

Pannexin 1 Signaling Metabolite Flux and Stoichiometry

Adishesh Kalya Narahari
Manassas, VA

Masters of Science in Biological and Physical Sciences, University of Virginia,
Charlottesville, VA 2017

Bachelors of Science in Biochemistry (Highest Honors) and Biology,
University of Virginia Charlottesville, VA 2014

A Dissertation Presented to the Graduate Faculty of the University of
Virginia in Candidacy for the Degree of Doctor of Philosophy

Department of Pharmacology
University of Virginia
May, 2021

Douglas A. Bayliss, Ph.D. (Advisor)

Kodi S. Ravichandran, Ph.D. (Committee Chair)

Paula Q. Barrett, Ph.D.

Mark P. Beenhakker, Ph.D.

Bimal N. Desai, Ph.D.

Mark J. Yeager, M.D., Ph.D.

ABSTRACT

Pannexin 1 (Panx1) channels are ion channels expressed in a wide range of tissues in vertebrate animals. Panx1 is predicted to be responsible for the release of ATP and other large signaling metabolites from cells. Panx1 has numerous activation mechanisms including via Gq-GPCRs and via C-terminal tail cleavage. The channel is important in this regard for various cell signaling pathways in numerous (patho)physiological processes. Despite works by previous groups, there are still numerous questions regarding important Panx1 channel properties: 1) Do caspase-activated Panx1 channels form a conduit that allows for the direct permeation of large signaling molecules and dye? 2) What is the functional oligomeric state of Panx1 channels? First, I utilize a biochemically-reduced proteoliposome system wherein I reconstitute Panx1 and show that caspase-activation of the channel forms a pore capable of fluxing dye, ATP, and other large signaling metabolites. Second, I use concatenated Panx1 constructs to demonstrate that Panx1 may be functional as both a hexamer and a heptamer. These works further our understanding of the Pannexin 1 channel and lead to new questions for which I have provided suggestions regarding future studies.

DEDICATION PAGE

I have been fortunate to have the most supportive group of friends, family, and mentors throughout the duration of my graduate career.

Arguably, without them none of this work would have been possible.

First and foremost, I am most grateful to my parents. Amma and Anna, you have instilled in me the value of hard work, dedication, a drive to answer questions, and for providing endless support over the years. I am eternally thankful for everything you have done to get me to this point both personally and professionally.

To my advisor Doug Bayliss, thank you very much for the opportunity to learn, work, and grow as a scientist under your guidance and mentorship. You have never ceased to amaze me with your work ethic, commitment to teaching, drive to answer questions as clearly as possible, and pushing me to be my best. I came into the lab as a naïve young scientist and was humbled many times by both science and life, but I always felt comfortable knocking on your door and knowing that you would help me get over the latest hurdle. I could not have picked a better mentor to help me learn how to “do science”. Thank you for all you have done and I am proud to have trained with you.

Eva, Ying-tang, Keyong, Liz, Christopher, and Pati, thank you for being fantastic lab mates. Science can be grueling at times and having friendly lab mates to spend time with and learn from has been a phenomenal experience.

The Bayliss lab experience would not have been the same without any of you.

I am thankful for my amazing committee members: Dr. Kodi Ravichandran, Dr. Bimal Desai, Dr. Mark Beenhakker, Dr. Paula Barrett, and Dr. Mark Yeager. I have spent time in each of your offices discussing my project or latest piece of data with you and advanced my project with your insightful comments.

To our collaborators: the Tamm lab (Lukas, Alex, Volker, and Binyong), the Ravichandran Lab (Ravi and Chris), the Yeager Lab (Mark, Susan, Vivian), and the Contreras Lab (Pablo and Jorge), I am so thankful for everything you have done to help me on this journey. You have all taught me so many techniques, provided so many resources, and importantly helped me learn many different facets of science.

To my MSTP friends Sham, Carol, Nadine, Jon, Dane, and Sarb. thank you all for running the MSTP marathon with me. We've all overlapped in different years and the numerous cups of coffee/hangouts we've had have been fantastic.

To the Beenhakker lab, Mark, Katie S., and Peter. Even though you've left our hallway, you still have adopted me as a member of your lab. I've spent many a day in your lab and learned so much about life from each one of you.

To my Pharm friends, Clint, Scott, Katie P., Mitch, Phil, Lily, Brittany and the Pharm front office (Ms. Tammy, Ms. Antoinette, Ms. Deborah, and

Ms. Jolene). Thank you all for keeping me sane on a day-to-day basis.

Whether it was in lab or out of lab, I've truly enjoyed getting to know each and every one of you and am lucky to have you as friends and colleagues.

To my undergraduates Ani, Julian, and Ann. Thank you for giving me the opportunity to teach and mentor. As harsh as I may sound at times, I'm extremely proud of each and every one of you and wish you three the best of luck in your future medical career pursuits.

To my clinical mentors Hunter, Eric, Zach, Vic, Dr. Kron, and Dr. Ailawadi, thank you for taking me under your wing and helping guide my clinical career through this time.

To my previous research mentors Dr. Diomedes E. Logothetis and Dr. Jochen Zimmer, I am eternally grateful for your efforts in preparing me for my graduate training. Dr. Logothetis, you ignited my interest in ion channels which has come full circle as presented in this dissertation. I will always be thankful for you pushing me to pursue an MD/PhD and not only attend medical school. Jochen, I have performed more protein preps during my doctoral research than I ever imagined I would. I'm glad I was able to learn science and especially membrane protein purification from one of the best in the business by doing preps with you! For this, thank you.

Thank you to some of the closest friends I have made over the years, Matt, Sankeerth, Kush, Nigel, Molly, Nish, Shelby, Amanda and Neil. Although some of you may not be geographically close anymore, you guys

are the best. You are always in my corner and you guys made this possible.

You all drive me to be the best possible physician-scientist I can be.

Finally, thank you to the funding agencies that made this work possible (NIH, UVA). I've been fortunate to be appointed to numerous training grants, receive scholarships, and have my NRSA (F30 CA236370).

TABLE OF CONTENTS

Title Page	i
Abstract	ii
Dedication	iii
Table of Contents	vii
List of Figures	viii
CHAPTER 1 Introduction: Structure, selectivity, and function of Pannexin 1 Channels.....	1
CHAPTER 2 ATP and large signaling metabolites flux through caspase- activated Pannexin 1 channels.....	41
CHAPTER 3 Stoichiometry and function of Pannexin 1 channels	110
CHAPTER 4 Conclusions and Future Studies	138

LIST OF FIGURES

Figure 1.1 Stoichiometry and subunit arrangement of large pore ion channels	12
Figure 2.1 Pannexin 1-eGFP construct and reconstitution	47
Figure 2.2 Liposome reconstitution and size	48
Figure 2.3 Pannexin 1 Caspase-3 cleavage sites and cleavage of Pannexin 1 in liposomes with recombinant Caspase-3	49
Figure 2.4 Whole-cell <i>in vitro</i> electrophysiology of fPanx1 in mammalian Cells	51
Figure 2.5 Single channel <i>in vitro</i> electrophysiology of fPanx1 in mammalian cells	52
Figure 2.6 Single channel electrophysiology of purified fPanx1 in planar lipid bilayers	54
Figure 2.7 Caspase has no effect on lipid bilayers that do not contain fPanx1	56
Figure 2.8 Bulk dye uptake in caspase-treated fPanx1-containing proteoliposomes	60
Figure 2.9 Dye uptake in caspase-treated fPanx1-containing proteoliposomes	62
Figure 2.10 GFP and Sulforhodamine-B Mean Fluorescence Intensity (MFI) in caspase-treated fPanx1-containing proteoliposomes	65
Figure 2.11 fPanx1 allows for permeation of anionic dye	66
Figure 2.12 Chemical structures of fluorescent dyes	68
Figure 2.13 fPanx1 allows for cation dye flux	70
Figure 2.14 Larger dyes flux through fPanx1 and fPanx1 is preferential to smaller, anionic dyes	71
Figure 2.15 Caspase-cleaved fPanx1 is a conduit for metabolite release	73

Figure 2.16 Chemical structures of metabolites.....	74
Figure 2.17 ATP and Spermidine can flux through Pannexin 1 concurrently	76
Figure 3.1 Concatemeric Constructs	113
Figure 3.2 Western Blot of Panx1KO HEK293T Cells.....	115
Figure 3.3 Heptameric Pannexin 1 Forms Functional Channels in wild- type HEK293T Cells	119
Figure 3.4 Hexameric Pannexin 1 Forms Functional Channels in Panx1KO HEK293T Cells	122
Figure 3.5 Heptameric Pannexin 1 Forms Functional Channels in Panx1KO HEK293T Cells	123
Figure 3.6 Both hexameric and heptameric Pannexin 1 concatemers form functional channels	124
Figure 3.7 ToPro3 Uptake into Jurkat T-cells expressing Panx1 concatemeric constructs	127
Figure 4.1 Alanine may not flux through Pannexin 1	147

CHAPTER 1

Introduction: Structure, selectivity, and function of Pannexin 1 Channels

The chapter is being prepared for submission as a review:
Adishesh K. Narahari*, Ann T. Mathew*, Yu-Hsin Chiu, Douglas A. Bayliss. Structure, selectivity, and Function of Pannexin 1 Channels

*These authors contributed equally

Please note: Ann and I wrote initial drafts of the review and I have modified the review to serve as an introduction to this dissertation based on comments from Doug Bayliss.

Abstract

Pannexin 1 (Panx1) is a membrane ion channel that is expressed through the body in vertebrate species. Panx1 plays an important role in various physiological and pathophysiological processes including blood pressure regulation, apoptosis, neuropathic pain, and ischemia-reperfusion injury. Numerous structural and functional studies have been reported recently. Understanding the structure-function relationship of Panx1 is critical to learning about its overall role in biology. Here, we review the structures of Panx1 and present them with the current functional understanding of the channel. Two important questions to keep in mind include: 1) Do activated Panx1 channels form conduits for large signaling metabolites and 2) What is the functional oligomeric state of Panx1 channels?

Introduction

Pannexin 1 (Panx1) channels are membrane channels that are expressed in a wide range of tissues (Baranova et al., 2004; Penuela, Gehi, & Laird, 2013). The three paralogues of the Pannexin family of channel proteins (Panx1, Panx2, and Panx3) share 50% sequence similarity with the greatest variability in the C-terminal region (Penuela, Bhalla, Nag, & Laird, 2009). Panx1 is expressed in numerous organs, central nervous system, skin, and vasculature; Panx2 is expressed in the central nervous system (Baranova et al., 2004); and Panx3 is localized in skin, cochlea, and developing hard tissues (cartilage, bones, and teeth) (Ishikawa et al., 2019). Panx1 channels have been implicated in numerous pathophysiological processes while less is known about the regulation and function of Panx2 and Panx3 channels.

Panx1 membrane channels are members of an extended family of channels that include Connexins, Innexins, Calcium homeostasis modulator 1 and 2 (CALHM 1 and CALHM2), and SWELL1 (LRRC8) (Abascal & Zardoya, 2012; Baranova et al., 2004; Deneka, Sawicka, Lam, Paulino, & Dutzler, 2018; Panchin et al., 2000; Siebert et al., 2013; Syrjanen et al., 2020). These channels display little sequence

homology but share a common subunit arrangement and some shared functional properties.

Panx1 is a unique ion channel with numerous activation mechanisms which are observed in various (patho)physiological processes. The channel is predicted to flux large signaling metabolites, most notably ATP when it is activated (L. Bao, Locovei, & Dahl, 2004; Chekeni et al., 2010; Lutter, Ullrich, Lueck, Kempa, & Jentsch, 2017; Medina et al., 2020; Siebert et al., 2013; Taruno, 2018).

In this Chapter, I discuss Panx1 in terms of its activation mechanisms, biological role, structure, permeation, and gating. I will describe the structures and permeation characteristics of Panx1 presented in recent studies, and cover some of the controversies that prompted the experiments presented in this dissertation.

Panx1 Activation Mechanisms

Numerous methods of activation for Panx1 have been suggested (e.g., elevated external K^+ , intracellular Ca^{2+} , Src family kinase-mediated phosphorylation, caspase-mediated cleavage of the C-terminal tail, and ionotropic/metabotropic receptor signaling) (Billaud et al., 2011; Chiu et al., 2017; Dahl, 2018; DeLalio et al., 2019; Locovei, Wang, &

Dahl, 2006; Medina et al., 2020; Y. Qu et al., 2011; Sandilos et al., 2012; Silverman et al., 2009; Suadicani et al., 2012; Thompson et al., 2008; Weilinger et al., 2016; D. Yang, He, Munoz-Planillo, Liu, & Nunez, 2015; reviewed in Chiu, Schappe, Desai, & Bayliss, 2018).

A few of the activation mechanisms are reversible: elevated external K^+ , (F. Qiu, Wang, Spray, Scemes, & Dahl, 2011; Silverman et al., 2009; Suadicani et al., 2012), intracellular Ca^{2+} (Locovei et al., 2006), hypotonicity (Seminario-Vidal et al., 2011), Src family kinase-mediated phosphorylation (DeLalio et al., 2019; Weilinger et al., 2016) and ionotropic/metabotropic receptor signaling (Billaud et al., 2015; Billaud et al., 2011; Chiu et al., 2017; reviewed in Chiu et al., 2018; Thompson et al., 2008; Weilinger et al., 2016). An irreversible mechanism of activation is via caspase-mediated cleavage of the C-terminal tail (Chekeni et al., 2010; Chiu et al., 2017; Medina et al., 2020; Y. Qu et al., 2011; Sandilos et al., 2012; D. Yang et al., 2015).

In expression systems, mouse Panx1 has basal activity and can be further activated whereas the human isoform is basally silent (Chiu et al., 2017; Nomura et al., 2017; Sandilos et al., 2012). Both GPCR- and cleavage-mediated activation have been shown to permit the flux of

atomic ions with similar unitary conductance, albeit with different mean open times (Chiu et al., 2017; Good, Chiu, et al., 2018).

Metabotropic GPCR-mediated activation of the channel occurs through an unknown signaling pathway through Gq-GPCRs (Billaud et al., 2015; Billaud et al., 2011; Chiu et al., 2017; Good, Chiu, et al., 2018). This mechanism may possibly involve phosphorylation of the channel. These GPCR-activated Panx1 channels open and close rapidly with 1.9 ms mean open times. Comparatively, Panx1 activated by Caspase-3-mediated C-tail cleavage renders a channel with a mean open time of 7.9 ms (Chiu et al., 2017).

Overview of Panx1 Biology

Panx1 has been studied as a therapeutic target in many contexts. Pathologically, it has been implicated in neuropathic pain (Bravo et al., 2014; Di Cesare Mannelli, Maresca, Farina, Scherz, & Ghelardini, 2015; Koyanagi et al., 2016; Weaver et al., 2017; Zhang, Laumet, Chen, Hittelman, & Pan, 2015; Zhang et al., 2017) epilepsy (Dossi et al., 2018), stroke (Bargiotas et al., 2011; Bargiotas, Krenz, Monyer, & Schwaninger, 2012; Good, Eucker, et al., 2018; Wei et al., 2020; Weilinger et al., 2016; Wicki-Stordeur et al., 2016), ischemia-reperfusion injury (Bargiotas et al., 2011; Freitas-Andrade,

Bechberger, MacVicar, Viau, & Naus, 2017; Sharma et al., 2018) and infertility (Sang et al., 2019; W. Wang et al., 2021). Panx1 is also important in normal physiological processes such as apoptosis (Chekeni et al., 2010; Medina et al., 2020; Poon et al., 2014), inflammation (Lemaire, Falzoni, Zhang, Pellegatti, & Di Virgilio, 2011; Lohman et al., 2015; Pelegrin & Surprenant, 2006; Saez et al., 2017; Schenk et al., 2008), blood pressure regulation (Billaud et al., 2011; DeLalio et al., 2019; DeLalio et al., 2020; Good, Chiu, et al., 2018; Nyberg et al., 2018; S. Wang et al., 2016) among others.

Panx1 channels have been implicated in cell death, particularly in various stages of apoptosis. Panx1 plays a role in apoptosis via the release of "find-me" signals to recruit phagocytes (Chekeni et al., 2010; Elliott et al., 2009; Medina et al., 2020; Y. Qu et al., 2011). In early phases, Panx1 has been found to increase membrane permeability and later maintain cell integrity (Chekeni et al., 2010; Poon et al., 2014). In apoptosis, Panx1 is activated by caspase cleavage of the C-terminal tail and dissociation of this auto-inhibitory domain (Chiu et al., 2017; Sandilos et al., 2012). In pyroptosis, Panx1 is activated by various caspases leading to P2X7 activation (D. Yang et al., 2015). The involvement of Panx1 in autophagy is not well defined. Current evidence for Panx1 and autophagy consists of its general

involvement in translocation of lysosome-associated protein 1 (Crespo Yanguas et al., 2017). The investigation of Panx1 in these contexts has introduced important insights on the involvement of Panx1 in cell death and cell clearance.

Panx1 is highly expressed in neurons, glia, and immune cells and activated by nerve injury-related mechanisms such as caspase cleavage, G protein-coupled receptors, inflammatory mediators or ionotropic receptors, causing it to be of relevance when investigating therapeutic targets for neuropathic pain (Bravo et al., 2014; Di Cesare Mannelli et al., 2015; Koyanagi et al., 2016; Weaver et al., 2017; Zhang et al., 2015; Zhang et al., 2017). These channels are upregulated in nerve injury models, particularly in the dorsal root ganglia (Zhang et al., 2015). Nerve injury often induces the release of pro-inflammatory cytokines that contribute to the development of neuropathic pain, which is in-part controlled by Panx1 to induce inflammation (Zhang et al., 2015). Panx1 channels mediate inflammation through two key mechanisms: activation of inflammasomes and release of pro-inflammatory cytokines and activation and release of leukocytes (Crespo Yanguas et al., 2017). In this context, Panx1 can activate P2X₇ receptors and promote multinucleated macrophage formation, cause T-cell activation, and

leukocyte/dendritic cell migration (Y. Bao, Chen, Ledderose, Li, & Junger, 2013; Lemaire et al., 2011; Lohman et al., 2015; Saez et al., 2017; Schenk et al., 2008). Activation of Panx1 in these contexts is dependent on extracellular ATP and P2 receptors (Lohman et al., 2015).

Panx1 is important in vascular contexts such as hypertension (DeLalio et al., 2019; Good, Chiu, et al., 2018; S. Wang et al., 2016) and ischemic stroke (Bargiotas et al., 2011; Bargiotas et al., 2012; Good, Eucker, et al., 2018; Wei et al., 2020; Weilinger et al., 2016; Wicki-Stordeur et al., 2016). Panx1 regulates blood pressure through its involvement in vasoconstriction in smooth muscle cells potentially via an ATP mechanism (Billaud et al., 2011; Good, Eucker, et al., 2018). α -adrenergic receptors in vascular smooth muscle cells are shown to activate Panx1 by signaling to the intracellular loop (Billaud et al., 2011). Caveolae structural protein Cav1 has been recently identified to interact with Panx1 in regulating blood pressure responses via an ATP-mediated response (DeLalio et al., 2018). Furthermore, endothelial Panx1 regulates leukocytes passing from the venous system to brain tissues in ischemia/reperfusion injury and regulates cerebral arterial function (Good, Eucker, et al., 2018). Myocardial, lung, and renal ischemia/reperfusion injuries and ischemia-induced neurodegeneration

have also been shown to involve Panx1 channels via a predicted ATP signaling mechanism (Bargiotas et al., 2012; Freitas-Andrade et al., 2017; Jankowski et al., 2018; Sharma et al., 2018; Su et al., 2019). Importantly, these (patho)physiological processes predict an important role for Panx1 and ATP; however, the permeants and selectivity of Panx1 have not been fully explored.

These various (patho)physiological processes represent the vast array of Panx1 involvement in numerous signaling pathways. Although there is much more to be studied to fully understand the scope of Panx1 involvement in these contexts, the evidence shows the importance of focusing research on Panx1 for treatments and preventative measures for various conditions. Yet, the mechanistic function of Panx1 in these various processes remains to be determined. Understanding Panx1 structure, function, activation, gating, and selectivity are important areas of study to elucidate the role of Panx1 in disease as well as homeostatic physiology.

Pannexin 1 Structure

Pannexin 1 is part of a group of large pore ion channels. Within this group -- which includes vertebrate and invertebrate gap junction channels (Connexins and Innexins), Calcium homeostasis modulator 1

and 2 (CALHM1 and CALHM2) and SWELL1 (LRRC8) -- Panx1 has the most sequence homology with Innexins, and shares general subunit topology with all members. Panx1 subunits all consist of four transmembrane domains with intracellular N- and C- terminal domains, but channels in this large-pore ion channel family vary in their oligomeric states (Boassa, Qiu, Dahl, & Sosinsky, 2008; Chiu et al., 2017; Deng et al., 2020; Jin et al., 2020; Michalski et al., 2020; Mou et al., 2020; R. Qu et al., 2020; Ruan, Orozco, Du, & Lu, 2020; J. Wang et al., 2014). Panx1 is heptameric, while Connexins are hexameric, Innexins and CALHM1 are octameric, and CALHM2 is undecameric. These channels are activated by a number of distinctly different mechanisms, and they can show mixed ionic selectivity (e.g., Connexins, CALHM1) and they are inhibited by extracellular Ca^{2+} (Choi, Clemente, Sun, Du, & Lu, 2019; Demura et al., 2020; W. Ma et al., 2012; Syrjanen et al., 2020; Taruno, Matsumoto, Ma, Marambaud, & Foskett, 2013). LRRC8, a hexameric, volume-regulating anionic channel whose channel activity is dependent on the osmolarity of its environment, also shares structural features with the previously noted channels (Abascal & Zardoya, 2012; Deneka et al., 2018; Kasuya et al., 2018; Kefauver et al., 2018; Z. Qiu et al., 2014; Siebert et al., 2013). For the majority of these channels, the subunit transmembrane regions assemble in a counter clockwise arrangement. The exceptions

are CALHM1 and CALHM2, for which the assembly occurs in a clockwise orientation (Ruan et al., 2020; Syrjanen et al., 2020) (**FIGURE 1**). As observed in CALHM1 (Dreses-Werringloer et al., 2008) and LRRC8 channels (Voss et al., 2014), Panx channels are also reported to undergo N-glycosylation (Penuela et al., 2007; Penuela et al., 2009). This glycosylation likely prevents gap junction formation because mutation of the relevant Asn site prevents glycosylation and allows formation of a gap junction (Ruan et al., 2020). This glycosylation further sets Panx channels apart from innexins and connexins (Beckmann, Grissmer, Krause, Tschernig, & Meier, 2016; Boassa et al., 2008; Sahu, Sukumaran, & Bera, 2014; Sosinsky et al., 2011).

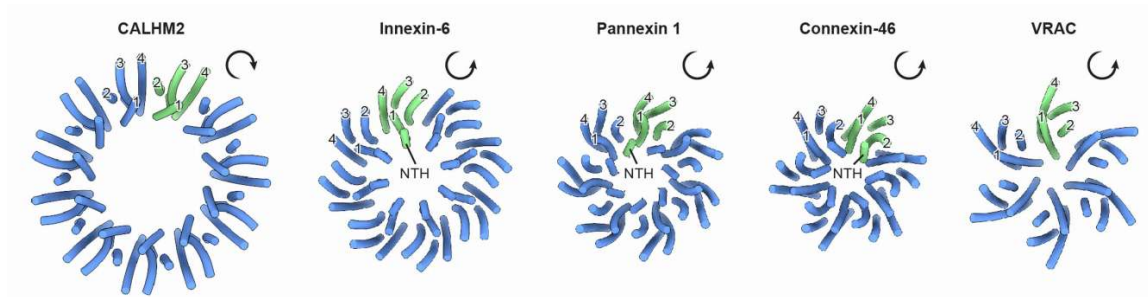


Figure 1.1 Stoichiometry and subunit arrangement of large pore ion channels (Adapted from Ruan et al. *Nature* 2020). Arrangement of transmembrane helices within large pore channels. Panx1 has a counter-clockwise arrangement similar to Innexin-6, Connexin-46 and VRAC. CALHM2 is an undecamer, Innexin-6 is an octomer, Pannexin 1 is a heptamer, Connexin-46 is a hexamer, and VRAC is also a hexamer.

Panx1 is a heptameric transmembrane channel

Until recently, Panx1 was believed to be a hexameric channel like connexins and innexins (Boassa et al., 2007; Chiu et al., 2017; J. Wang et al., 2014). However, recent cryo-EM structures and 2D class averages of human and frog Panx1 demonstrate the formation of a symmetric heptamer (Deng et al., 2020; Jin et al., 2020; Michalski et al., 2020; Mou et al., 2020; R. Qu et al., 2020; Ruan et al., 2020).

Similar to innexins, connexins, and LRRC8 channels, Panx1 has four transmembrane domains, with the N- and C-termini on the cytoplasmic side; there are two extracellular loops (between TM1-TM2 and TM3-TM4) and a single intracellular loop (between TM2-TM3) (Deng et al., 2020; Jin et al., 2020; Michalski et al., 2020; Mou et al., 2020; R. Qu et al., 2020; Ruan et al., 2020). Seven identical subunits form a symmetric central axis that constitutes the permeation pathway (Deng et al., 2020). Each protomer consists of an extracellular domain and intracellular domain that are connected by a transmembrane domain (Ruan et al., 2020). The two extracellular loops in the extracellular domain are connected via β -strands which are strengthened by two disulfide bonds (Deng et al., 2020; Michalski et al., 2020; R. Qu et al., 2020). An alpha helix within the extracellular domain extends into the central pore creating the extracellular

constriction site at the entrance of the channel (Deng et al., 2020; Ruan et al., 2020). The transmembrane domain is two-layered where it is composed of the interior N-terminal helix that lines the pore and exterior helix bundle arranged in an anticlockwise manner (Deng et al., 2020; Ruan et al., 2020). Finally, the intracellular domain is a helix-rich structure that is linked with the N-terminal loop (Deng et al., 2020; Michalski et al., 2020; Ruan et al., 2020). The cytoplasmic domain, an important regulatory part of each subunit, has not been resolved in any of the structures (Ruan et al., 2020; Sandilos et al., 2012).

Panx1 permeation pathway(s)

The available structures indicate that Panx1 channels have a central pore and, in one case, have been predicted to have additional side tunnels (Ruan et al., 2020). The main pore is characterized as a “truncated cone” with a wide transmembrane domain and intracellular domain, but narrow extracellular domain (Deng et al., 2020). The extracellular domain consists of a ring of seven W74 residues that line the outer constriction site of the pore (Deng et al., 2020; Jin et al., 2020; Michalski et al., 2020; Mou et al., 2020; R. Qu et al., 2020; Ruan et al., 2020). The pore radius for the structures is quite consistent (~4.4-4.7 Å). The R75 residues in the extracellular domain

may contribute to the anionic preference of the channel (Michalski et al., 2020). This theory was tested by Michalski et al. by performing mutagenesis experiments at this residue to either a neutral or negatively charged residue. Changing the residue to a negative residue (R75E) rendered the channel more permeable to cations (Michalski et al., 2020).

Hydrophobic amino acids of one of the transmembrane helices predominantly lines the transmembrane domain of the pore, (Deng et al., 2020). The helix is predicted to not play a role in gating due to its limited mobility and limited interactions with other helices (Ruan et al., 2020). The intracellular domain is positively charged and may contribute to the anion preference of the channel by creating a positive electrostatic potential to recruit anions and other negatively charged molecules (Michalski et al., 2020; Ruan et al., 2020). However, a lack of resolution of the C-terminus which forms a part of the intracellular domain does not allow for further interpretation of a second region of selectivity -- an intracellular "shrink ring" made up of T21, E22, and P23 residues on an inter-protomer helix in the N-terminus (Mou et al., 2020). However, other structures identified K26 as the site of this intracellular constriction (Deng et al., 2020; Ruan et al., 2020). Again, the C-terminal tails of the channel are further intracellular to this

constriction point and may form a smaller pore diameter compared to the 10 Å radius at the K26 site. The C-terminal tails may either have direct steric effects (smaller pore not allowing channel activity) or allosteric effects (pore size formed by C-terminal tails is not as important) which prevent channel gating and activity. Once the direct steric or allosteric block is removed, the channel can open and close.

In addition to the main permeation pathway, there are seven side tunnels found in the upper intracellular domain that may allow for an alternative pathway for the conduction of ions into the main vestibule (i.e., not via the central pore made accessible by cleavage of C-terminal tails) (Ruan et al., 2020). Ruan et al. describe small outwardly-rectifying currents that are inhibited by carbenoxolone. The current is ameliorated by mutagenesis to shrink the constriction point at the entrance of the tunnel (A33W) or the current is increased by enlarging the tunnel (R29A). This can be interpreted as basal currents that are present without any further channel activation via an alternative ion conduction pathway. Ruan et al. performed molecular dynamics simulations that predict that the tunnels are large enough for hydrated chloride ions, but not for larger molecules. A few issues with this prediction is that many previous studies have found that human and *Xenopus* Panx1 is basally silent (Chekeni et al., 2010; Chiu

et al., 2017; Dahl, 2018; Sandilos et al., 2012) in whole cell recordings. Further, single channel recordings of these channels yield silent channels until they are activated. Although, mouse Panx1 does support basal current, the current in these channels is far larger than the current reported by Ruan et al. and likely not via the same mechanism (W. Ma et al., 2012; Nomura et al., 2017).

Caspase-cleavage activation and CBX inhibition in the context of structure

The caspase-cleavage activation and CBX-dependent inhibition mechanisms have also been studied in relation to these new structural findings (Jin et al., 2020; R. Qu et al., 2020; Ruan et al., 2020). Many studies have highlighted the caspase activation of Panx1 channels by removing the C-terminal tail, an autoinhibitory region (Chekeni et al., 2010; Chiu et al., 2017; Deng et al., 2020; Imamura et al., 2020; Ruan et al., 2020; Sandilos et al., 2012). A few available structures have provided the first visualization of the channel with a C- tail deletion, a mimetic of caspase cleavage of the C-terminal tail (Jin et al., 2020; Mou et al., 2020; R. Qu et al., 2020; Ruan et al., 2020). Numerous groups also attempted to resolve the full-length structure and the studies fail to illustrate the disordered C-terminal region at high resolution. Ruan et al. has provided disordered visualization of

the C-terminal tail (Ruan et al., 2020). However, when comparing full-length and C-terminal tail-cleaved Panx1 channels, no differences in channel architecture or pore dilation are apparent. The pore is too constricted at the extracellular domain W74 ring (8.8 Å diameter) to allow for the passage of molecules larger than atomic ions or small molecules (Diameters: Cl⁻: 6.6 Å, Mg-ATP: ~18 Å) (Israelachvili, 2011; Liao, Sun, Chandler, & Oster, 2004). Even with the activated channel (C-terminal tail cleaved), a permeation pathway for large molecules is not apparent. The channel may have different states when it is activated or the pore could dilate to permit large molecule flux. A similar dilation mechanism has been proposed with P2X7 receptor (Karasawa, Michalski, Mikhelzon, & Kawate, 2017). In non-cleavage methods of activation, the C-tails need to spread apart to form a passage way for permeants. In C-terminal tail cleavage-based activation, the extracellular domain must dilate to allow for passage of large molecules (up to 1.2 kDa) (Chiu et al., 2017; Poon et al., 2014; J. Wang, Ma, Locovei, Keane, & Dahl, 2007). Finally, no gating mechanism for the channel when it is activated by C-terminal tail cleavage has been shown. The C-terminal tail is clearly one potential “lock” that needs to be released before the gate of the channel can open and close. Further complicating Panx1 gating is the fact that the channel can open and close even without C-terminal tail cleavage,

possibly via a different gate opening mechanism. These questions may need to be explored by capturing the channel in different states of opening and closing via cryo-EM or by other microscopy methods such as atomic force microscopy (AFM).

In regards to inhibition, the W74 residue has been acknowledged as a key determinant of CBX inhibition of Panx1 channels (Michalski & Kawate, 2016). However, recent mutagenesis experiments of these residues and other residues in the helices in the extracellular domain were also found to influence CBX-dependent inhibition (Michalski et al., 2020; Ruan et al., 2020).

Over the past two decades, we have advanced our understanding of Panx1 channels; however, there are still multiple questions that need to be answered. Despite numerous groups attempting to show how C-tail cleavage may lead to channel opening, no apparent differences are visible in C-tail deleted structures. Further, the auto inhibitory C-terminal region is disordered and not well resolved in full-length Panx1 structures. Many questions remain regarding the gating mechanism, the unresolved areas of the channel, conductance states, and permeability.

Permeants and Selectivity

With the recent publication of numerous structural studies and works relating to the physiological relevance of Panx1, determining the permselectivity of Panx1 is of utmost importance in understanding the mechanistic role Panx1 plays in these various (patho)physiological processes. Various groups have described the permeation characteristics of this unique large-pore channel and we will consider those according to three main permeant types: atomic ions, fluorescent dyes, and signaling metabolites.

Ions

First and foremost, Panx 1 is a bona fide ion channel with an outwardly-rectifying current in whole cell recordings (Chekeni et al., 2010; Chiu et al., 2017; Good, Chiu, et al., 2018; Pelegrin & Surprenant, 2006; Sandilos et al., 2012)) and channel openings and closings in single channel recordings (L. Bao et al., 2004; Chiu et al., 2017; Locovei et al., 2006; Mou et al., 2020; Romanov et al., 2012). Currently available structures of Panx1 are the full length channel and a channel with the C-terminus deleted at the caspase cleavage sequence (Deng et al., 2020; Jin et al., 2020; Michalski et al., 2020; Mou et al., 2020; R. Qu et al., 2020; Ruan et al., 2020). Unfortunately, no appreciable differences are apparent with regard to

pore size or pore architecture between the full-length channel and the “caspase-cleavage mimetic” channel (Jin et al., 2020; Mou et al., 2020; R. Qu et al., 2020; Ruan et al., 2020). As described earlier, a secondary ion permeation pathway has been suggested, with a side tunnel leading into the main vestibule (Ruan et al., 2020). This pathway does not require C-terminal cleavage for activation. However, single channel recordings by other groups show silent channels without any ion permeation and therefore this proposed mechanism of an alternative ion permeation pathway in addition to the main large pore needs to be further explored (Chiu et al., 2017; Sandilos et al., 2012). Once the mechanism of GPCR activation of Panx1 is well characterized, potential phosphomimetic or other channel activating mutations can be used for future structural studies. Attempts to characterize the selectivity of the channel using mutagenesis or traditional impermeant ion replacement strategies has not yielded conclusive results likely because the “impermeant” ions are too small and may in fact flux through the channel (Chiu, Ravichandran, & Bayliss, 2014; Deng et al., 2020; Michalski et al., 2020; Nielsen et al., 2020; Nomura et al., 2017; Ruan et al., 2020; J. Wang & Dahl, 2018). Conventional studies of selectivity in ion channels are performed by whole-cell patch-clamp experiments where the predicted permeant ion is replaced in the bath solution with another ion that is predicted to not permeate or be less

permeable through the channel (creating asymmetric solutions). In an ideal scenario, the replacement of the predicted permeating ion with a less permeable ion, changes the reversal potential (E_{rev}) of the recording due to the channel's selectivity. For example, if chloride (-) can flux through the channel and is replaced with a larger anion such as gluconate (-) only in the bath solution while maintaining $[Cl^-]$ in the pipette solution, the E_{rev} is shifted to a more positive potential, suggesting that Panx1 favors the permeation of chloride compared to gluconate (Michalski et al., 2020). If a cation (such as sodium) does not contribute to the current being measured, and a larger cation (NMDG⁺) is replaced in the bath solution, the E_{rev} should not change as the isolated whole-cell current is not affected by the introduced ion.

At this point, few conclusions about the atomic ion selectivity of the channel can be made. Our group and other groups have employed proteoliposome flux assays to test putative permeants in an isolated system (Karasawa et al., 2017; Nimigean, 2006). A very similar system can be employed for testing atomic ion permeability with proteoliposomes filled with dyes that fluoresce when bound to the ion of interest.

Dye

Dye permeation into cells has been used as a surrogate for Panx1 channel activity (Chekeni et al., 2010; Chiu et al., 2017; Nielsen et al., 2020; Poon et al., 2014; F. Qiu et al., 2011; Silverman et al., 2009). This method of determining channel activity has suggested that dye uptake into cells occurs in a Panx1-dependent fashion. However, other channels (e.g. Connexins, CALHMs) are also capable of dye uptake and may be potential dye conduits. Both cationic (To-Pro3, Yo-Pro3, Ethidium, Propidium Iodide) and anionic dyes (Lucifer Yellow) up to 1300 daltons have been shown to flux into cells with active Panx1 (basally or through intentional activation). For example, Panx1 is active during apoptosis and pyroptosis (caspase-activation dependent) and dye uptake is diminished in cells expressing dominant-negative Panx1 (Caspase-3 site is mutated) or when a Panx1 inhibitor is utilized (Boyd-Tressler, Penuela, Laird, & Dubyak, 2014; Chekeni et al., 2010; Chiu et al., 2017; Dolmatova et al., 2012; Hansen et al., 2014; Nielsen et al., 2020; Poon et al., 2014; Sandilos et al., 2012). Further, other modes of Panx1 activation such as Gq-GPCR mediated activation or TNF- α receptor mediated activation also lead to ToPro3 uptake (Good, Chiu, et al., 2018; Lohman et al., 2015). Hypotonicity has also been shown to permit propidium iodide (+) permeation into cells (Seminario-Vidal et al., 2011). Finally, high extracellular K⁺ has also

been shown to permit dye uptake into cells expressing Panx1 and this dye uptake was abolished with the use of a Panx1 inhibitor or in Panx1KO neurons (Santiago et al., 2011). However, secondary methods of dye uptake through other channels cannot be excluded. For example, the channel forming a dye-permeable pore was disputed with P2X₇ receptors where Panx1 was actually a candidate for the dye conducting pore (Pelegriin & Surprenant, 2006). However, the P2X₇ receptor itself was found to form the dye-permeable pore (Karasawa et al., 2017). To dispel concerns with secondary mechanisms of permeation, in Chapter 2, I utilized a proteoliposome system wherein I reconstituted purified Panx1 into proteoliposomes to test for dye flux. In our system, I demonstrated that caspase-activated Panx1 itself forms a conduit that permits dye flux. I tested dye flux (uptake and release) using three methods: ImageStream flow cytometry, a bulk size-exclusion column assay, and a TIRF-based dye release assay. We find that both anionic and cationic dyes are able to permeate through the channel with a preference towards smaller, anionic dyes. The mechanism for this relative selectivity still needs to be explored further.

Metabolites

For nearly two decades, Panx1 has been canonically dubbed as an ATP channel (L. Bao et al., 2004; Chekeni et al., 2010; Dahl, 2018; Medina et al., 2020; Poon et al., 2014; R. Qu et al., 2020; Seminario-Vidal et al., 2011; Siebert et al., 2013; Taruno, 2018; J. Wang & Dahl, 2018). ATP release has been demonstrated in association with numerous Panx1 activation mechanisms such as $\alpha 1D$ -Receptor mediated signaling (Billaud et al., 2015), high K^+ (R. Qu et al., 2020; J. Wang & Dahl, 2018), TNF-induced activation (Lohman et al., 2015), stretch (L. Bao et al., 2004; Locovei et al., 2006), Caspase-3 mediated cleavage (Chekeni et al., 2010; Chiu et al., 2017; Medina et al., 2020; Siebert et al., 2013; D. Yang et al., 2015). In one report, Panx1 ionic currents were dissociated from ATP release, suggesting that Panx1 is perhaps not a conduit for ATP release; however, in that case, ion channel activity was measured in heterologously expressed mouse Panx1 (which has basal activity) that had not been intentionally activated (Romanov et al., 2012). As with dye uptake, possible primary and secondary modalities of ATP release cannot be excluded (Dahl, 2018). For example, ATP may be released through other channels (e.g., CALHM1/2, Connexons) or through vesicular release (Bahima et al., 2006; Cotrina et al., 1998; Dosch et al., 2019; J. Ma et al., 2018; Taruno, Vingtdoux, et al., 2013). A previous approach to determine

ATP permeability has been used Bao et al. by demonstrating different E_{rev} by varying K_2ATP concentrations. However, a few issues with this study make the results difficult to interpret: a potassium driven current cannot be excluded, osmolality driven stretch activation may result in the current seen, and no inhibitors were utilized to show that the current was indeed Panx1 (L. Bao et al., 2004).

Finally, recent work has suggested that Panx1 is a large-pore channel implicated in the release of “good-bye” signals other than ATP that may play roles in anti-inflammatory signaling and other important cell signaling pathways (Medina et al., 2020; Nielsen et al., 2020). For example, glutamate (-), spermidine (+), and lactate (-) are all predicted permeants of the channel (Medina et al., 2020; Nielsen et al., 2020). However, other molecules of similar size (e.g., alanine (0) and glucose (0)) do not permeate the channel (Medina et al., 2020; Nielsen et al., 2020). It is possible that the size, shape, and charge of the molecule are important characteristics of permeants.

Charge Selectivity

A key characteristic for any ion channel is its selectivity for different potential permeants. Numerous attempts to characterize the selectivity of Panx1 channels have been difficult to interpret due to the large pore nature of the channel (Chiu et al., 2014; Deng et al., 2020; W. Ma et

al., 2012; Michalski et al., 2020; Ruan et al., 2020; J. Wang & Dahl, 2018). These studies have largely relied on patch-clamp studies with E_{rev} changes as described earlier. Some studies have claimed outright that the channel is anion selective (W. Ma et al., 2012; Michalski et al., 2020; J. Wang & Dahl, 2018). Other studies have claimed that the channel is a cationic channel (Kienitz, Bender, Dermietzel, Pott, & Zoidl, 2011; Y. Yang et al., 2020). Further complicating the issue is that both cationic and anionic dyes/large molecules have been shown to permeate through the channel (see Dye and Metabolites section). Two residues, (W74 and R75) were identified as potentially important in selectivity via structural studies because they are the narrowest part of the pore. Interestingly, W74 has also been predicted to play an important role in the binding of carbenoxolone, a Panx1 inhibitor (Michalski & Kawate, 2016). Further careful analysis with mutagenesis in isolated systems, such as a proteoliposome assay or lipid bilayer recordings, needs to be performed to further refine our understanding of Panx1 selectivity.

Gating

Lastly, very little is known about the gating of the channel. The C-terminal tail has been shown to be an autoinhibitory domain that allows for channel activity once cleaved (Chiu et al., 2017; Sandilos et

al., 2012). However, the channel does not remain permanently open after this method of activation and therefore another gate in the channel must exist that causes the channel to open and close. Further complicating the issue is that the channel can also open and close upon non-cleavage based activation (GPCR, SRC-mediated, etc.). This suggests that even with the C-terminal tail present, the channel can still open and close. Capturing the channel in an open state structurally or by atomic force microscopy after C-tail cleavage or utilizing phosphomimetic mutations to force the channel open may yield further information regarding channel gating.

Conclusion

Our understanding of Panx1 channels has greatly been furthered by recent structural and functional studies. Panx1 plays an important role in numerous (patho)physiological processes and understanding the mechanism by which the channel functions is crucial in understanding the complex role it plays in cell signaling. Functional studies of the channel have suggested that Panx1 may form a conduit for large signaling metabolites. The charge preference of the channel for large molecules is not known. Finally, the structural studies have suggested that Panx1 assembles into a heptamer with two potential permeation pathways for ions. In Chapter 2, I will address if caspase-activated

Panx1 is a large metabolite conduit with a charge preference using purified Panx1 reconstituted in proteoliposomes. In Chapter 3, I will test two oligomeric conformations of Panx1 for functionality using hexameric and heptameric concatemers.

References

- Abascal, F., & Zardoya, R. (2012). LRRC8 proteins share a common ancestor with pannexins, and may form hexameric channels involved in cell-cell communication. *Bioessays*, *34*(7), 551-560. doi:10.1002/bies.201100173
- Bahima, L., Aleu, J., Elias, M., Martin-Satue, M., Muhaisen, A., Blasi, J., . . . Solsona, C. (2006). Endogenous hemichannels play a role in the release of ATP from *Xenopus* oocytes. *J Cell Physiol*, *206*(1), 95-102. doi:10.1002/jcp.20440
- Bao, L., Locovei, S., & Dahl, G. (2004). Pannexin membrane channels are mechanosensitive conduits for ATP. *FEBS Lett*, *572*(1-3), 65-68. doi:10.1016/j.febslet.2004.07.009
- Bao, Y., Chen, Y., Ledderose, C., Li, L., & Junger, W. G. (2013). Pannexin 1 channels link chemoattractant receptor signaling to local excitation and global inhibition responses at the front and back of polarized neutrophils. *J Biol Chem*, *288*(31), 22650-22657. doi:10.1074/jbc.M113.476283
- Baranova, A., Ivanov, D., Petrash, N., Pestova, A., Skoblov, M., Kelmanson, I., . . . Panchin, Y. (2004). The mammalian pannexin family is homologous to the invertebrate innexin gap junction proteins. *Genomics*, *83*(4), 706-716. doi:10.1016/j.ygeno.2003.09.025
- Bargiotas, P., Krenz, A., Hormuzdi, S. G., Ridder, D. A., Herb, A., Barakat, W., . . . Schwaninger, M. (2011). Pannexins in ischemia-induced neurodegeneration. *Proc Natl Acad Sci U S A*, *108*(51), 20772-20777. doi:10.1073/pnas.1018262108
- Bargiotas, P., Krenz, A., Monyer, H., & Schwaninger, M. (2012). Functional outcome of pannexin-deficient mice after cerebral ischemia. *Channels (Austin)*, *6*(6), 453-456. doi:10.4161/chan.22315
- Beckmann, A., Grissmer, A., Krause, E., Tschernig, T., & Meier, C. (2016). Pannexin-1 channels show distinct morphology and no gap junction characteristics in mammalian cells. *Cell Tissue Res*, *363*(3), 751-763. doi:10.1007/s00441-015-2281-x
- Billaud, M., Chiu, Y. H., Lohman, A. W., Parpaite, T., Butcher, J. T., Mutchler, S. M., . . . Isakson, B. E. (2015). A molecular signature in the pannexin1 intracellular loop confers channel activation by the alpha1 adrenoreceptor in smooth muscle cells. *Sci Signal*, *8*(364), ra17. doi:10.1126/scisignal.2005824
- Billaud, M., Lohman, A. W., Straub, A. C., Looft-Wilson, R., Johnstone, S. R., Araj, C. A., . . . Isakson, B. E. (2011). Pannexin1 regulates alpha1-adrenergic receptor- mediated

- vasoconstriction. *Circ Res*, 109(1), 80-85.
doi:10.1161/CIRCRESAHA.110.237594
- Boassa, D., Ambrosi, C., Qiu, F., Dahl, G., Gaietta, G., & Sosinsky, G. (2007). Pannexin1 channels contain a glycosylation site that targets the hexamer to the plasma membrane. *J Biol Chem*, 282(43), 31733-31743. doi:10.1074/jbc.M702422200
- Boassa, D., Qiu, F., Dahl, G., & Sosinsky, G. (2008). Trafficking dynamics of glycosylated pannexin 1 proteins. *Cell Commun Adhes*, 15(1), 119-132. doi:10.1080/15419060802013885
- Boyd-Tressler, A., Penuela, S., Laird, D. W., & Dubyak, G. R. (2014). Chemotherapeutic drugs induce ATP release via caspase-gated pannexin-1 channels and a caspase/pannexin-1-independent mechanism. *J Biol Chem*, 289(39), 27246-27263. doi:10.1074/jbc.M114.590240
- Bravo, D., Ibarra, P., Retamal, J., Pelissier, T., Laurido, C., Hernandez, A., & Constandil, L. (2014). Pannexin 1: a novel participant in neuropathic pain signaling in the rat spinal cord. *Pain*, 155(10), 2108-2115. doi:10.1016/j.pain.2014.07.024
- Chekeni, F. B., Elliott, M. R., Sandilos, J. K., Walk, S. F., Kinchen, J. M., Lazarowski, E. R., . . . Ravichandran, K. S. (2010). Pannexin 1 channels mediate 'find-me' signal release and membrane permeability during apoptosis. *Nature*, 467(7317), 863-867. doi:10.1038/nature09413
- Chiu, Y. H., Jin, X., Medina, C. B., Leonhardt, S. A., Kiessling, V., Bennett, B. C., . . . Bayliss, D. A. (2017). A quantized mechanism for activation of pannexin channels. *Nat Commun*, 8, 14324. doi:10.1038/ncomms14324
- Chiu, Y. H., Ravichandran, K. S., & Bayliss, D. A. (2014). Intrinsic properties and regulation of Pannexin 1 channel. *Channels (Austin)*, 8(2), 103-109. doi:10.4161/chan.27545
- Chiu, Y. H., Schappe, M. S., Desai, B. N., & Bayliss, D. A. (2018). Revisiting multimodal activation and channel properties of Pannexin 1. *J Gen Physiol*, 150(1), 19-39. doi:10.1085/jgp.201711888
- Choi, W., Clemente, N., Sun, W., Du, J., & Lu, W. (2019). The structures and gating mechanism of human calcium homeostasis modulator 2. *Nature*, 576(7785), 163-167. doi:10.1038/s41586-019-1781-3
- Cotrina, M. L., Lin, J. H., Alves-Rodrigues, A., Liu, S., Li, J., Azmi-Ghadimi, H., . . . Nedergaard, M. (1998). Connexins regulate calcium signaling by controlling ATP release. *Proc Natl Acad Sci U S A*, 95(26), 15735-15740. doi:10.1073/pnas.95.26.15735

- Crespo Yanguas, S., Willebrords, J., Johnstone, S. R., Maes, M., Decrock, E., De Bock, M., . . . Vinken, M. (2017). Pannexin1 as mediator of inflammation and cell death. *Biochim Biophys Acta Mol Cell Res*, 1864(1), 51-61. doi:10.1016/j.bbamcr.2016.10.006
- Dahl, G. (2018). The Pannexin1 membrane channel: distinct conformations and functions. *FEBS Lett*, 592(19), 3201-3209. doi:10.1002/1873-3468.13115
- DeLalio, L. J., Billaud, M., Ruddiman, C. A., Johnstone, S. R., Butcher, J. T., Wolpe, A. G., . . . Isakson, B. E. (2019). Constitutive SRC-mediated phosphorylation of pannexin 1 at tyrosine 198 occurs at the plasma membrane. *J Biol Chem*, 294(17), 6940-6956. doi:10.1074/jbc.RA118.006982
- DeLalio, L. J., Keller, A. S., Chen, J., Boyce, A. K. J., Artamonov, M. V., Askew-Page, H. R., . . . Isakson, B. E. (2018). Interaction Between Pannexin 1 and Caveolin-1 in Smooth Muscle Can Regulate Blood Pressure. *Arterioscler Thromb Vasc Biol*, 38(9), 2065-2078. doi:10.1161/ATVBAHA.118.311290
- DeLalio, L. J., Masati, E., Mendu, S., Ruddiman, C. A., Yang, Y., Johnstone, S. R., . . . Isakson, B. E. (2020). Pannexin 1 channels in renin-expressing cells influence renin secretion and blood pressure homeostasis. *Kidney Int*, 98(3), 630-644. doi:10.1016/j.kint.2020.04.041
- Demura, K., Kusakizako, T., Shihoya, W., Hiraizumi, M., Nomura, K., Shimada, H., . . . Nureki, O. (2020). Cryo-EM structures of calcium homeostasis modulator channels in diverse oligomeric assemblies. *Sci Adv*, 6(29), eaba8105. doi:10.1126/sciadv.aba8105
- Deneka, D., Sawicka, M., Lam, A. K. M., Paulino, C., & Dutzler, R. (2018). Structure of a volume-regulated anion channel of the LRRC8 family. *Nature*, 558(7709), 254-259. doi:10.1038/s41586-018-0134-y
- Deng, Z., He, Z., Maksaev, G., Bitter, R. M., Rau, M., Fitzpatrick, J. A. J., & Yuan, P. (2020). Cryo-EM structures of the ATP release channel pannexin 1. *Nat Struct Mol Biol*, 27(4), 373-381. doi:10.1038/s41594-020-0401-0
- Di Cesare Mannelli, L., Maresca, M., Farina, C., Scherz, M. W., & Ghelardini, C. (2015). A model of neuropathic pain induced by sorafenib in the rat: Effect of dimiracetam. *Neurotoxicology*, 50, 101-107. doi:10.1016/j.neuro.2015.08.002
- Dolmatova, E., Spagnol, G., Boassa, D., Baum, J. R., Keith, K., Ambrosi, C., . . . Duffy, H. S. (2012). Cardiomyocyte ATP release through pannexin 1 aids in early fibroblast activation. *Am J*

- Physiol Heart Circ Physiol*, 303(10), H1208-1218.
doi:10.1152/ajpheart.00251.2012
- Dosch, M., Zindel, J., Jebbawi, F., Melin, N., Sanchez-Taltavull, D., Stroka, D., . . . Beldi, G. (2019). Connexin-43-dependent ATP release mediates macrophage activation during sepsis. *Elife*, 8. doi:10.7554/eLife.42670
- Dossi, E., Blauwblomme, T., Moulard, J., Chever, O., Vasile, F., Guinard, E., . . . Rouach, N. (2018). Pannexin-1 channels contribute to seizure generation in human epileptic brain tissue and in a mouse model of epilepsy. *Sci Transl Med*, 10(443). doi:10.1126/scitranslmed.aar3796
- Dreses-Werringloer, U., Lambert, J. C., Vingtdoux, V., Zhao, H., Vais, H., Siebert, A., . . . Marambaud, P. (2008). A polymorphism in CALHM1 influences Ca²⁺ homeostasis, Abeta levels, and Alzheimer's disease risk. *Cell*, 133(7), 1149-1161. doi:10.1016/j.cell.2008.05.048
- Elliott, M. R., Chekeni, F. B., Trampont, P. C., Lazarowski, E. R., Kadl, A., Walk, S. F., . . . Ravichandran, K. S. (2009). Nucleotides released by apoptotic cells act as a find-me signal to promote phagocytic clearance. *Nature*, 461(7261), 282-286. doi:10.1038/nature08296
- Freitas-Andrade, M., Bechberger, J. F., MacVicar, B. A., Viau, V., & Naus, C. C. (2017). Pannexin1 knockout and blockade reduces ischemic stroke injury in female, but not in male mice. *oncotarget*, 8(23), 36973-36983. doi:10.18632/oncotarget.16937
- Good, M. E., Chiu, Y. H., Poon, I. K. H., Medina, C. B., Butcher, J. T., Mendu, S. K., . . . Ravichandran, K. S. (2018). Pannexin 1 Channels as an Unexpected New Target of the Anti-Hypertensive Drug Spironolactone. *Circ Res*, 122(4), 606-615. doi:10.1161/CIRCRESAHA.117.312380
- Good, M. E., Eucker, S. A., Li, J., Bacon, H. M., Lang, S. M., Butcher, J. T., . . . Isakson, B. E. (2018). Endothelial cell Pannexin1 modulates severity of ischemic stroke by regulating cerebral inflammation and myogenic tone. *JCI Insight*, 3(6). doi:10.1172/jci.insight.96272
- Hansen, D. B., Ye, Z. C., Calloe, K., Braunstein, T. H., Hofgaard, J. P., Ransom, B. R., . . . MacAulay, N. (2014). Activation, permeability, and inhibition of astrocytic and neuronal large pore (hemi)channels. *J Biol Chem*, 289(38), 26058-26073. doi:10.1074/jbc.M114.582155
- Imamura, H., Sakamoto, S., Yoshida, T., Matsui, Y., Penuela, S., Laird, D. W., . . . Kakizuka, A. (2020). Single-cell dynamics of

- pannexin-1-facilitated programmed ATP loss during apoptosis. *Elife*, 9. doi:10.7554/eLife.61960
- Ishikawa, M., Williams, G., Forcinito, P., Ishikawa, M., Petrie, R. J., Saito, K., . . . Yamada, Y. (2019). Pannexin 3 ER Ca(2+) channel gating is regulated by phosphorylation at the Serine 68 residue in osteoblast differentiation. *Sci Rep*, 9(1), 18759. doi:10.1038/s41598-019-55371-9
- Israelachvili, J. (2011). *Intermolecular and Surface Forces*.
- Jankowski, J., Perry, H. M., Medina, C. B., Huang, L., Yao, J., Bajwa, A., . . . Okusa, M. D. (2018). Epithelial and Endothelial Pannexin1 Channels Mediate AKI. *J Am Soc Nephrol*, 29(7), 1887-1899. doi:10.1681/ASN.2017121306
- Jin, Q., Zhang, B., Zheng, X., Li, N., Xu, L., Xie, Y., . . . Ye, S. (2020). Cryo-EM structures of human pannexin 1 channel. *Cell Res*, 30(5), 449-451. doi:10.1038/s41422-020-0310-0
- Karasawa, A., Michalski, K., Mikhelzon, P., & Kawate, T. (2017). The P2X7 receptor forms a dye-permeable pore independent of its intracellular domain but dependent on membrane lipid composition. *Elife*, 6. doi:10.7554/eLife.31186
- Kasuya, G., Nakane, T., Yokoyama, T., Jia, Y., Inoue, M., Watanabe, K., . . . Nureki, O. (2018). Cryo-EM structures of the human volume-regulated anion channel LRRC8. *Nat Struct Mol Biol*, 25(9), 797-804. doi:10.1038/s41594-018-0109-6
- Kefauver, J. M., Saotome, K., Dubin, A. E., Pallesen, J., Cottrell, C. A., Cahalan, S. M., . . . Patapoutian, A. (2018). Structure of the human volume regulated anion channel. *Elife*, 7. doi:10.7554/eLife.38461
- Kienitz, M. C., Bender, K., Dermietzel, R., Pott, L., & Zoidl, G. (2011). Pannexin 1 constitutes the large conductance cation channel of cardiac myocytes. *J Biol Chem*, 286(1), 290-298. doi:10.1074/jbc.M110.163477
- Koyanagi, S., Kusunose, N., Taniguchi, M., Akamine, T., Kanado, Y., Ozono, Y., . . . Ohdo, S. (2016). Glucocorticoid regulation of ATP release from spinal astrocytes underlies diurnal exacerbation of neuropathic mechanical allodynia. *Nat Commun*, 7, 13102. doi:10.1038/ncomms13102
- Lemaire, I., Falzoni, S., Zhang, B., Pellegatti, P., & Di Virgilio, F. (2011). The P2X7 receptor and Pannexin-1 are both required for the promotion of multinucleated macrophages by the inflammatory cytokine GM-CSF. *J Immunol*, 187(7), 3878-3887. doi:10.4049/jimmunol.1002780

- Liao, J. C., Sun, S., Chandler, D., & Oster, G. (2004). The conformational states of Mg.ATP in water. *Eur Biophys J*, 33(1), 29-37. doi:10.1007/s00249-003-0339-2
- Locovei, S., Wang, J., & Dahl, G. (2006). Activation of pannexin 1 channels by ATP through P2Y receptors and by cytoplasmic calcium. *FEBS Lett*, 580(1), 239-244. doi:10.1016/j.febslet.2005.12.004
- Lohman, A. W., Leskov, I. L., Butcher, J. T., Johnstone, S. R., Stokes, T. A., Begandt, D., . . . Isakson, B. E. (2015). Pannexin 1 channels regulate leukocyte emigration through the venous endothelium during acute inflammation. *Nat Commun*, 6, 7965. doi:10.1038/ncomms8965
- Lutter, D., Ullrich, F., Lueck, J. C., Kempa, S., & Jentsch, T. J. (2017). Selective transport of neurotransmitters and modulators by distinct volume-regulated LRRC8 anion channels. *J Cell Sci*, 130(6), 1122-1133. doi:10.1242/jcs.196253
- Ma, J., Qi, X., Yang, C., Pan, R., Wang, S., Wu, J., . . . Yuan, Z. (2018). Calhm2 governs astrocytic ATP releasing in the development of depression-like behaviors. *Mol Psychiatry*, 23(4), 883-891. doi:10.1038/mp.2017.229
- Ma, W., Compan, V., Zheng, W., Martin, E., North, R. A., Verkhatsky, A., & Surprenant, A. (2012). Pannexin 1 forms an anion-selective channel. *Pflugers Arch*, 463(4), 585-592. doi:10.1007/s00424-012-1077-z
- Medina, C. B., Mehrotra, P., Arandjelovic, S., Perry, J. S. A., Guo, Y., Morioka, S., . . . Ravichandran, K. S. (2020). Metabolites released from apoptotic cells act as tissue messengers. *Nature*, 580(7801), 130-135. doi:10.1038/s41586-020-2121-3
- Michalski, K., & Kawate, T. (2016). Carbenoxolone inhibits Pannexin1 channels through interactions in the first extracellular loop. *J Gen Physiol*, 147(2), 165-174. doi:10.1085/jgp.201511505
- Michalski, K., Syrjanen, J. L., Henze, E., Kumpf, J., Furukawa, H., & Kawate, T. (2020). The Cryo-EM structure of pannexin 1 reveals unique motifs for ion selection and inhibition. *Elife*, 9. doi:10.7554/eLife.54670
- Mou, L., Ke, M., Song, M., Shan, Y., Xiao, Q., Liu, Q., . . . Deng, D. (2020). Structural basis for gating mechanism of Pannexin 1 channel. *Cell Res*, 30(5), 452-454. doi:10.1038/s41422-020-0313-x
- Nielsen, B. S., Toft-Bertelsen, T. L., Lolansen, S. D., Anderson, C. L., Nielsen, M. S., Thompson, R. J., & MacAulay, N. (2020). Pannexin 1 activation and inhibition is permeant-selective. *J Physiol*, 598(2), 361-379. doi:10.1113/JP278759

- Nimigean, C. M. (2006). A radioactive uptake assay to measure ion transport across ion channel-containing liposomes. *Nat Protoc*, *1*(3), 1207-1212. doi:10.1038/nprot.2006.166
- Nomura, T., Taruno, A., Shiraishi, M., Nakahari, T., Inui, T., Sokabe, M., . . . Marunaka, Y. (2017). Current-direction/amplitude-dependent single channel gating kinetics of mouse pannexin 1 channel: a new concept for gating kinetics. *Sci Rep*, *7*(1), 10512. doi:10.1038/s41598-017-10921-x
- Nyberg, M., Piil, P., Kiehn, O. T., Maagaard, C., Jorgensen, T. S., Egelund, J., . . . Hellsten, Y. (2018). Probenecid Inhibits alpha-Adrenergic Receptor-Mediated Vasoconstriction in the Human Leg Vasculature. *Hypertension*, *71*(1), 151-159. doi:10.1161/HYPERTENSIONAHA.117.10251
- Panchin, Y., Kelmanson, I., Matz, M., Lukyanov, K., Usman, N., & Lukyanov, S. (2000). A ubiquitous family of putative gap junction molecules. *Curr Biol*, *10*(13), R473-474. doi:10.1016/s0960-9822(00)00576-5
- Pelegri, P., & Surprenant, A. (2006). Pannexin-1 mediates large pore formation and interleukin-1beta release by the ATP-gated P2X7 receptor. *EMBO J*, *25*(21), 5071-5082. doi:10.1038/sj.emboj.7601378
- Penuela, S., Bhalla, R., Gong, X. Q., Cowan, K. N., Celetti, S. J., Cowan, B. J., . . . Laird, D. W. (2007). Pannexin 1 and pannexin 3 are glycoproteins that exhibit many distinct characteristics from the connexin family of gap junction proteins. *J Cell Sci*, *120*(Pt 21), 3772-3783. doi:10.1242/jcs.009514
- Penuela, S., Bhalla, R., Nag, K., & Laird, D. W. (2009). Glycosylation regulates pannexin intermixing and cellular localization. *Mol Biol Cell*, *20*(20), 4313-4323. doi:10.1091/mbc.E09-01-0067
- Penuela, S., Gehi, R., & Laird, D. W. (2013). The biochemistry and function of pannexin channels. *Biochim Biophys Acta*, *1828*(1), 15-22. doi:10.1016/j.bbamem.2012.01.017
- Poon, I. K., Chiu, Y. H., Armstrong, A. J., Kinchen, J. M., Juncadella, I. J., Bayliss, D. A., & Ravichandran, K. S. (2014). Unexpected link between an antibiotic, pannexin channels and apoptosis. *Nature*, *507*(7492), 329-334. doi:10.1038/nature13147
- Qiu, F., Wang, J., Spray, D. C., Scemes, E., & Dahl, G. (2011). Two non-vesicular ATP release pathways in the mouse erythrocyte membrane. *FEBS Lett*, *585*(21), 3430-3435. doi:10.1016/j.febslet.2011.09.033
- Qiu, Z., Dubin, A. E., Mathur, J., Tu, B., Reddy, K., Miraglia, L. J., . . . Patapoutian, A. (2014). SWELL1, a plasma membrane protein, is

- an essential component of volume-regulated anion channel. *Cell*, 157(2), 447-458. doi:10.1016/j.cell.2014.03.024
- Qu, R., Dong, L., Zhang, J., Yu, X., Wang, L., & Zhu, S. (2020). Cryo-EM structure of human heptameric Pannexin 1 channel. *Cell Res*, 30(5), 446-448. doi:10.1038/s41422-020-0298-5
- Qu, Y., Misaghi, S., Newton, K., Gilmour, L. L., Louie, S., Cupp, J. E., . . . Dixit, V. M. (2011). Pannexin-1 is required for ATP release during apoptosis but not for inflammasome activation. *J Immunol*, 186(11), 6553-6561. doi:10.4049/jimmunol.1100478
- Romanov, R. A., Bystrova, M. F., Rogachevskaya, O. A., Sadovnikov, V. B., Shestopalov, V. I., & Kolesnikov, S. S. (2012). The ATP permeability of pannexin 1 channels in a heterologous system and in mammalian taste cells is dispensable. *J Cell Sci*, 125(Pt 22), 5514-5523. doi:10.1242/jcs.111062
- Ruan, Z., Orozco, I. J., Du, J., & Lu, W. (2020). Structures of human pannexin 1 reveal ion pathways and mechanism of gating. *Nature*, 584(7822), 646-651. doi:10.1038/s41586-020-2357-y
- Saez, P. J., Vargas, P., Shoji, K. F., Harcha, P. A., Lennon-Dumenil, A. M., & Saez, J. C. (2017). ATP promotes the fast migration of dendritic cells through the activity of pannexin 1 channels and P2X7 receptors. *Sci Signal*, 10(506). doi:10.1126/scisignal.aah7107
- Sahu, G., Sukumaran, S., & Bera, A. K. (2014). Pannexins form gap junctions with electrophysiological and pharmacological properties distinct from connexins. *Sci Rep*, 4, 4955. doi:10.1038/srep04955
- Sandilos, J. K., Chiu, Y. H., Chekeni, F. B., Armstrong, A. J., Walk, S. F., Ravichandran, K. S., & Bayliss, D. A. (2012). Pannexin 1, an ATP release channel, is activated by caspase cleavage of its pore-associated C-terminal autoinhibitory region. *J Biol Chem*, 287(14), 11303-11311. doi:10.1074/jbc.M111.323378
- Sang, Q., Zhang, Z., Shi, J., Sun, X., Li, B., Yan, Z., . . . Wang, L. (2019). A pannexin 1 channelopathy causes human oocyte death. *Sci Transl Med*, 11(485). doi:10.1126/scitranslmed.aav8731
- Santiago, M. F., Veliskova, J., Patel, N. K., Lutz, S. E., Caille, D., Charollais, A., . . . Scemes, E. (2011). Targeting pannexin1 improves seizure outcome. *PLoS One*, 6(9), e25178. doi:10.1371/journal.pone.0025178
- Schenk, U., Westendorf, A. M., Radaelli, E., Casati, A., Ferro, M., Fumagalli, M., . . . Grassi, F. (2008). Purinergic control of T cell activation by ATP released through pannexin-1 hemichannels. *Sci Signal*, 1(39), ra6. doi:10.1126/scisignal.1160583

- Seminario-Vidal, L., Okada, S. F., Sesma, J. I., Kreda, S. M., van Heusden, C. A., Zhu, Y., . . . Lazarowski, E. R. (2011). Rho signaling regulates pannexin 1-mediated ATP release from airway epithelia. *J Biol Chem*, *286*(30), 26277-26286. doi:10.1074/jbc.M111.260562
- Sharma, A. K., Charles, E. J., Zhao, Y., Narahari, A. K., Baderdinni, P. K., Good, M. E., . . . Laubach, V. E. (2018). Pannexin-1 channels on endothelial cells mediate vascular inflammation during lung ischemia-reperfusion injury. *Am J Physiol Lung Cell Mol Physiol*, *315*(2), L301-L312. doi:10.1152/ajplung.00004.2018
- Siebert, A. P., Ma, Z., Grevet, J. D., Demuro, A., Parker, I., & Foskett, J. K. (2013). Structural and functional similarities of calcium homeostasis modulator 1 (CALHM1) ion channel with connexins, pannexins, and innexins. *J Biol Chem*, *288*(9), 6140-6153. doi:10.1074/jbc.M112.409789
- Silverman, W. R., de Rivero Vaccari, J. P., Locovei, S., Qiu, F., Carlsson, S. K., Scemes, E., . . . Dahl, G. (2009). The pannexin 1 channel activates the inflammasome in neurons and astrocytes. *J Biol Chem*, *284*(27), 18143-18151. doi:10.1074/jbc.M109.004804
- Sosinsky, G. E., Boassa, D., Dermietzel, R., Duffy, H. S., Laird, D. W., MacVicar, B., . . . Dahl, G. (2011). Pannexin channels are not gap junction hemichannels. *Channels (Austin)*, *5*(3), 193-197. doi:10.4161/chan.5.3.15765
- Su, L., Jiang, X., Yang, C., Zhang, J., Chen, B., Li, Y., . . . Peng, Z. (2019). Pannexin 1 mediates ferroptosis that contributes to renal ischemia/reperfusion injury. *J Biol Chem*, *294*(50), 19395-19404. doi:10.1074/jbc.RA119.010949
- Suadicani, S. O., Iglesias, R., Wang, J., Dahl, G., Spray, D. C., & Scemes, E. (2012). ATP signaling is deficient in cultured Pannexin1-null mouse astrocytes. *Glia*, *60*(7), 1106-1116. doi:10.1002/glia.22338
- Syrjanen, J. L., Michalski, K., Chou, T. H., Grant, T., Rao, S., Simorowski, N., . . . Furukawa, H. (2020). Structure and assembly of calcium homeostasis modulator proteins. *Nat Struct Mol Biol*, *27*(2), 150-159. doi:10.1038/s41594-019-0369-9
- Taruno, A. (2018). ATP Release Channels. *Int J Mol Sci*, *19*(3). doi:10.3390/ijms19030808
- Taruno, A., Matsumoto, I., Ma, Z., Marambaud, P., & Foskett, J. K. (2013). How do taste cells lacking synapses mediate neurotransmission? CALHM1, a voltage-gated ATP channel. *Bioessays*, *35*(12), 1111-1118. doi:10.1002/bies.201300077

- Taruno, A., Vingtdoux, V., Ohmoto, M., Ma, Z., Dvoryanchikov, G., Li, A., . . . Foskett, J. K. (2013). CALHM1 ion channel mediates purinergic neurotransmission of sweet, bitter and umami tastes. *Nature*, *495*(7440), 223-226. doi:10.1038/nature11906
- Thompson, R. J., Jackson, M. F., Olah, M. E., Rungta, R. L., Hines, D. J., Beazely, M. A., . . . MacVicar, B. A. (2008). Activation of pannexin-1 hemichannels augments aberrant bursting in the hippocampus. *Science*, *322*(5907), 1555-1559. doi:10.1126/science.1165209
- Voss, F. K., Ullrich, F., Munch, J., Lazarow, K., Lutter, D., Mah, N., . . . Jentsch, T. J. (2014). Identification of LRRC8 Heteromers as an Essential Component of the Volume-Regulated Anion Channel VRAC. *Science*, *344*(6184), 634-638. doi:10.1126/science.1252826
- Wang, J., Ambrosi, C., Qiu, F., Jackson, D. G., Sosinsky, G., & Dahl, G. (2014). The membrane protein Pannexin1 forms two open-channel conformations depending on the mode of activation. *Sci Signal*, *7*(335), ra69. doi:10.1126/scisignal.2005431
- Wang, J., & Dahl, G. (2018). Pannexin1: a multifunction and multiconductance and/or permeability membrane channel. *Am J Physiol Cell Physiol*, *315*(3), C290-C299. doi:10.1152/ajpcell.00302.2017
- Wang, J., Ma, M., Locovei, S., Keane, R. W., & Dahl, G. (2007). Modulation of membrane channel currents by gap junction protein mimetic peptides: size matters. *Am J Physiol Cell Physiol*, *293*(3), C1112-1119. doi:10.1152/ajpcell.00097.2007
- Wang, S., Chennupati, R., Kaur, H., Iring, A., Wettschureck, N., & Offermanns, S. (2016). Endothelial cation channel PIEZO1 controls blood pressure by mediating flow-induced ATP release. *J Clin Invest*, *126*(12), 4527-4536. doi:10.1172/JCI87343
- Wang, W., Qu, R., Dou, Q., Wu, F., Wang, W., Chen, B., . . . Sang, Q. (2021). Homozygous variants in PANX1 cause human oocyte death and female infertility. *Eur J Hum Genet*. doi:10.1038/s41431-020-00807-4
- Weaver, J. L., Arandjelovic, S., Brown, G., S, K. M., M, S. S., Buckley, M. W., . . . Bayliss, D. A. (2017). Hematopoietic pannexin 1 function is critical for neuropathic pain. *Sci Rep*, *7*, 42550. doi:10.1038/srep42550
- Wei, R., Bao, W., He, F., Meng, F., Liang, H., & Luo, B. (2020). Pannexin1 Channel Inhibitor ((10)panx) Protects Against Transient Focal Cerebral Ischemic Injury by Inhibiting RIP3 Expression and Inflammatory Response in Rats. *Neuroscience*, *437*, 23-33. doi:10.1016/j.neuroscience.2020.02.042

- Weilinger, N. L., Lohman, A. W., Rakai, B. D., Ma, E. M., Bialecki, J., Maslieieva, V., . . . Thompson, R. J. (2016). Metabotropic NMDA receptor signaling couples Src family kinases to pannexin-1 during excitotoxicity. *Nat Neurosci*, *19*(3), 432-442. doi:10.1038/nn.4236
- Wicki-Stordeur, L. E., Sanchez-Arias, J. C., Dhaliwal, J., Carmona-Wagner, E. O., Shestopalov, V. I., Lagace, D. C., & Swayne, L. A. (2016). Pannexin 1 Differentially Affects Neural Precursor Cell Maintenance in the Ventricular Zone and Peri-Infarct Cortex. *J Neurosci*, *36*(4), 1203-1210. doi:10.1523/JNEUROSCI.0436-15.2016
- Yang, D., He, Y., Munoz-Planillo, R., Liu, Q., & Nunez, G. (2015). Caspase-11 Requires the Pannexin-1 Channel and the Purinergic P2X7 Pore to Mediate Pyroptosis and Endotoxic Shock. *Immunity*, *43*(5), 923-932. doi:10.1016/j.immuni.2015.10.009
- Yang, Y., Delalio, L. J., Best, A. K., Macal, E., Milstein, J., Donnelly, I., . . . Johnstone, S. R. (2020). Endothelial Pannexin 1 Channels Control Inflammation by Regulating Intracellular Calcium. *J Immunol*, *204*(11), 2995-3007. doi:10.4049/jimmunol.1901089
- Zhang, Y., Laumet, G., Chen, S. R., Hittelman, W. N., & Pan, H. L. (2015). Pannexin-1 Up-regulation in the Dorsal Root Ganglion Contributes to Neuropathic Pain Development. *J Biol Chem*, *290*(23), 14647-14655. doi:10.1074/jbc.M115.650218
- Zhang, Y., Zhu, D., Wang, J., Yang, L., Wang, L., & Wang, Y. (2017). Expression of pannexin-1 in the trigeminal ganglion after chronic constriction injury of the infraorbital nerve in a rat model. *Neuroreport*. doi:10.1097/WNR.0000000000000958

CHAPTER 2

ATP and large signaling metabolites flux through caspase-activated Pannexin 1 channels

The chapter is modified from the following publication:

Adishesh K. Narahari, Alex J.B. Kreutzberger, Pablo S. Gaete, Yu-Hsin Chiu, Susan A. Leonhardt, Christopher B. Medina, Xueyao Jin, Patrycja W. Oleniacz, Volker Kiessling, Paula Q. Barrett, Kodi S. Ravichandran, Mark Yeager, Jorge E. Contreras, Lukas K. Tamm, Douglas A. Bayliss. (2021). ATP and large signaling metabolites flux through caspase-activated Pannexin 1 channels. *ELife*. [PMID: 33410749]

Please note: I performed protein purification, proteoliposome reconstitution, dye/metabolite assays with assistance from Alex Kreutzberger (Tamm Lab at UVA) on TIRF assays, and ImageStream flow cytometry with help from Christopher Medina (Ravichandran Lab, UVA). Susan Leonhardt performed negative stain EM and developed the Panx1 purification protocol with Xueyao Jin. Planar lipid bilayer recordings were performed by Pablo Gaete (Contreras Lab at NJMS). Whole-cell electrophysiology and single-channel recordings from HEK293T cells were performed by Yu-Hsin Chiu (Bayliss Lab at UVA, now independent PI).

Abstract

Pannexin 1 (Panx1) is a membrane channel implicated in numerous physiological and pathophysiological processes via its ability to support release of ATP and other cellular metabolites for local intercellular signaling. However, to date, there has been no direct demonstration of large molecule permeation via the Panx1 channel itself, and thus the permselectivity of Panx1 for different molecules remains unknown. To address this, we expressed, purified and reconstituted Panx1 into proteoliposomes and demonstrated that channel activation by caspase

cleavage yields a dye-permeable pore that favors flux of anionic, large-molecule permeants (up to ~1 kDa). Large cationic molecules can also permeate the channel, albeit at a much lower rate. We further show that Panx1 channels provide a molecular pathway for flux of ATP and other anionic (glutamate) and cationic signaling metabolites (spermidine). These results verify large molecule permeation directly through activated Panx1 channels that can support their many physiological roles.

Introduction

Pannexin 1 (Panx1) is a widely-expressed homo-heptameric membrane channel that plays a critical role in numerous physiological and pathophysiological processes. Among others, this includes cell clearance after apoptosis (Chekeni et al., 2010; Medina et al., 2020; Poon et al., 2014), blood pressure regulation (Billaud et al., 2011; Good, Chiu, et al., 2018), stroke (Bargiotas et al., 2011; Good, Eucker, et al., 2018; Thompson, 2015), and neuropathic pain (Bravo et al., 2014; Weaver et al., 2017; Zhang, Laumet, Chen, Hittelman, & Pan, 2015). Individual Panx1 subunits consist of a four-transmembrane α -helical bundle with a cytoplasmic loop between TM2 and TM3; the N- and C-termini also reside on the cytoplasmic surface (Baranova et al., 2004; Penuela, Gehi, & Laird, 2013). These channels

are broadly similar to a subset of mammalian large-pore ion channels that include connexin gap junctions (Panchin et al., 2000), calcium homeostasis modulator 1 (CALHM1) (Siebert et al., 2013; Syrjanen et al., 2020) and SWELL1 (LRRC8) (Abascal & Zardoya, 2012; Deneka, Sawicka, Lam, Paulino, & Dutzler, 2018). Despite a conserved subunit topology, recent cryoEM structures revealed that these different channels exist in a variety of oligomeric states (from hexameric to undecameric) (Deng et al., 2020; Michalski et al., 2020). Of interest here, activation of these channels has been associated with both ionic current and large molecule permeation. In particular, channel activation is associated with release of metabolites (often ATP) that are critical for their roles in intercellular signaling (Bao, Locovei, & Dahl, 2004; Chekeni et al., 2010; Lutter, Ullrich, Lueck, Kempa, & Jentsch, 2017; Medina et al., 2020; Siebert et al., 2013; Taruno, 2018).

In the two decades since their discovery, much has been learned about the functional properties of Panx1 channels. Panx1 ionic currents have occasionally been detected under unstimulated conditions (Ma et al., 2012; Romanov et al., 2012; Ruan, Orozco, Du, & Lu, 2020), but that basal activity does not appear to be associated with large molecule permeation (Romanov et al., 2012). By contrast, transmembrane permeation of large fluorescent dyes and ATP occurs when Panx1 is

activated by various mechanisms (e.g., stretch, elevated external K^+ , ionotropic and metabotropic receptor signaling, and caspase-mediated cleavage at a C-terminal site) (Beckel et al., 2015; Chekeni et al., 2010; Chiu et al., 2017; Iglesias et al., 2008; Silverman et al., 2009; Weilinger et al., 2016). Among these, caspase-mediated activation is a well characterized mechanism in which cleavage of the channel C-tails, as occurs during apoptosis or pyroptosis, is accompanied by uptake of dyes indicative of cell death (e.g., Yo-Pro-1, To-Pro-3) and release of ATP and UTP that serve as “find-me” signals to direct phagocytic clearance of cell corpses (Chekeni et al., 2010; Chiu et al., 2017; Poon et al., 2014; Y. Qu et al., 2011; Yang, He, Munoz-Planillo, Liu, & Nunez, 2015). Moreover, Panx1 cleavage elicits efflux of additional metabolites from apoptotic cells, which function as local “good-bye” signals with anti-inflammatory, wound healing, and cell proliferative actions (Medina et al., 2020). Notably, all studies to date have been performed using intact cells. Therefore, this previous work does not demonstrate that large molecule permeation occurs directly via the channel itself or exclude a secondary release mechanism. Moreover, recently-available Panx1 channel structures from both intact (inactive) and caspase-cleaved (activated) channels reveal a central pore with an extracellular constriction that has a diameter of $\sim 9 \text{ \AA}$, which would appear to be too small to enable large molecule permeation (Deng et

al., 2020; Jin et al., 2020; Michalski et al., 2020; Mou et al., 2020; R. Qu et al., 2020; Ruan et al., 2020). Thus, the ability of caspase-activated Panx1 to support metabolite release remains uncertain.

In this study, we developed a proteoliposome system for reconstitution of purified Panx1 and channel activation by caspase-mediated cleavage. By combining lipid bilayer electrophysiology, flow cytometry, total internal reflection fluorescence (TIRF) microscopy, and radioactive metabolite uptake assays, we characterized the large molecule permeation properties of cleavage-activated Panx1. We determined that the caspase-activated Panx1 channel forms a permeation pathway that favors anionic over cationic molecules, and supports flux of ATP and other important signaling metabolites, such as glutamate and spermidine.

Results

For these studies, we used the Panx1 ortholog from *Xenopus tropicalis* (i.e. frog Panx1, fPanx1) that has been examined in recent structural studies (Deng et al., 2020; Michalski et al., 2020).

Preparation of Pannexin 1 Proteoliposomes

An fPanx1-eGFP fusion construct, containing a thrombin cleavage site and a Strep-tag®, was inserted into pFastBac for expression in Sf9 cells (**Figure 2.1 A**) and purified by affinity chromatography and size-exclusion chromatography (SEC) (**Figure 2.1 B,C**). Purified fPanx1-eGFP was incorporated into proteoliposomes that appeared in fractions 1-3 of a co-floatation assay on a Nycodenz density gradient (**Figure 2.2 A,B**) (Hernandez et al., 2012). When analyzed by negative-stain electron microscopy, we observed a normal distribution of circular proteoliposomes in projection images, with the expected mean diameter of 97.3 ± 22 nm (**Figure 2.2 C,D**). Panx1 cleavage by caspases is a prominent mechanism for channel activation. Therefore, we verified that purified fPanx1 incorporated into proteoliposomes was cleaved at the expected sites following overnight incubation with recombinant Caspase 3 (Casp3) (**Figure 2.3**). Note that although the channel can be cleaved at multiple sites, cleavage at the C-terminal

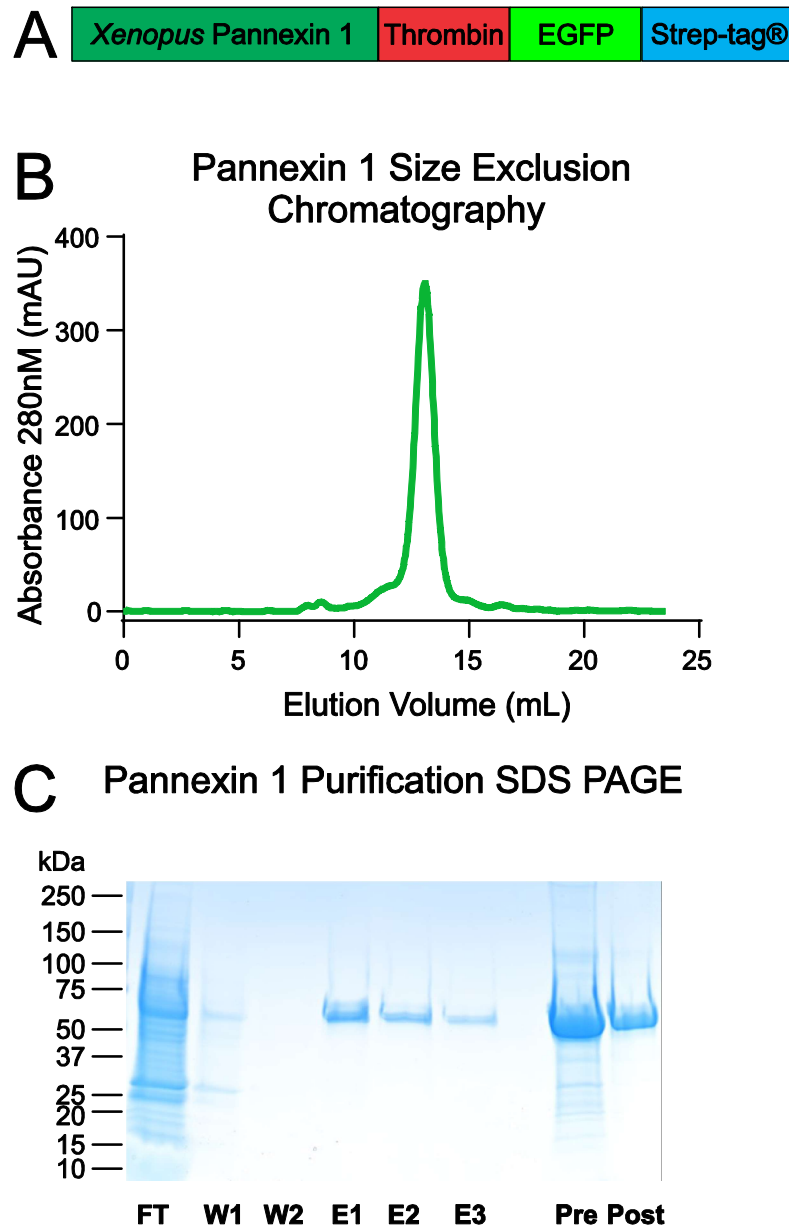


Figure 2.1 Pannexin 1-eGFP construct and reconstitution

A) Schematic of recombinant *Xenopus* Panx1 (fPanx1) construct incorporating a thrombin cleavage site, eGFP, and a Strep-Tag®. **B)** Size-exclusion chromatogram showing the purification of fPanx1-eGFP. **C)** Simply Blue-stained SDS-PAGE gel showing samples taken during the purification process: flow through after gravity flow chromatography (FT), low salt wash (W1), high salt wash (W2), desthiobiotin elution fractions (e1, e2, e3), blank, concentrated sample before size-exclusion chromatography (Pre), and concentrated sample after size-exclusion chromatography (Post).

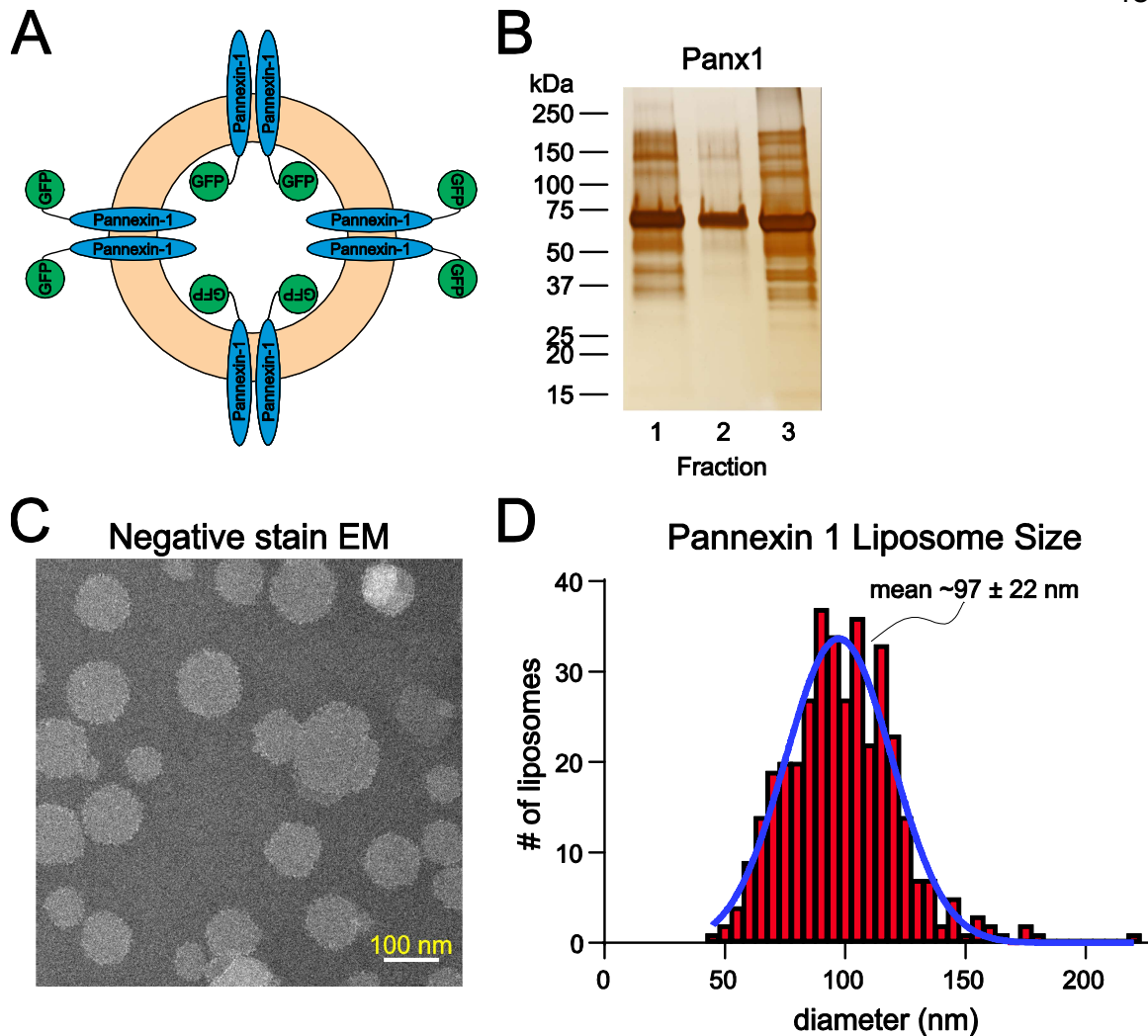


Figure 2.2 Liposome reconstitution and size

A) Schematic of proteoliposomes containing fPanx1-eGFP fusion proteins, in either orientation. **B)** fPanx1-containing fractions from Nycodenz co-floatation assay (fractions 1-3, 20 μ L each) were run on a polyacrylamide gel and analyzed by silver stain. **C)** Negative stain electron microscopy image of fPanx1-eGFP proteoliposomes extruded at 100 nm shown at 29,000x magnification. **D)** Distribution of liposome diameters measured from negative stain EM images (97.3 ± 22 nm, 374 liposomes from 12 images).

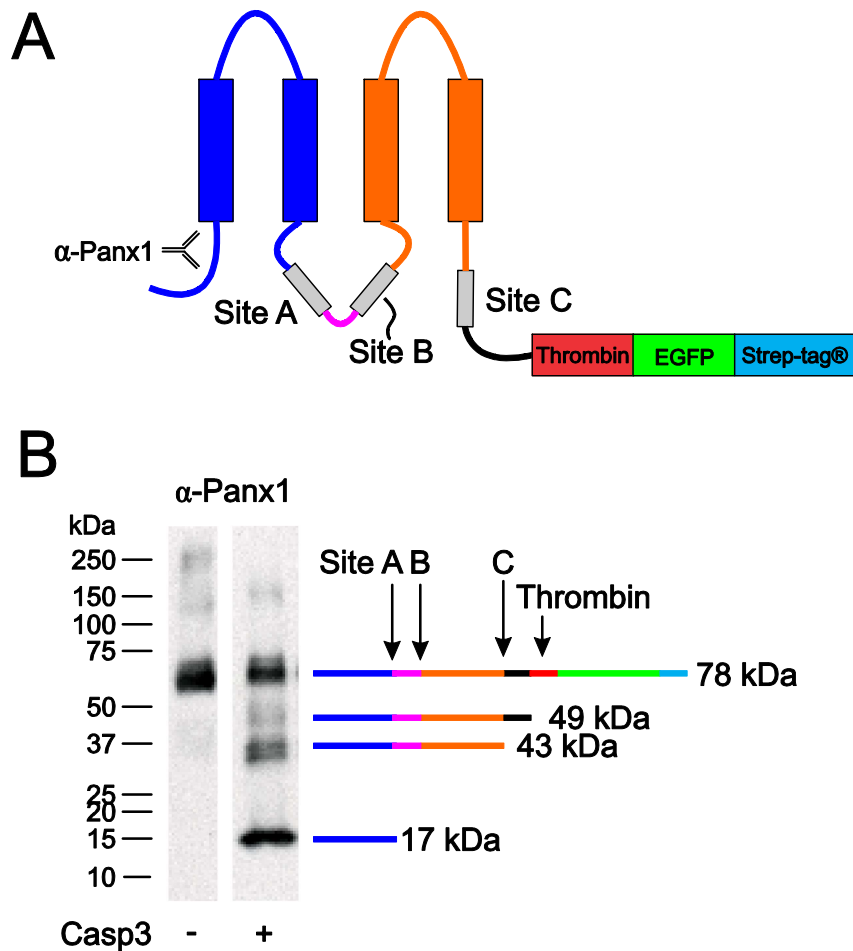


Figure 2.3 Pannexin 1 Caspase-3 cleavage sites and cleavage of Pannexin 1 in liposomes with recombinant Caspase-3

A) The schematics illustrate the location of: caspase cleavage sites, N-terminally-directed α -Panx1 antibody, and corresponding cleavage products. Note that residual thrombin from activating recombinant caspase cleaves at its cognate C-terminal site. **B)** Western blot of fPanx1-eGFP from proteoliposomes after overnight incubation in the absence and presence of recombinant Casp3.

site is necessary and sufficient for channel activation (Chekeni et al., 2010; Chiu et al., 2017; Sandilos et al., 2012).

Properties of caspase-activated fPanx1 in cells and lipid bilayers

In recordings from transfected HEK293T cells, we found that fPanx1 was basally silent and could be activated by intracellular dialysis with Casp3 to generate whole cell currents with an outwardly-rectifying current-voltage profile (**Figure 2.4 A,B**) similar to that observed with cleavage-activated human Pannexin 1 (hPANX1) channels (**Figure 2.4 C**) (Chiu et al., 2017; Sandilos et al., 2012). These currents were blocked by the Panx1 inhibitor carbenoxolone (CBX). In addition, and also similar to hPANX1, single fPanx1 channels were silent in excised inside-out patches until activated by Casp3 (Chiu et al., 2017); the cleavage-activated channels were inhibited by CBX and displayed a unitary conductance of 91.4 ± 13.5 pS ($n= 3$, **Figure 2.5 A,B**). Thus, whole cell and single channel properties of fPanx1 are essentially identical to hPANX1 after caspase activation (Chiu et al., 2017).

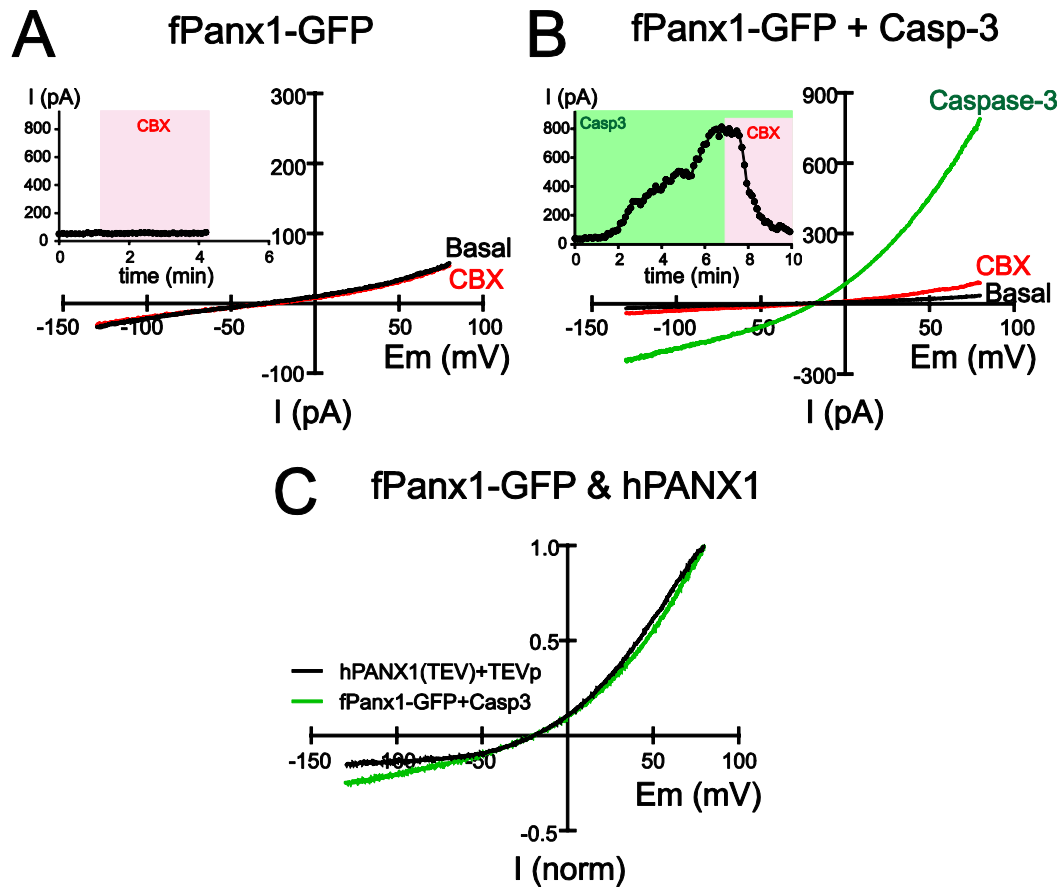


Figure 2.4 Whole-cell *in vitro* electrophysiology of fPanx1 in mammalian cells

A) Current-voltage traces for fPanx1-eGFP expressed in HEK 293T with normal internal solution (**A**) and with recombinant Casp3 in the internal solution (**B**; 2 $\mu\text{g}/\text{mL}$). The current activated by Casp3 was inhibited by bath application of 50 μM CBX. **C)** Normalized current-voltage curves from whole-cell patch-clamp electrophysiology comparing hPANX1 and fPanx1-eGFP.

A Inside-out patch recording (full length fPanx1-eGFP)

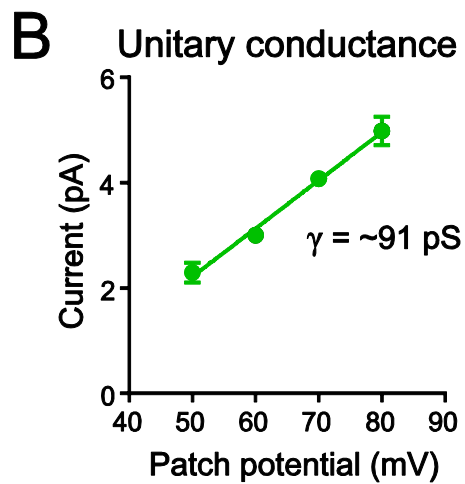
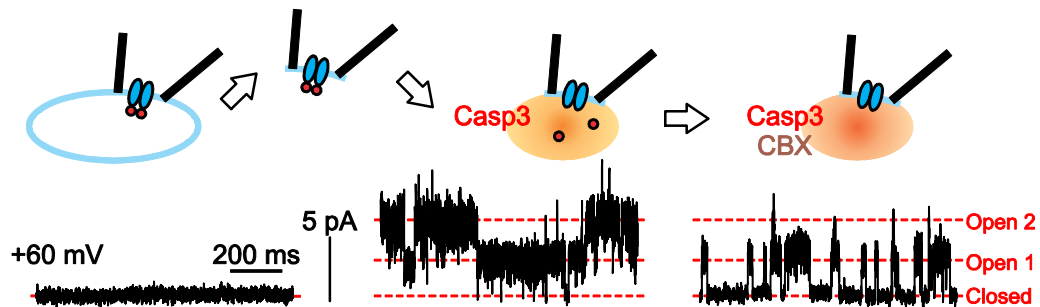


Figure 2.5 Single channel *in vitro* electrophysiology of fPanx1 in mammalian cells

A) Schematic showing protocol for inside-out patch-clamp recordings of fPanx1-eGFP (upper) and channel activity evoked by Casp3 and inhibited by CBX. **B)** Unitary current-voltage relationship with estimated slope conductance from inside-out patches of fPanx1 ($n = 3$).

We next used lipid bilayer recordings to characterize single channel properties of purified fPanx1 after caspase cleavage. The purified channels were added to DPhPC (1,2-diphytanoyl-sn-glycero-3-phosphocholine, 4ME16:0 PC) lipid bilayers and Casp3 was added to the bath to activate those channels with their C-terminus facing the *cis* side of the chamber (**Figure 2.6 A**). Prior to application of caspase, large “flickery” currents were occasionally observed at extreme potentials (e.g., +140 mV; **Figure 2.7 A**), and this often signified successful incorporation of fPanx1 into the bilayer. However, before caspase addition, fPanx1 channel activity was not observed at physiological potentials, even in a bath solution containing 200 mM K⁺ (**Figure 2.7 B**). After caspase addition, channel currents with discrete openings and closings became apparent across a wide range of physiological voltages (**Figure 2.6 A, Figure 2.7 B**); this activity was not seen when caspase was applied to plain lipid bilayers (i.e., with no channel added; **Figure 2.7 C**), indicating that measured currents reflected cleavage activation of the bilayer-incorporated fPanx1 channels.

The properties of caspase-activated fPanx1 channels in bilayers were similar, but not identical, to those of heterologously-expressed

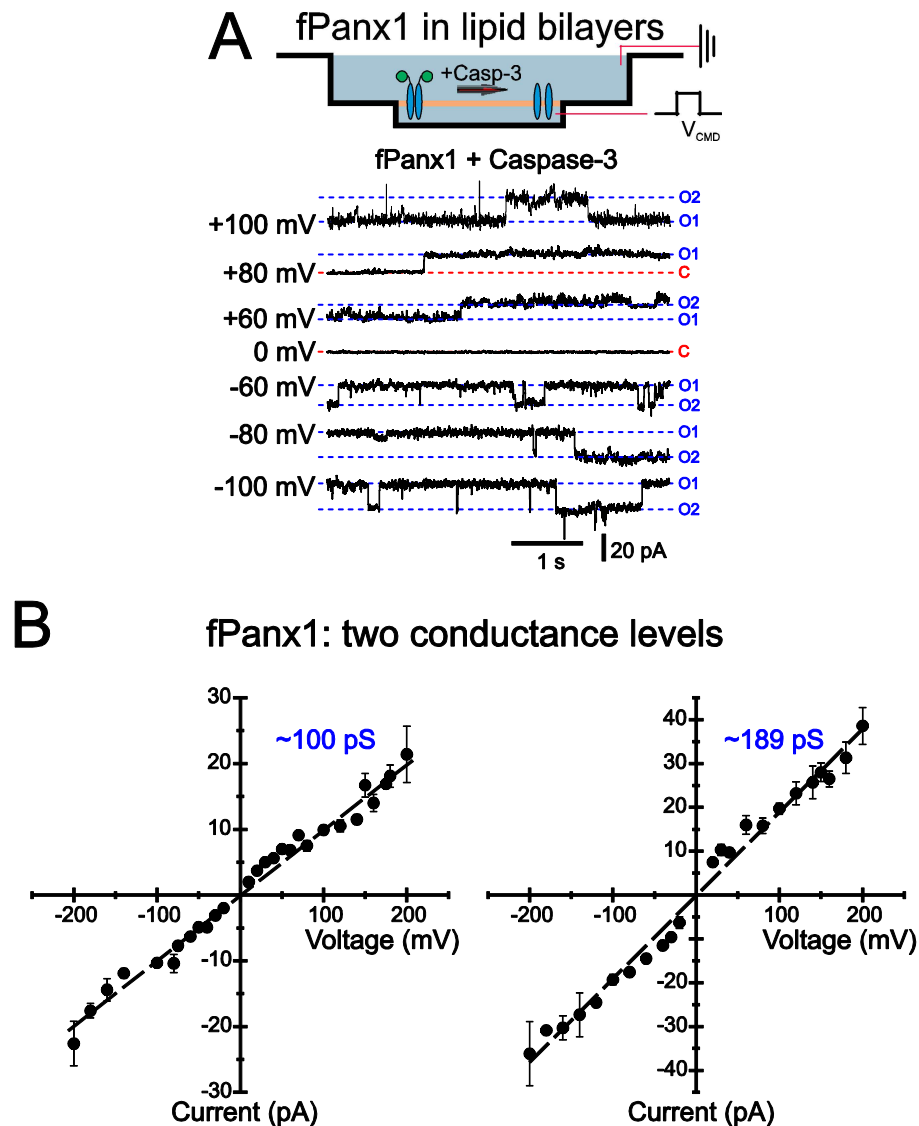


Figure 2.6 Single channel electrophysiology of purified fPanx1 in planar lipid bilayers

A) *Upper:* Schematic of fPanx1-eGFP embedded in bilayer in recording chambers in NanIon® Orbit mini; only channels in the orientation shown are activated by recombinant Casp3 added to the chamber. Positions of recording and ground electrodes are depicted. *Lower:* Recordings of purified fPanx1 channels in planar lipid bilayers at the indicated voltages following activation by recombinant Casp3; current levels are indicated that correspond to closed (C) state and apparent openings of one or two channels (O1, O2). **B)** Unitary

current voltage relationships for caspase-activated fPanx1 show two different conductance states ($n = 3$ bilayers with each conductance level).

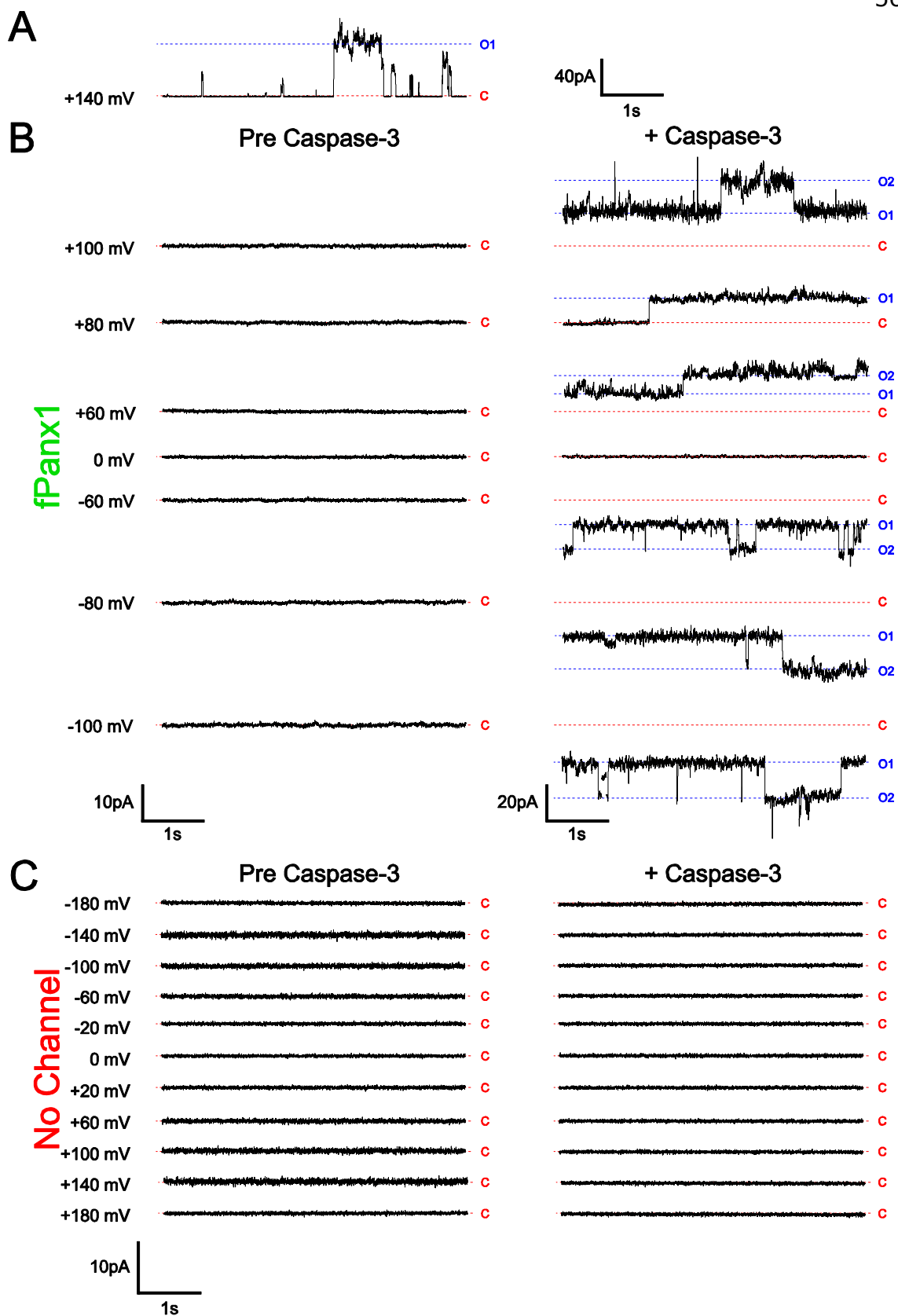


Figure 2.7 Caspase has no effect on lipid bilayers that do not contain fPanx1.

A) "Flickery" currents observed after addition of fPanx1 to lipid bilayers at +140 mV before addition of caspase. **B)** Current recordings from DPhPC lipid bilayers with fPanx1, before (left) and after addition of Casp3 (right) (n = 3).

C) Current recordings from DPhPC lipid bilayers without incorporation of fPanx1, before (left) and after addition of Casp3 (right) (n = 3).

recombinant fPanx1 channels recorded in mammalian cells (**Figure 2.5 A,B**). The individual bilayers usually included multiple active channels that presented with either of two distinct conductance levels: one set had a unitary conductance of ~ 100 pS, similar to that recorded in mammalian cells, and the second displayed a larger unitary conductance of ~ 189 pS (**Figure 2.6 B**). For both, the open channel I-V relationships were approximately ohmic (**Figure 2.6 B**), unlike the outwardly-rectifying single channel conductance observed for recombinant caspase-activated Panx1 in mammalian cells (Chekeni et al., 2010; Chiu et al., 2017; Romanov et al., 2012; Sandilos et al., 2012). These differences may be due to species variants and/or the fact that the bilayer recordings were obtained in symmetrical solutions across a non-native membrane composed of non-physiological lipids (e.g., without cholesterol, phosphatidylinositol 4,5-bisphosphate (PIP₂), etc.). Nevertheless, the purified fPanx1 channel is clearly activated by caspase.

Pannexin 1 forms a dye permeable pore

Caspase-mediated activation of Panx1 is associated with transmembrane flux of various metabolites and fluorescent dyes (Chekeni et al., 2010; Medina et al., 2020; Nielsen et al., 2020; Y. Qu et al., 2011). Importantly, all previous experiments have been

performed with Panx1 expressed in cells, either endogenously or heterologously. Therefore, a secondary mechanism of Panx1-dependent large molecule flux could not be excluded. To address this directly, we tested whether large molecule permeation can occur upon caspase cleavage-based activation of fPanx1 reconstituted in proteoliposomes (containing phosphatidylcholine, total brain lipid extract, cholesterol and PIP₂).

In a first set of studies, we examined whether caspase-cleaved fPanx1 is capable of forming a dye permeable pore. After overnight treatment with Casp3 (or buffer alone), liposomes were incubated with the anionic fluorescent dye, Sulforhodamine B (SR-B), and eluted through G25 spin columns for analysis on a fluorescence plate reader. Uptake of SR-B into liposomes was observed only when they contained fPanx1 and were treated with caspase. In addition, dye uptake was inhibited when caspase-treated fPanx1-containing proteoliposomes were treated with CBX before and during the dye incubation period (**Figure 2.8**).

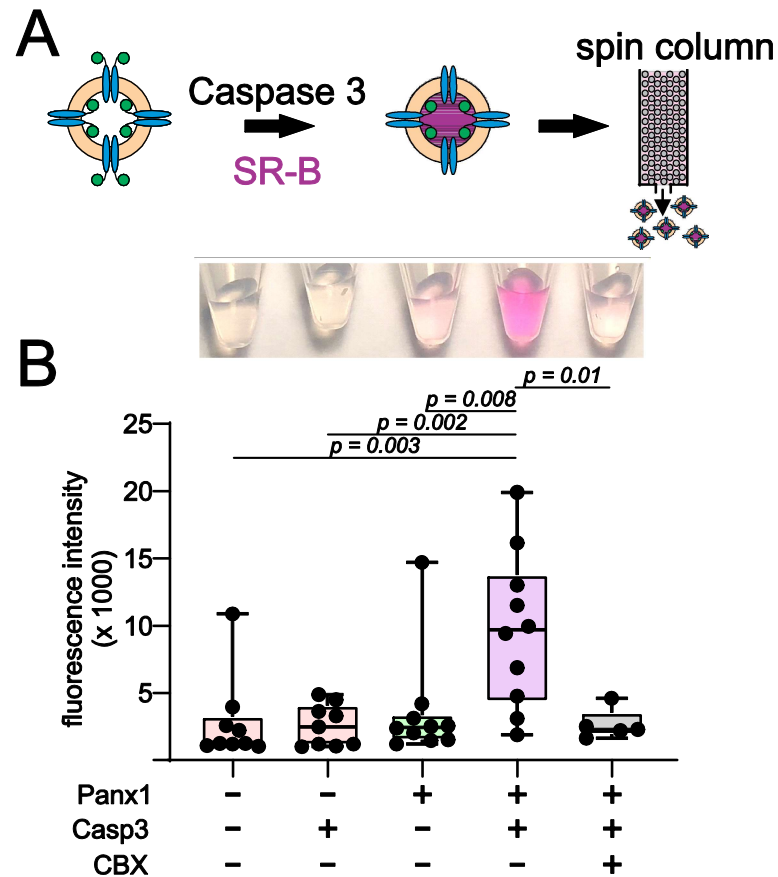


Figure 2.8 Bulk dye uptake in caspase-treated fPanx1-containing proteoliposomes.

A) Schematic depicting experimental design for treating fPanx1-containing proteoliposomes with recombinant Casp3 overnight at 4°C before incubation with SR-B (B, 1 mM) for 3 h and loading on a G-25 spin column. **B)** SR-B fluorescence (mean \pm SEM) in eluted proteoliposomes under the indicated conditions (9 assays: >3 proteoliposome preparations). ANOVA ($F_{4,34} = 5.95$, $p = 0.001$) and Tukey's multiple comparisons test (p -values from comparisons are shown).

To quantify this dye uptake, and verify that the dye was indeed associated with proteoliposomes containing fPanx1-GFP, we analyzed SR-B uptake in Casp3-treated and control proteoliposomes by ImageStream flow cytometry (**Figure 2.9 A**). As depicted in the representative images (**Figure 2.9 B**), SR-B was only observed in proteoliposomes that were treated with Casp3. A high GFP signal was present in the proteoliposomes that were not exposed to caspase, verifying the presence of GFP-tagged fPanx1 in those proteoliposomes that did not accumulate SR-B. Normalized frequency histograms of the mean fluorescence intensity (MFI) for GFP and SR-B quantify results from this exemplar experiment. Compared to untreated proteoliposomes, a larger fraction of Casp3-treated proteoliposomes contained SR-B (83.6% vs. 20.4%; **Figure 2.9 C**), and at ~10-fold higher MFI levels. We found a concomitant, albeit modest, leftward shift in the GFP signal after caspase treatment, reflecting cleavage of the outward-facing fPanx1 C-tail (exposed to caspase) and the associated removal of the C-terminal GFP tag (**Figure 2.9 C**); the retained GFP signal in the caspase-treated proteoliposomes may reflect uncut channels or channels with their GFP-tagged C-tails oriented into the proteoliposome. In multiple independent experiments and proteoliposome preparations, Casp3 treatment of fPanx1 proteoliposomes resulted in a decrease in GFP signal and a

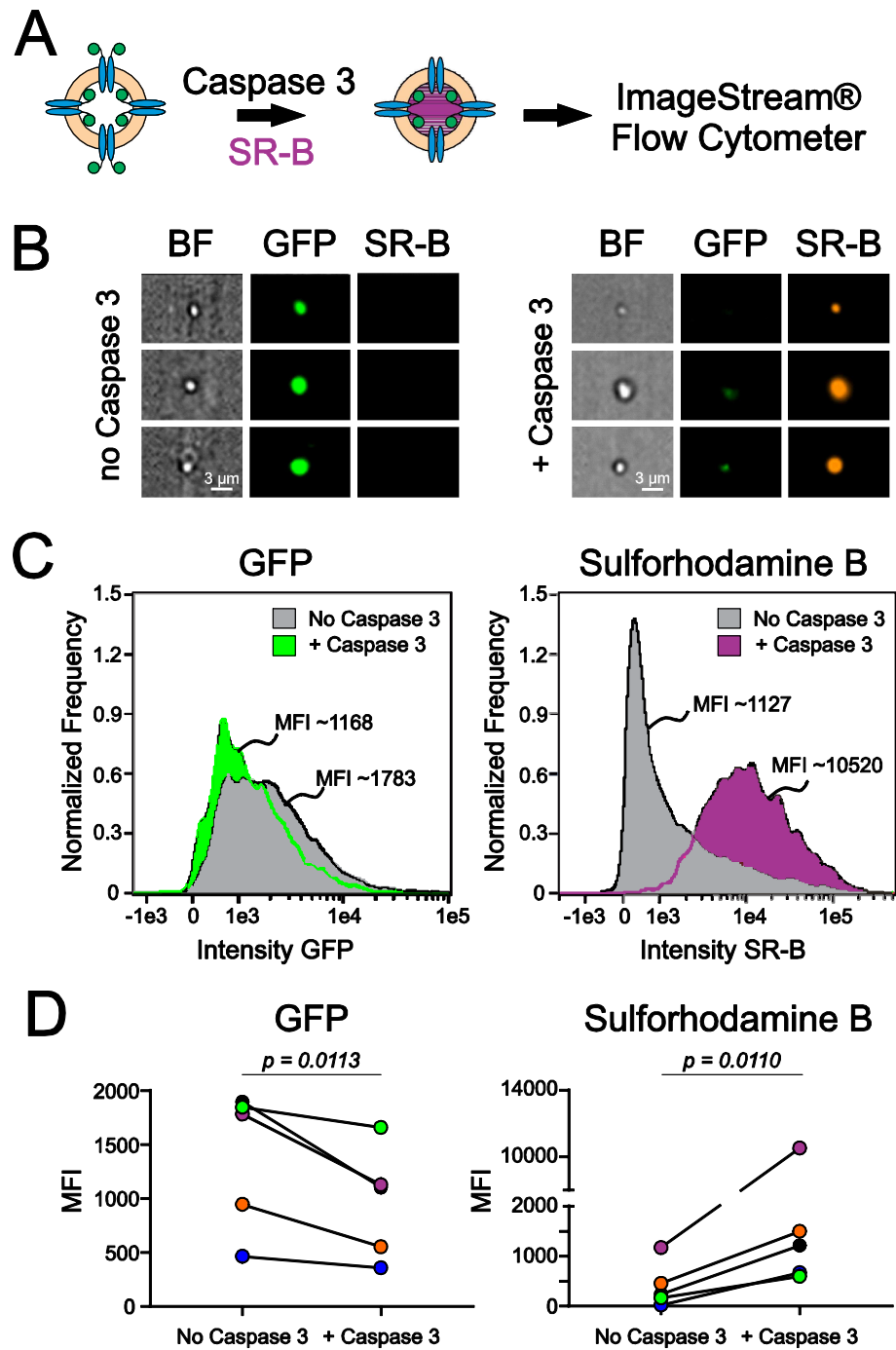


Figure 2.9 Dye uptake in caspase-treated fPanx1-containing proteoliposomes.

A) Proteoliposomes containing fPanx1 were incubated overnight with recombinant Casp3 and for 3 hours with sulforhodamine B (SR-B) dye prior to analysis by ImageStream® flow cytometry. **B)** Representative images of liposomes treated with vehicle (left) or Casp3 (right) viewed by brightfield, or on channels for GFP and SR-B fluorescence. **C)** Frequency distributions of fluorescence intensity show that proteoliposomes treated with recombinant Casp3 show a reduction in mean GFP intensity (*left*) and an increase in SR-B intensity (*right*), relative to vehicle treated proteoliposomes. **D)** Mean fluorescence intensity (MFI) of GFP fluorescence (*left*) ($p = 0.0096$) and SR-B fluorescence (*right*) ($p = 0.0104$) before and after caspase treatment are shown with individual experiments depicted according to the color shown ($N = 5$). A paired t-test was performed.

concomitant increase in SR-B signal (**Figure 2.9D, Figure 2.10**), indicating that caspase-cleaved fPanx1 channels generate a pore that is large enough for permeation of the SR-B dye.

Pannexin 1 is an anion-preferring molecular sieve

We exploited the dye permeation properties of fPanx1 channels to develop a single-particle assay, in which total internal reflection fluorescence (TIRF) microscopy was used to characterize the kinetics of dye flux and the charge/size determinants of fPanx1 permeants in proteoliposomes (**Figure 2.11 A**) (Farsi et al., 2016).

For these experiments, liposomes were pre-filled with SR-B and visualized by TIRF microscopy before and after the addition of Casp3 to the bath solution. For each liposome, we recorded changes in the fluorescence intensity of both GFP, representing fPanx1 C-tail channel cleavage, and SR-B, representing dye release from the proteoliposome (**Figure 2.11 B**). In a prominent subset of fPanx1-containing proteoliposomes, both GFP and SR-B fluorescence decreased following Casp3 application (**Figure 2.11 B,C, purple**). For other fPanx1-containing proteoliposomes, the GFP fluorescence was not reduced by

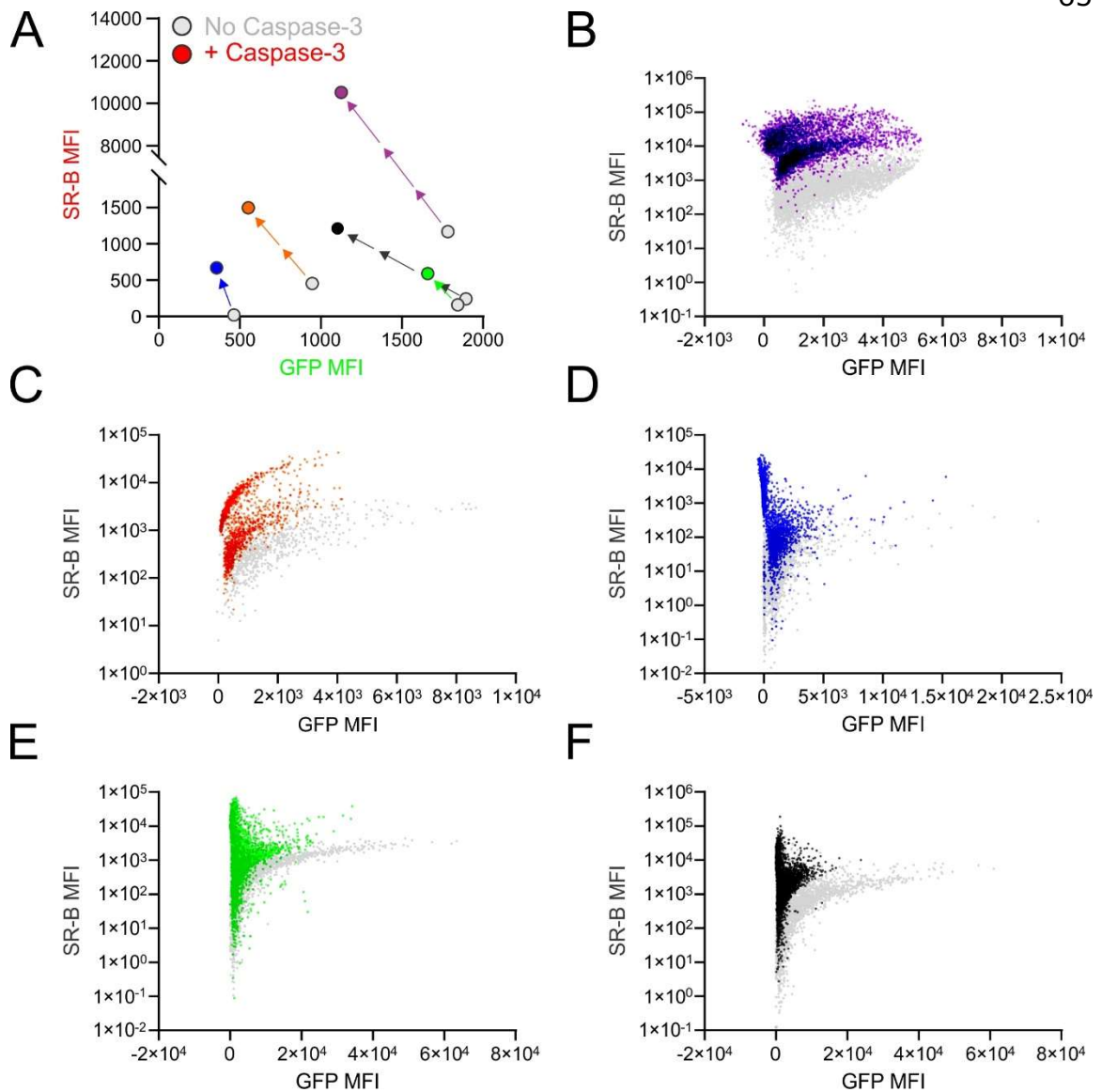


Figure 2.10 GFP and Sulforhodamine-B Mean Fluorescence Intensity (MFI) in caspase-treated fPanx1-containing proteoliposomes.

A) Changes in GFP and SR-B fluorescence in individual experiments are shown (N = 5). **B-F)** Flow cytometry plots are shown for individual experiments from **A** (color-coded accordingly). Gray dots indicate proteoliposomes not treated with Casp3 and colored dots indicate proteoliposomes after treatment with Casp3. Only positive SR-B values are plotted on the logarithmic y-axis.

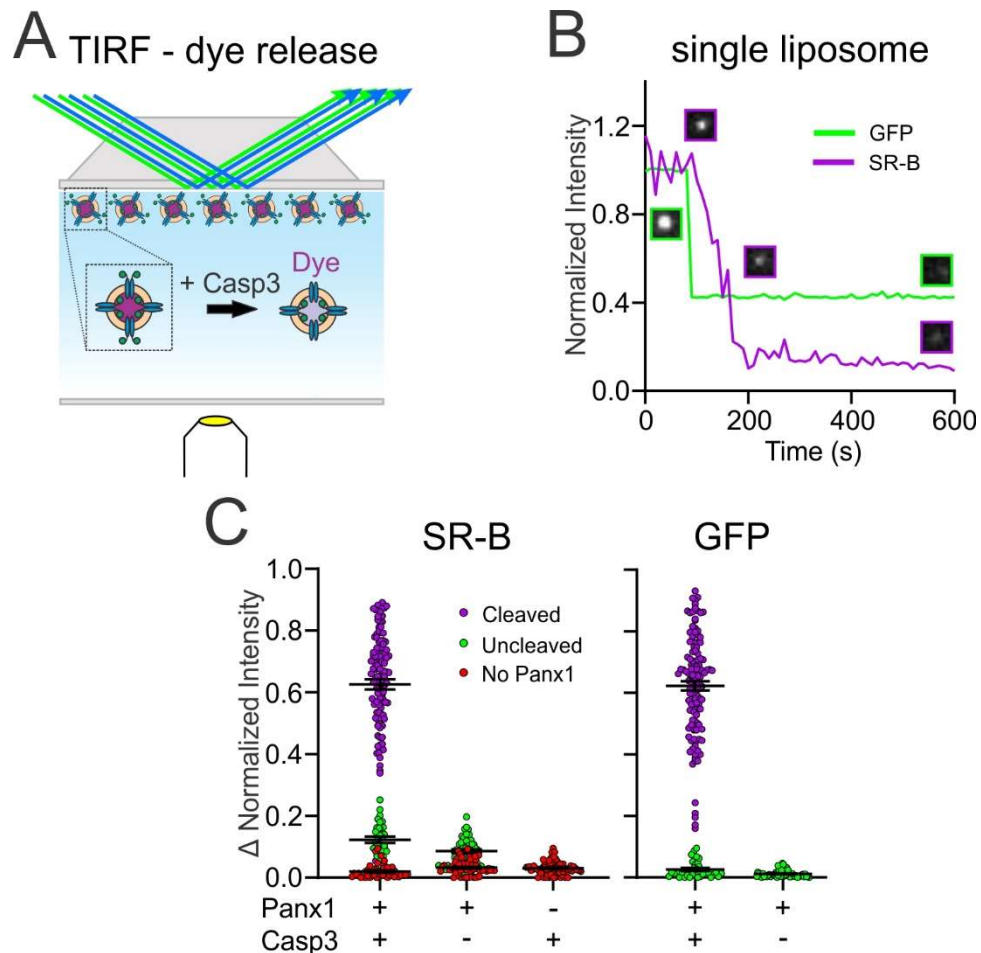


Figure 2.11 fPanx1 allows for permeation of anionic dye

A) Schematic of experimental design to assay dye release kinetics from caspase-treated fPanx1-containing proteoliposomes by TIRF microscopy. **B)** Example fluorescence intensity traces for sulforhodamine B (SR-B, anionic dye, 559 Da) and GFP (caspase cleavage) over time in proteoliposomes after caspase treatment. Sample images of the proteoliposome fluorescence at the different time points are also provided. **C)** Steady state change in normalized fluorescence intensity for SR-B (*left*) and GFP (*right*) from fPanx1-GFP-containing proteoliposomes treated with either Casp3 or vehicle, or from empty liposomes (no fPanx1-GFP) treated with Casp3. Data from fPanx1-containing proteoliposomes were grouped according to whether they showed a reduction in GFP fluorescence (cleaved) or no change in GFP fluorescence (<10%, uncleaved) (N = 5 (+)Panx 1 (+)Casp3, N = 5 (+)Panx1 (-)Casp3, N = 4 (-)Panx1 (+)Casp3).

Casp3, suggesting that the GFP-tagged fPanx1 C-tail was oriented into the proteoliposome and remained uncleaved; in those cases, the SR-B fluorescence was also unchanged (**Figure 2.11 C**, *green*). Likewise, SR-B fluorescence was unaffected following Casp3 application in particles that were devoid of GFP fluorescence, likely representing liposomes that did not incorporate any fPanx1-GFP (**Figure 2.11 C**, *red*). In other controls, SR-B fluorescence was retained in liposomes, either with or without GFP fluorescence (i.e., with or without fPanx1) when they were not exposed to Casp3; and SR-B fluorescence was also unaffected by Casp3 in liposomes that did not contain fPanx1 (i.e., empty liposomes) (**Figure 2.11 C**). Thus, this TIRF-based assay verifies that caspase cleavage activation of fPanx1 elicits dye efflux from fPanx1-containing proteoliposomes.

The TIRF assay was also used to examine the kinetics of dye permeation by imaging dye release from proteoliposomes, thereby enabling flux measurements between fluorescent dyes of different charge and size. To examine charge effects, we assessed the release of a cationic dye, Rhodamine B (RhB), which is slightly smaller than the anionic SR-B (480 Da vs. 559 Da; **Figure 2.12**). Like SR-B, RhB was released from proteoliposomes, and this release was also

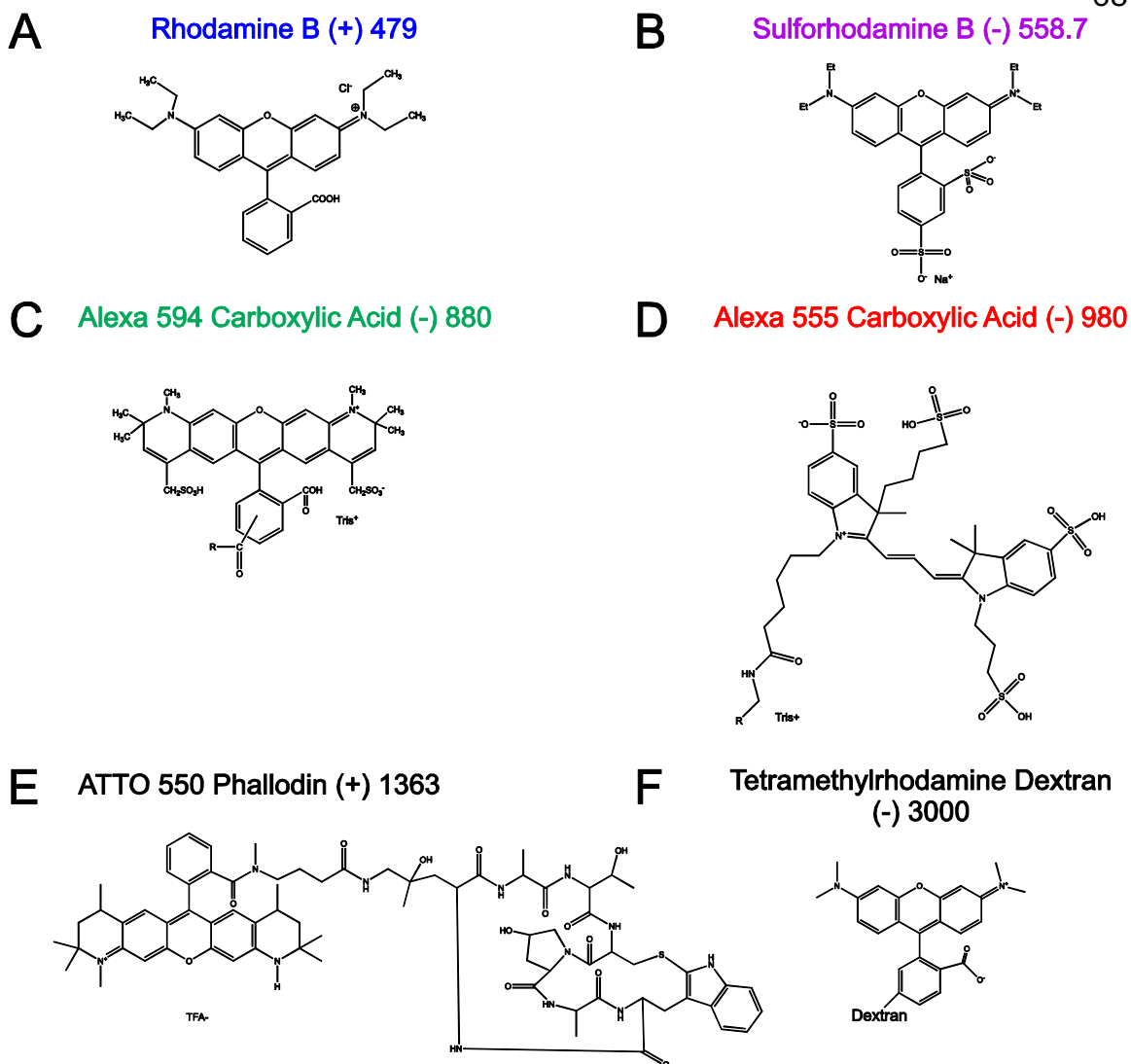


Figure 2.12 Chemical structures of fluorescent dyes.

Chemical structures, net charge, and molecular weight are shown for **A**) Rhodamine B, **B**) Sulforhodamine-B, **C**) Alexa 594 Carboxylic Acid, **D**) Alexa 555 Carboxylic Acid, **E**) ATTO 550 Phalloidin, and **F**) Tetramethylrhodamine Dextran 3000. Note, the precise site of the conjugate for proprietary dyes was not provided so the figures depict approximate structures, and the size of the dextran is approximate. The chemical structure of ATTO 550 Phalloidin was provided by ATTO-TEC.

dependent on caspase-mediated cleavage of fPanx1 (**Figure 2.13 A,B**). The rate of dye efflux, obtained from fits to mono-exponential decay curves of the fluorescent signal for each proteoliposome, was positively correlated to the fraction of fPanx1 cleavage (i.e., reduction in GFP fluorescence) for both SR-B and RhB dyes (**Figure 2.13 C**). Notably, despite the smaller size of RhB, the efflux rate was significantly slower than for SR-B due to the cationic charge (**Figure 2.13 C**).

To examine the effect of size on efflux rates, we tested two additional anionic fluorescent dyes of increasing size, Alexa 594 and Alexa 555 (880 Da and 980 Da, respectively; **Figure 2.14 A, Figure 2.12**). These larger dyes permeated caspase-cleaved fPanx1 at rates substantially slower than the smaller SR-B (**Figure 2.14 B**). Of note, however, despite being ~2-times larger, these anionic dyes transited the channel at rates comparable to the cationic dye RhB (**Figure 2.14 B**). Finally, we also examined two larger dyes (ATTO 550 (+), 1363 Da; and Dextran 3000 (-), 3000 Da; **Figure 2.12**), and neither of those were able to permeate caspase-activated fPanx1 (**Figure 2.14 A**). The permeation properties of these dyes were not related to the relative amounts of GFP cleavage, which were comparable in all cases

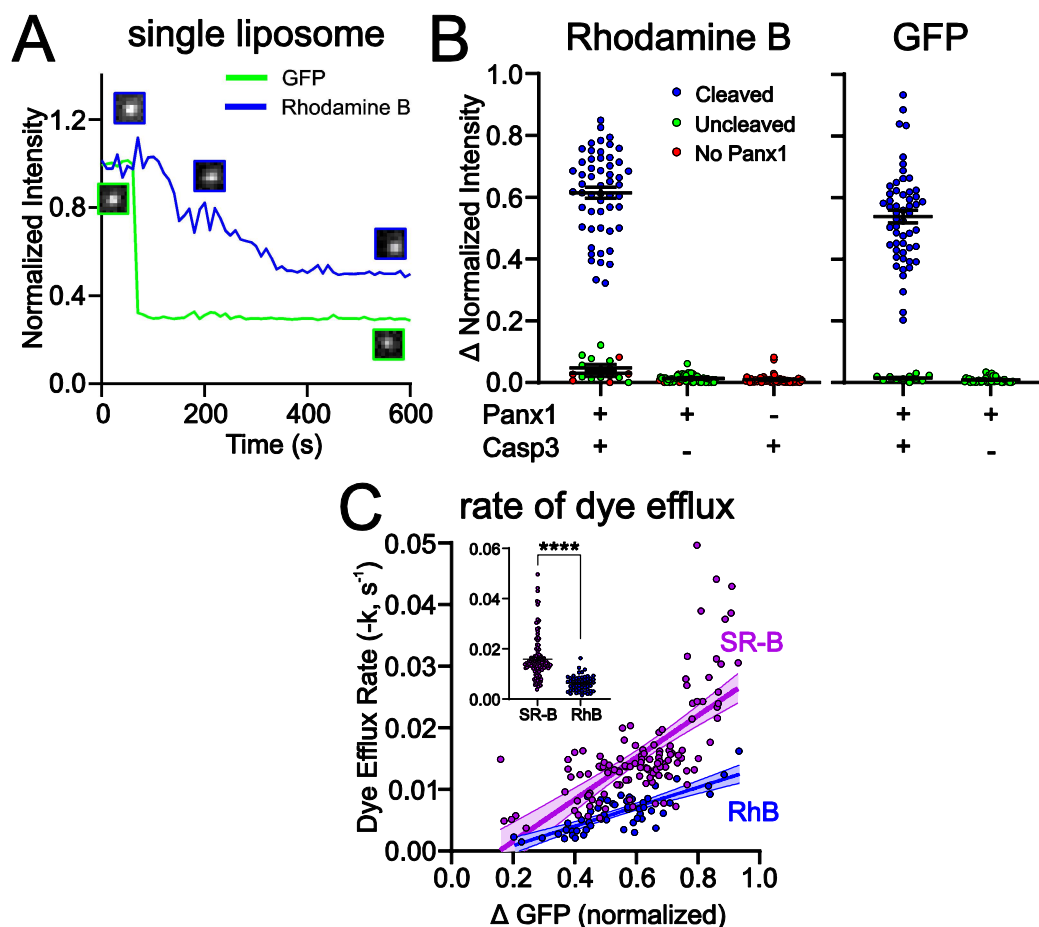


Figure 2.13 fPanx1 allows for cation dye flux and favors permeation of anionic dyes

A,B) Fluorescence intensity traces (**A**) and steady state change in normalized fluorescence intensity (**B**) for Rhodamine B (RhB, cationic dye, 479 Da) and GFP, as described for **Figure 2.11 B,C** ($N = 5$ (+)Panx1 (+)Casp3, $N = 3$ (+)Panx1(-)Casp3, $N = 4$ (-)Panx1 (+)Casp3). **C)** Efflux rates for SR-B and RhB were determined from fits of mono-exponential to the fluorescence intensity decay curves for individual caspase-treated proteoliposomes and plotted relative to the change in GFP fluorescence (i.e., fPanx1 cleavage); overlaid regression lines are depicted (with 95% confidence interval; slopes were significantly different, $p = 0.0014$). Inset shows dye efflux rates for individual liposomes. Individual liposome dye efflux rates were analyzed by a Mann-Whitney test ($p < 0.0001$).

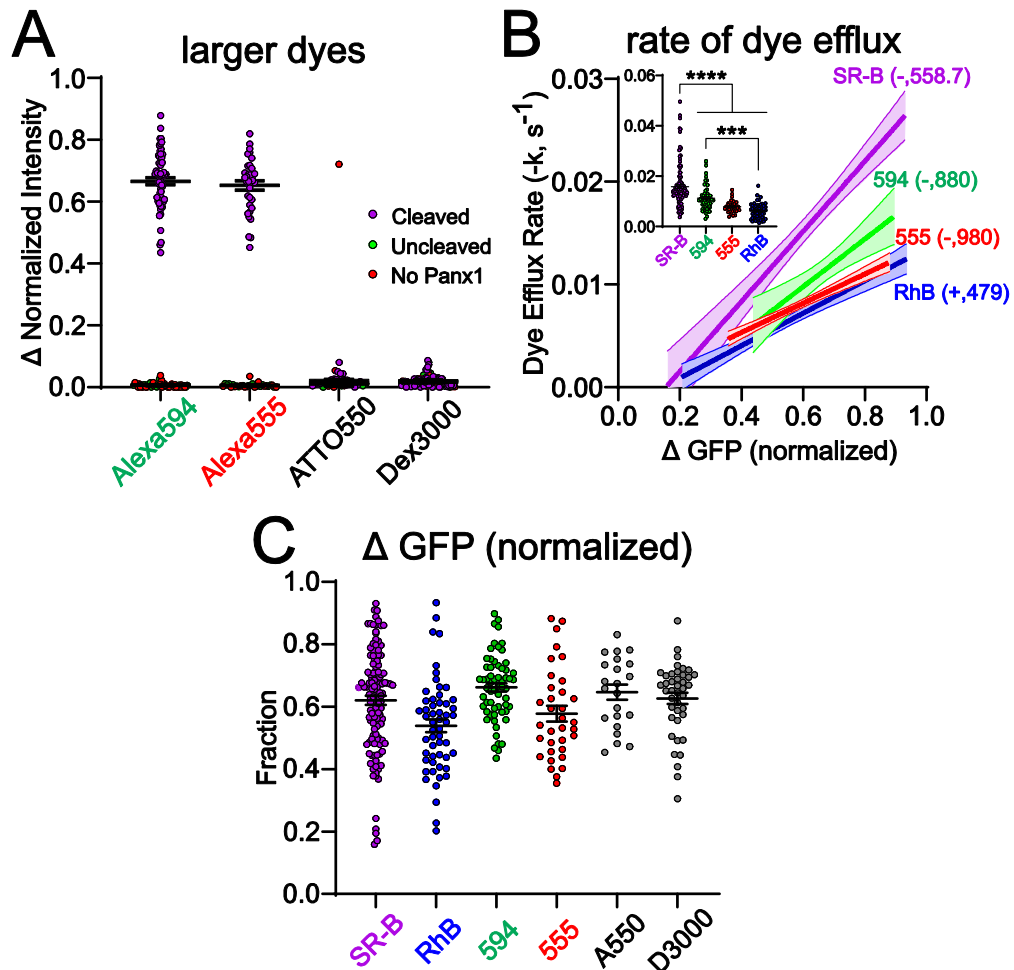


Figure 2.14 Larger dyes flux through fPanx1 and fPanx1 is preferential to smaller, anionic dyes

A) Steady state change in normalized fluorescence intensity for Alexa594 (anionic, 880 Da), Alexa555 (anionic, 980 Da), ATTO550 (cationic, 1363 Da) and Dextran 3000 (anionic, 3000 Da) from fPanx-GFP-containing proteoliposomes treated with Casp3 (Alexa 594 N = 6, Alexa 555 N = 5, ATTO 550 N = 3, Dextran 3000 N = 5). **B)** Efflux rates for the indicated dyes represented by associated regression lines (with 95% confidence interval), with pairwise comparison of slopes: SR-B vs. RhB ($p = 0.0014$), SR-B vs. 594 ($p = 0.16$), SR-B vs. 555 ($p = 0.0074$), 594 vs. 555 ($p = 0.15$), 594 vs. RhB ($p = 0.16$), 555 vs. RhB ($p = 0.53$). Inset shows dye efflux rates for individual liposomes (ANOVA: $F_{3,267} = 36.18$, $p < 0.0001$; with Tukey's multiple comparisons test: ****, $p < 0.0001$; ***, $p = 0.0002$). **C)** Relative change (upper) and rate (lower) of GFP fluorescence in cleaved fPanx1-containing proteoliposomes filled with the indicated dyes.

(**Figure 2.14 C**). Together, these data indicate that the channel favors anionic over cationic permeants, and reveal that the pore size is sufficient to accommodate molecules up to 980 Da.

Pannexin 1 is a conduit for anionic and cationic metabolites

Panx1 is commonly characterized as an ATP-release channel (Chekeni et al., 2010; Chiu et al., 2017; Chiu, Schappe, Desai, & Bayliss, 2018; Dahl, 2015; Medina et al., 2020; Taruno, 2018) and recent work provides compelling evidence that caspase cleavage-based activation of Panx1 can also lead to release of multiple additional metabolites (e.g., spermidine) that mediate important intercellular signaling processes (Medina et al., 2020). To test whether ATP and other metabolites permeate directly through caspase-activated fPanx1 channels, we developed a filtration-based assay for uptake of radiolabeled metabolites in proteoliposomes (**Figure 2.15 A**). We performed this assay with select metabolites that have been proposed to permeate cleavage-activated fPanx1 (Medina et al., 2020), including anionic (α - ^{32}P ATP and ^3H -glutamate) and cationic (^3H -spermidine) metabolites (**Figure 2.16**). Indeed, we found that uptake of α - ^{32}P ATP, ^3H -glutamate, and ^3H -spermidine into proteoliposomes required caspase-activated fPanx1; uptake was not

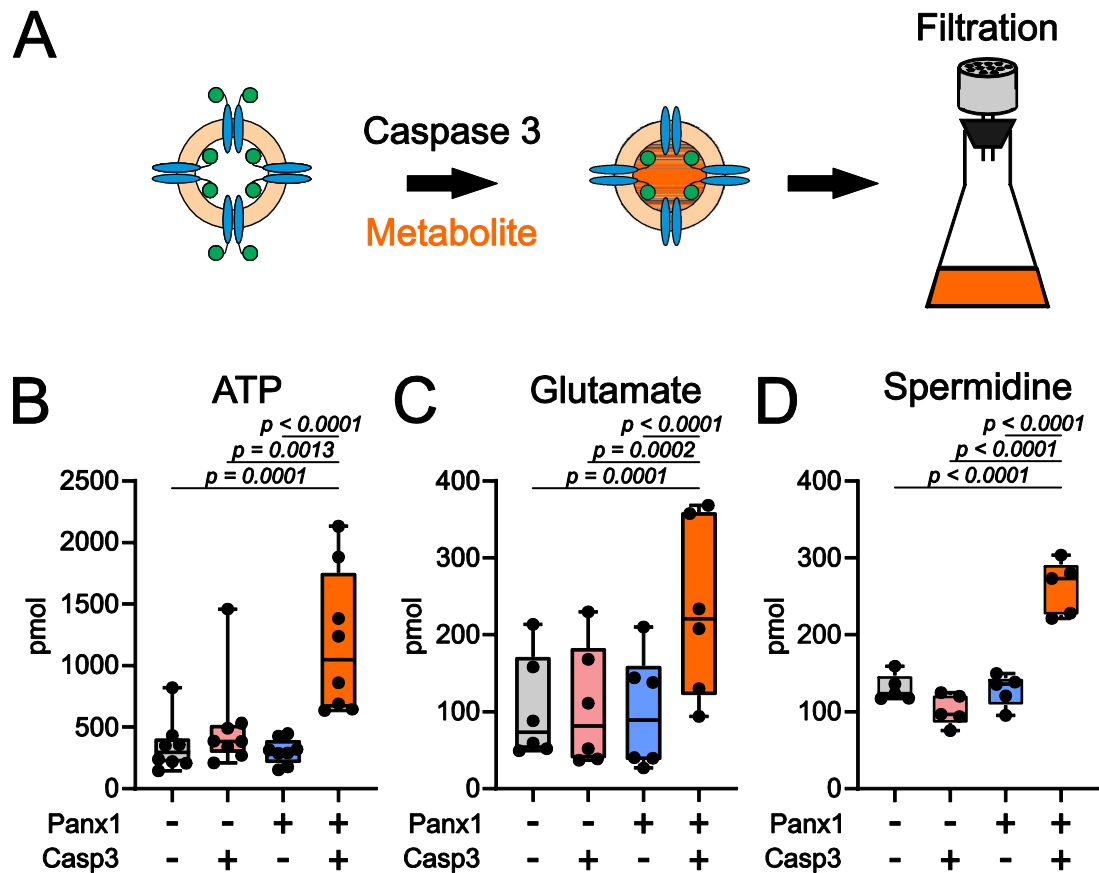


Figure 2.15 Caspase-cleaved fPanx1 is a conduit for metabolite release.

A) Schematic depicting experimental design for treating fPanx1-containing proteoliposomes with recombinant Casp3 overnight at 4°C before incubation with 4 μCi each of α [^{32}P]-ATP (**B**, 1 mM; \sim 1:150000, hot:cold), [^3H]-Glutamate (**C**, 0.8 mM; \sim 1:2000), and [^3H]-Spermidine (**D**, 8 μM ; \sim 1:24) for 3 h and filtration using a Whatman GF/B filter. **B-D)** Metabolites taken up by proteoliposomes under the indicated conditions for α [^{32}P]-ATP (N = 8), [^3H]-Glutamate (N = 6), and [^3H]-Spermidine (N = 5); molar quantities should not be compared between compounds due to different assay conditions. A box plot with the box depicting the quartiles/median, and lines drawn to points outside 25th/75th percentiles are shown. By repeated-measures one-way ANOVA (ATP: $F_{3,28} = 14.18$, $p < 0.0001$; Glutamate: $F_{3,20} = 18.29$, $p < 0.0001$; Spermidine: $F_{3,16} = 40.50$, $p < 0.0001$), with p-values provided from Tukey's multiple comparisons tests.

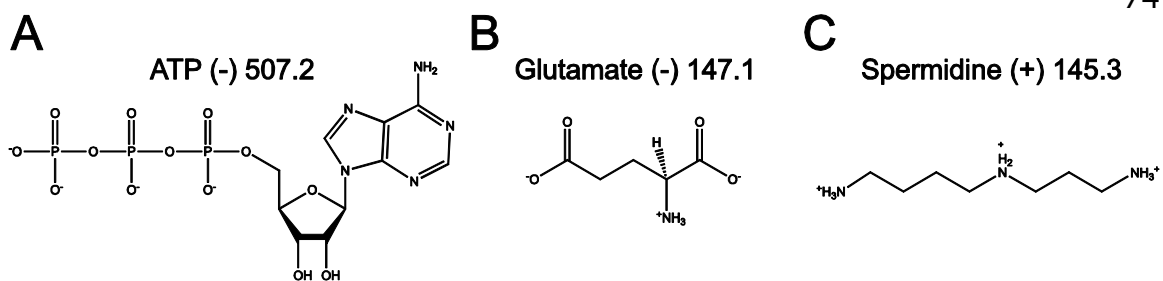


Figure 2.16 Chemical structures of metabolites.

Chemical structures, net charge, and molecular weight are shown for **A**) Adenosine triphosphate, **B**) glutamate, and **C**) spermidine.

observed when liposomes did not contain fPanx1 or when the channel was not activated by Casp3 (**Figure 2.15 B-D**). We also tested whether ATP and spermidine could flux via caspase-activated Panx1 when included together in the same assay, rather than independently. Under these conditions, we again found uptake of both ATP and spermidine into caspase-cleaved Panx1-containing proteoliposomes, albeit at slightly lower levels (**Figure 2.17**). These data indicate that cleavage-activated fPanx1 itself is sufficient to form a membrane conduit capable of simultaneously conducting ATP and other important signaling metabolites.

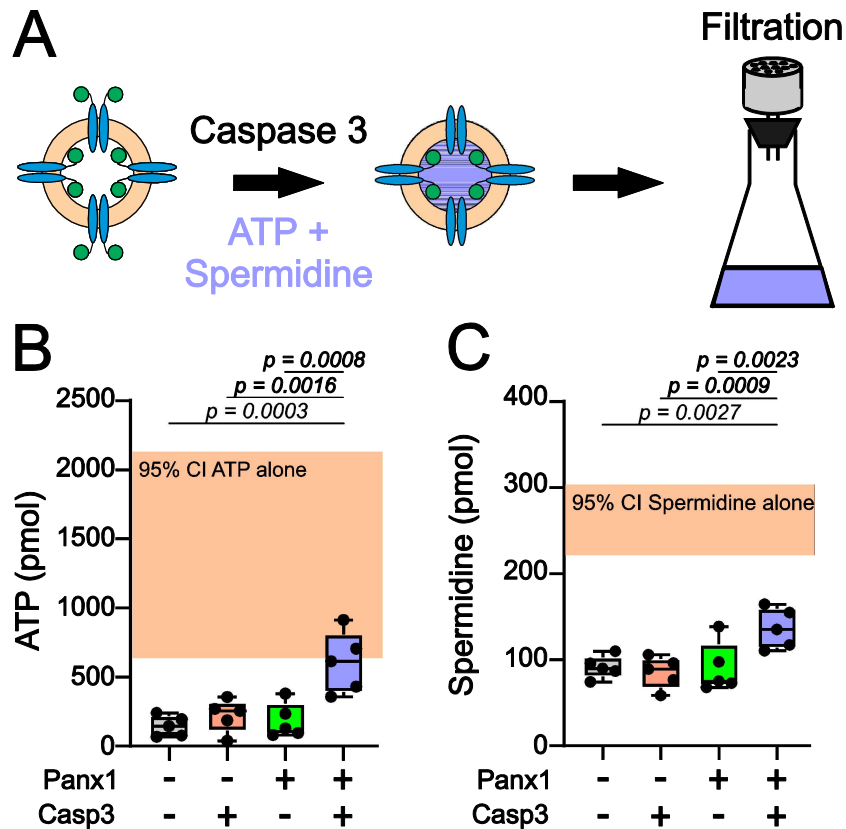


Figure 2.17 ATP and Spermidine can flux through Pannexin 1 concurrently.

A) Schematic depicting experimental design for treating fPanx1-containing proteoliposomes with recombinant Casp3 overnight at 4°C before concurrent incubation with 4 μ Ci each of α [32 P]-ATP (**B**, 1 mM; \sim 1:150000, hot:cold) and [3 H]-Spermidine (**C**, 8 μ M; \sim 1:24) for 3 h and filtration using a Whatman GF/B filter. Orange boxes depict 95% confidence intervals of Casp3-treated fPanx1 proteoliposome metabolite uptake of compounds incubated individually (from **Fig 4B,D**). By repeated-measures one-way ANOVA (ATP: $F_{3,19} = 15.14$, $p = 0.0002$; Spermidine: $F_{3,16} = 12.17$, $p < 0.0006$), with p-values provided from Tukey's multiple comparisons tests.

Discussion

Panx1 membrane channels are best known for their purported ability to support transmembrane flux of large molecules such as fluorescent dyes and, of more physiological relevance, metabolites and intercellular signaling molecules (e.g., most notably, ATP) (Chekeni et al., 2010; Chiu et al., 2017; Yang et al., 2015). The widespread acceptance of this idea is based on a wealth of data obtained from more intact systems, including those that implicated caspase-activated Panx1 as the likely transmembrane flux pathway for large molecule permeation (Chekeni et al., 2010; Chiu et al., 2017; Medina et al., 2020; Nielsen et al., 2020; Poon et al., 2014). In particular, the dye/metabolite permeation associated with apoptosis requires Panx1 expression, caspase activation and an intact C-terminal caspase cleavage site; it is blocked by Panx1 channel inhibitors, indicating that ongoing channel activity is required (Chekeni et al., 2010; Chiu et al., 2017; Poon et al., 2014; Y. Qu et al., 2011). This dye and metabolite permeation occurs not only during cell death, but is also observed when the channels are activated by C-terminal truncation independent of apoptosis (Chiu et al., 2017; Sandilos et al., 2012). In addition, ATP release and dye uptake closely parallel the quantized channel activation associated with individual subunit C-tail removal, further implicating the Panx1 channel as the permeation pathway for large

molecules (Chiu et al., 2017). Despite this substantial body of evidence, this previous work was all based on experiments in intact cells, where secondary release mechanisms could not be excluded, and it has been suggested based on other channel properties (i.e., preferential anion selectivity, single channel conductance) that caspase-cleaved Panx1 is not compatible with large molecule permeation (Wang & Dahl, 2018). The present data demonstrate dye and metabolite permeation directly through purified Panx1 channels reconstituted in proteoliposomes to convincingly dispel this conflicting idea and clearly establish that dye/metabolite flux can indeed occur directly through caspase-activated Panx1 channels.

Channel properties of Panx1 channels in bilayers and cells

Similar to electrophysiological measurements of fPanx1 and hPANX1 recorded in inside-out patches from mammalian cells, we found that fPanx1 was silent in planar lipid bilayers until activated by caspase cleavage. In native cell membranes, caspase-cleaved hPANX1 and fPanx1 generate outwardly-rectifying currents with a single channel conductance of ~ 90 pS at depolarized potentials (Chiu et al., 2017). However, different conductance levels for channels attributed to Panx1 have been observed in various cell systems after different forms of activation, reportedly up to ~ 500 pS (Bao et al., 2004; reviewed in

Chiu et al., 2018; Wang et al., 2014). Here, we observed two main, non-rectifying conductance levels from purified fPanx1 channels in bilayers after caspase activation (~ 100 pS; ~ 190 pS). In lipid bilayer recordings of purified hPANX1 reported during preparation of this work, Mou et al. detected a ~ 30 pS channel in *E. coli* polar lipid extract, although these recordings were in the absence of any specific form of activation and were not accompanied by open-closed transitions; the C-tail-cleaved channels, by contrast, yielded a number of extremely large open channel conductance states (i.e., 750 pS, 1.3 nS, and 1.8 nS; at +100 mV) (Mou et al., 2020). There have been other reports of constitutive Panx1 channel activity (i.e., in the absence of stimulation), and although these channels display a unitary conductance similar that of channels stimulated by Casp3 cleavage (~ 70 -80 pS), they do not appear to support ATP release (Ma et al., 2012; Romanov et al., 2012). It was recently proposed that a second permeation pathway, visible as a side tunnel in the structure of hPANX1, could support atomic ion flux through unstimulated and C-tail-intact channels in the absence of large molecule permeation (Ruan et al., 2020); this intriguing idea will need to be explored further (e.g., with single channel recordings of hPANX1 with intact C-termini). At this point, the mechanisms controlling basal and stimulated channel activity, and the factors that determine the vast range of reported

Panx1 channel conductance levels, remain to be determined and may be related to any number of cell specific factors (e.g., channel-interacting proteins, different lipid composition in native cell membranes and bilayers).

A preference for anion versus cation selectivity

In ion substitution experiments, obvious shifts in reversal potential (E_{rev}) were observed when Cl^- was exchanged with other negatively charged counterions (Ma et al., 2012; Michalski et al., 2020; Romanov et al., 2012; Ruan et al., 2020; Wang & Dahl, 2018). These shifts in E_{rev} were strongly affected by mutations in R75, a positively-charged residue next to W74, the narrowest pore constriction site identified in multiple recent structural reports (Deng et al., 2020; Michalski et al., 2020; Ruan et al., 2020). These results provide strong evidence for anion permeation through Panx1. By contrast, negligible changes in E_{rev} accompany substitution with different positively-charged counterions (Michalski et al., 2020; Ruan et al., 2020). On this basis, it has been inferred that the channel is exclusively anion-selective and impermeable to cations (Ma et al., 2012). Our data likewise reveal permeation of anionic dyes and signaling molecules (ATP, glutamate), with a clear preference for anionic over cationic dyes. However, we also detected flux through the channel of a positively-charged dye

(RhB) and metabolite (spermidine), indicating that cationic molecules can also traverse the channel. In addition, we observed simultaneous Panx1-mediated flux of both ATP and spermidine when assessed in combination. This supports the previous observation from apoptotic T cells that multiple important signaling metabolites can be released via caspase-activated channels in a complex milieu containing numerous permeants (Medina et al., 2020).

Permeant size considerations and pore architecture

Our data reveal a negative correlation between dye size and permeation rate – larger dyes were associated with slower permeation. Previous studies have predicted the maximum size of a Panx1 permeant to be less than 1270 Da (7-AAD) (Chiu et al., 2017; Poon et al., 2014) or 1500 Da (PEG 1500) (Wang, Ma, Locovei, Keane, & Dahl, 2007). We found that Alexa555 (980 Da) could transit via the cleavage-activated Panx1 channel while ATTO550 (1363 Da) was unable to permeate. This indicates that the pore of the activated channel must be able to accommodate a molecule at least up to ~1 kDa.

A major breakthrough in the field was achieved with the recent determination of several high-resolution cryoEM structures of frog and

human Panx1 by multiple groups (Deng et al., 2020; Jin et al., 2020; Michalski et al., 2020; Mou et al., 2020). The architecture and contours of the transmembrane pore were remarkably similar for all constructs analyzed, despite those including full length (presumably inactive) and C-terminal cleaved/truncated (presumably activated) (Deng et al., 2020; Michalski et al., 2020; Ruan et al., 2020). The narrowest pore constriction was formed by a ring of seven W74 residues on the extracellular surface of the channel, with a diameter of $\sim 8-10$ Å. This constriction appears to be too small to accommodate large dyes or even hydrated ATP, although this may be influenced by the shape and flexibility of the permeant molecule and/or the pore itself. Moreover, upon activation by cleavage (or truncation) at the C-terminal caspase site, Panx1 transitions between open and closed states (Chiu et al., 2017). Thus, the available structures may have captured the channel in a state that is “open” for atomic ions but remains “closed” for large molecules. The possibility of multiple open conformations, or separate permeation pathways for ions and large molecules in both Panx1 channels and in CALHM1 channels, have been proposed (Gaete et al., 2020; Nielsen et al., 2020; Ruan et al., 2020; Wang et al., 2014). If those distinct conformations exist, the dye/metabolite flux data we present indicate that Panx1 cleavage by caspase is permissive for conformations that allow large molecule

permeation, perhaps by removing a physical block to pore access while allowing open-closed transitions (Sandilos et al., 2012).

Summary

Examination of dye and metabolite flux through purified Panx1 channels reconstituted in proteoliposomes demonstrates directly that molecules up to ~1 kDa are capable of permeating caspase cleavage-activated fPanx1. Moreover, anionic and cationic metabolites and dyes can traverse caspase-activated Panx1 channels, albeit with a marked preference for anionic molecules. These data validate caspase-activated Panx1 as a direct conduit for release of ATP and other signaling molecules that facilitate immunologically-silent cell clearance in the context of caspase-dependent cell death (apoptosis, pyroptosis) (Chekeni et al., 2010; Medina et al., 2020; Y. Qu et al., 2011; Yang et al., 2015).

Materials and Methods

Key Resources Table				
Reagent type (species) or resource	Designation	Source or reference	Identifiers	Additional information
gene (<i>Xenopus tropicalis</i>)	fPanx1	GenBank	NM_001130256.1	
gene (<i>Homo sapiens</i>)	hPANX1	GenBank	NM_015368.4	
Cell line (<i>Spodoptera frugiperda</i>)	Sf9	Expression Systems, Davis, CA	Parent cell line: IPLB-Sf-21-AE, RRID:CVCL_0518	clonal isolate derived from the parental cell line
Cell line (<i>Homo sapiens</i>)	HEK293T	ATCC	CRL-3216, RRID:CVCL_0063	Negative for mycoplasma contamination at ATCC (obtained from Kodi Ravichandran lab)
Biological sample (<i>Homo sapiens</i>)	Caspase-3	Kang et al.		

Antibody	Anti-human/mouse/rat Pannexin-1 (rabbit monoclonal)	Cell Signaling Technology	D9M1C, RRID:AB_28000167	1:1000 dilution
Chemical compound, drug	Brain PC	Avanti Polar Lipids	840053	
Chemical compound, drug	Brain Total Lipid Extract	Avanti Polar Lipids	131101	
Chemical compound, drug	Brain PI(4,5)P2	Avanti Polar Lipids	840046	
Chemical compound, drug	DPhPC	Avanti Polar Lipids	860337	
Chemical compound, drug	Sulforhodamine-B	Sigma Aldrich	S1402	
Chemical compound, drug	Rhodamine B	Sigma Aldrich	83689	
Chemical compound, drug	Dextran, Tetramethylrhodamine, 3000 MW,	ThermoFisher Scientific	D3307	

Chemical compound, drug	Alexa 594 Carboxylic Acid, tris salt	ThermoFisher Scientific	A33082	
Chemical compound, drug	Alexa 555 Carboxylic Acid, tris salt	ThermoFisher Scientific	A33080	
Chemical compound, drug	ATTO 550 Phalloidin	ATTO-TEC	AD 550-8	
Chemical compound, drug	α - ³² P-ATP	PerkinElmer	BLU003H250 UC	
Chemical compound, drug	³ H-Glutamate	PerkinElmer	NET490250UC	
Chemical compound, drug	³ H-Spermidine	PerkinElmer	NET522001MC	
Software, algorithm	LabView	Kiessling et al.		https://github.com/VolkerKirchheim/VK_TIRF_singlevesicleStep1

Pannexin 1 Expression

A cDNA encoding *Xenopus tropicalis* Pannexin 1 (fPanx1; Genscript-OXa25378, Accession NM_001130256.1) was inserted upstream of a thrombin protease cleavable linker (LVPRGS), enhanced green

fluorescent protein (eGFP), and a Strep II epitope (WSHPQFEK) in a modified pFastBacI vector (Invitrogen, Carlsbad, CA) by In-Fusion cloning (Takara Bio USA, Inc. Mountain View, CA). Briefly, a PCR amplicon containing fPANX1, with a 5' NotI and XhoI site at its 3' end was prepared using Pfu DNA polymerase and inserted into a modified pFastBacI vector that contained a unique XhoI site upstream of the thrombin proteolytic site. The Strep II tag was fused in frame to the C-terminus of eGFP. The construct was verified by DNA sequencing.

The Bac-to-Bac expression system (Invitrogen, Carlsbad, CA) was used to generate baculovirus for expression in *Spodoptera frugiperda* (Sf9) insect cells. Recombinant fPanx1-eGFP baculovirus was used to infect Sf9 insect cells grown at 27°C to a density of $2 \times 10^6 \text{ ml}^{-1}$, at a multiplicity of infection (MOI) of ~ 3 . Cells were collected 48 h after infection by low-speed centrifugation at 2,000 x g and stored at -80°C.

Pannexin 1 Protein Purification

To isolate membrane-localized fPanx1-eGFP, Sf9 cell pellets were resuspended in low salt buffer (50 mM HEPES, pH 7.5, 50 mM NaCl, 0.5 mM EDTA, with protease inhibitor cocktails (Roche, Basel Switzerland)) and lysed by Dounce homogenization (~ 30 strokes). Nucleic acids were digested by adding 2.5 mM MgCl_2 and ~ 12.5 units

of Benzonase (EMD Millipore, Burlington MA) per 1 ml lysate, with gentle stirring at 4°C for 10 min. Membranes were collected by ultracentrifugation at 100,000 x g and washed with stepwise Dounce homogenization again in low salt buffer and twice in high salt buffer (50 mM HEPES, pH 7.5, 1 M NaCl, 0.5 mM EDTA, with protease inhibitor cocktails). Pellets were isolated by ultracentrifugation at 100,000 x g between steps. Finally, membranes were resuspended (5 mL/g) in membrane freezing buffer (10 mM HEPES, pH 7.5, 20 mM KCl, 10 mM MgCl₂, and 40% glycerol), flash frozen, and stored at -80°C.

The frozen membrane pellet was thawed and solubilized at 4°C for 3 h with 1% (w/v) n-dodecyl-β-D-maltopyranoside (DDM; Anatrace, Maumee, OH) and 0.2% (w/v) cholesteryl hemisuccinate (CHS; Anatrace, Maumee, OH) in ~50 ml of buffer containing 50 mM HEPES, pH 7.5, 300 mM NaCl, 3 mM CaCl₂, 2.5% glycerol and protease inhibitor cocktails. Insoluble material was removed by ultracentrifugation at 100,000 x g, and the supernatant was incubated with ~1.0 ml of Strep-Tactin Superflow Plus resin (QIAGEN, Hilden, Germany) overnight at 4°C. The resin was packed in an Econo-column (1.0 x 10 cm; Bio-Rad, Hercules, CA) and washed with low salt buffer (50 mM HEPES, pH 7.5, 300 mM NaCl, 3 mM CaCl₂ and 0.2% DDM

with 0.04% CHS) for 20 column volumes/wash, high salt buffer (50 mM HEPES, pH 7.5, 1 M NaCl, 3 mM CaCl₂ and 0.05% DDM with 0.01% CHS), for 20 column volumes/wash, and eluted with 2.5 mM Desthiobiotin (Sigma-Aldrich, St. Louis, MO) in buffer (50 mM HEPES, pH 7.5, 500 mM NaCl, 3 mM CaCl₂ and 0.02% DDM with 0.004% CHS). The eluted protein was concentrated to ~500 μL using an 100kDa Amicon ultracel-100 centrifugal filter unit (EMD Millipore, Burlington MA). Preparative size-exclusion chromatography (SEC) was performed on a Superose 6 Increase 10/300 GL column (GE Healthcare, Chicago, IL) interfaced to an AKTA Purifier 10 FPLC system (GE Healthcare, Chicago, IL), equilibrated with buffer (50 mM HEPES, pH 7.5, 500 mM NaCl, 3 mM CaCl₂ and 0.02% DDM with 0.004% CHS). Fractions containing fPanx1-eGFP were collected and the protein was concentrated to ~2-3 mg ml⁻¹ using a 100 kDa Amicon ultracel-100 centrifugal filter unit and stored at 4°C for proteoliposome reconstitution, or snap frozen and stored at -80°C for lipid bilayer recordings.

Liposome Preparation and Reconstitution of Pannexin 1

Liposomes were prepared from lipids of the following composition: 70% brain phosphatidylcholine (PC), 15% total brain lipid extract, 14% cholesterol, 1% phosphatidylinositol 4,5-bisphosphate (PIP₂; all

from Avanti Polar Lipids, Alabaster, AL), with 40 μ l of methanol, dried under nitrogen flow with gentle agitation and then in a vacuum desiccator overnight. Dried lipids were resuspended in liposome buffer (20 mM Tris, 140 mM NaCl, pH 7.4), vortexed vigorously, incubated at room temperature for 45 minutes, and the lipid mixture was extruded at least 21 times through a LiposoFast-Basic extruder (Avestin Inc., Ottawa, Canada) with a 100 nm polycarbonate membrane. After extrusion, sodium cholate (3.9 mM final concentration) was added, and the solution was gently agitated for 3 hours. Purified detergent-solubilized fPanx1-eGFP (21.6 μ M) was added in a 1:1000 protein:lipid molar ratio and gently agitated for 1 hour at room temperature. Following protein incubation, the proteoliposome-containing solution was transferred to 10 kDa dialysis cassettes (Slide-A-Lyzer™; Thermo Scientific, Waltham, MA) and immersed in liposome buffer containing BioBeads (Bio-Rad, Hercules, CA) for detergent removal (5 L at 4 °C, with gentle stirring), first for 5 hours and then overnight at 4°C with fresh BioBead-containing liposome buffer. Proteoliposomes were collected by 100,000 x g spin for 60 minutes at 4°C and resuspended to 1 mL with liposome buffer and utilized immediately or snap frozen in liposome buffer containing 200 mM sucrose. After snap freezing in liquid N₂, liposomes were stored at -80°C until use. For dye uptake experiments, proteoliposomes were thawed at 4°C, diluted 10x in

liposome buffer, spun at 100,000 x g, and resuspended to desired volume.

Liposomes for radiolabeled metabolite uptake were prepared as previously described (Johnson & Lee, 2015). Briefly, the dried lipid mixture described above was resuspended in liposome buffer (20 mM Tris, 140 mM NaCl, pH 7.4), incubated at room temperature for 45 minutes, vortexed vigorously, and sonicated in cycles of 1 minute in a bath sonicator followed by 1 minute on ice until the solution was clear. Liposomes were incubated with 3.9 mM Na Cholate (Sigma-Aldrich, St. Louis, MO) and rotated for 1 hour under nitrogen. After addition of fPanx1-eGFP (1:1000 protein:lipid molar ratio), the mixture was rotated for 2-3 hours at room temperature under nitrogen. The proteoliposome-containing solution was transferred to 10 kDa dialysis cassettes (Slide-A-Lyzer™; Thermo Scientific, Waltham, MA) and immersed in liposome buffer containing BioBeads for detergent removal (5 L at 4°C, with gentle stirring), first for 5 hours and then overnight at 4°C with fresh BioBead-containing liposome buffer. Proteoliposomes were snap frozen in liquid N₂ and stored at -80°C until use.

Nycodenz Cofloatation Assay

Nycodenz cofloatation was performed as previously described (Hernandez et al., 2012). Briefly, 50 μ L proteoliposomes were mixed with 50 μ L 80% w/v Nycodenz in liposome buffer. A 50 μ L layer of 30% w/v Nycodenz solution was applied on top of the liposome-Nycodenz mixture, and an additional 50 μ L of liposome buffer layered on top. The density gradient was spun at 197,000 g for 90 minutes at 4°C in a TL-100 ultracentrifuge (TLS55 Rotor; Beckman-Coulter, Brea, CA). Upon completion, 20 μ L fractions were collected and analyzed via SDS PAGE and silver staining.

Gel Electrophoresis and Silver Staining

SDS PAGE gels (BioRad AnyKD™ Mini-PROTEAN® TGX™; BioRad, Hercules, CA) were run at 120 mV for 45 minutes and gels were fixed in 50 mL of 40% methanol solution containing 0.0185% formaldehyde, washed in DI water (2 x 5 minutes), immersed in 0.02% sodium thiosulfate solution (1 min), and washed again with in DI water (2 x 20 s). The gel was incubated in 50 mL of 0.1% silver nitrate solution for 10 minutes. The gel was quickly washed with 10 mL of DI water and then washed with 10 mL of thiosulfate developing solution (0.0185% formaldehyde, 28.3 mM sodium carbonate, and 0.0004% Sodium Thiosulfate). The gel was incubated in 50 mL of thiosulfate developing

solution until bands were visualized. A volume of 2.5 mL of 2.3 M citric acid was added for 10 minutes to stop developing. The gel was washed with water and imaged.

Negative Stain Electron Microscopy

For negative staining, 3.5 μ l of proteoliposomes were applied to a glow-discharged, carbon-coated, 300-mesh, copper grid (Electron Microscopy Sciences, Hatfield, PA) and stained with 2% uranyl acetate (Adair & Yeager, 2007). Low-dose EM was performed at the Molecular Electron Microscopy Core facility at UVA using a Tecnai F20 electron microscope (FEI, Hillsboro, OR), operating at 120 kV. Images were recorded at a nominal magnification of 29,000x and a defocus of 3 μ m using a 4 \times 4 K charge-coupled device camera (UltraScan 4000; Gatan, Pleasanton, CA), corresponding to a pixel size of 3.7 \AA on the specimen. Proteoliposome diameters were obtained using ImageJ (NIH, Bethesda, MD) from the average of two measurements per proteoliposome.

Caspase 3 purification

Recombinant Casp3 precursors were prepared as previously described (Kang et al., 2008). In brief, BL21(DE3) cells were transformed with the pro-Casp3 Δ 28/175TS deletion in pET-22b (+) vector and treated

with 1 mM IPTG (18 °C, 18 h). Cells were lysed using a microfluidizer, pro-Casp3 precursors were purified, and then activated by thrombin as previously described (Kang et al., 2008).

Western blotting

Proteoliposomes (25 μ L, 1:1000 protein:lipid ratio) were incubated with purified Casp3 (6 μ L, $k_{cat} = \sim 1.9 \pm 0.1$) and analyzed via SDS PAGE electrophoresis (BioRad AnyKD™ Mini-PROTEAN® TGX™; BioRad, Hercules, CA). Samples were transferred to 0.45 μ M nitrocellulose membranes (Perkin Elmer), which were blocked for 1 h at room temperature in 5% non-fat milk, 10 mM Tris, 150 mM NaCl, 0.1% Tween 20, pH 7.4 and then incubated overnight at 4°C with fPax1 antibody (Rabbit mAb #91137, 1:1000; Cell Signaling Technology, Danvers, MA). After 3 washes in a Tris-based buffer (10 mM Tris, 150 mM NaCl, 0.1% Tween 20, pH 7.4), the membranes were incubated with horseradish peroxidase-conjugated secondary antibody, (Na9340; Amersham, Little Chalfont, UK), immunoreactive signals were detected by enhanced chemiluminescence (Western Lightning Plus-ECL; PerkinElmer, Waltham, MA), and visualized using Amersham Hyperfilm ECL (GE Healthcare, Chicago, IL).

Planar Lipid Bilayer Recordings

Single-channel activity was evaluated in planar lipid bilayers using the Orbit mini system (Nanion Technologies, Munich, Germany). Briefly, Multi Electrode Cavity Array (MECA4) chips (Ionera, Freiburg, Germany) were filled with 150 μL of solution containing 200 mM KCl, 5 mM HEPES, and 0.2 mM EDTA; adjusted to pH 7.6. Lipid bilayers were formed by painting the chips with 10 mg/mL 1,2-diphytanoyl-sn-glycero-3-phosphocholine (DPhPC; Avanti Polar Lipids, Alabaster, AL) dissolved in octane. Purified fPanx1-eGFP (2-5 μL) was added at the cis (ground) side of the bilayer. After channel reconstitution, the current was recorded in a range of voltages (± 200 mV). Activity at extreme potentials (> 140 mV) was indicative of channel presence in the bilayer. Then, 2 μL of Casp3 (~ 0.4 mg/mL) was added to the cis side of the bilayer. After channel activation, Casp3 was gently washed out to keep symmetrical ionic composition on both sides of the bilayer. After treatment with caspase, the current was recorded again in a range of voltages (± 200 mV). Recordings were performed at 20 kHz using Element Data Recorder 3.8.0 software and further analyzed with Clampfit 10 software (Axon Instruments, San Jose, CA). Measurements were performed at 37°C using a temperature control unit (Nanion Technologies, Munich, Germany).

Whole Cell Recordings

Whole cell voltage clamp recordings of fPanx1 and hPANX1 were performed in transiently transfected HEK293T cells (ATCC, Manassas, VA. Cells were authenticated originally by ATCC STR profiling and negative for mycoplasma at time of purchase), as described previously (Chiu et al., 2017). In short, expression plasmids for fPanx1-eGFP or hPANX-TEV and TEV protease (1:3) (Sandilos et al., 2012), were transfected into HEK293T cells using Lipofectamine 2000 (Thermo Fisher Scientific, Waltham, MA). After 16-18 hours, whole cell recordings were performed at room temperature using borosilicate glass micropipettes (Harvard Apparatus, Holliston, MA) that were pulled on a P-97 puller (Sutter Instrument Company, Novato, CA) to a resistance of 3-5 M Ω and coated with Sylgard 184 (Dow Corning Corporation, Midland, MI). Recordings were obtained with an Axopatch 200B amplifier, a Digidata 1322 A board, and Clampex software (all Molecular Devices, San Jose, CA) with a HEPES-bath solution composed of (mM): 140 NaCl, 3 KCl, 2 MgCl₂, 2 CaCl₂, 10 HEPES and 10 glucose (pH 7.3) and an internal solution composed of (mM): 100 CsMeSO₄, 30 TEACl, 4 NaCl, 1 MgCl₂, 10 HEPES, 10 EGTA, 3 ATP-Mg, and 0.3 GTP-Tris (pH 7.3). Purified and activated Casp3 was added in the internal solution (2 μ g/mL) to cleave and activate fPanx1-eGFP before bath application of CBX (50 μ M). CBX-sensitive currents from

fPanx1-eGFP or hPANX-TEV were obtained from ramp voltage commands, and normalized to the peak current to compare current-voltage relationships of fPanx1-eGFP and hPANX-TEV.

Single Channel Recordings

We examined single channel activity of caspase-activated fPanx1-GFP in transfected HEK293T cells (as above). For inside-out patch recordings, Sylgard-coated patch pipettes were pulled to a DC resistance of 7-10 M Ω and filled with the HEPES-bath solution. After seal formation (≥ 10 G Ω) and patch excision, the bath solution was exchanged to an inside-out solution containing 150 mM CsCl, 5 mM EGTA, 10 mM HEPES, and 1 mM MgCl₂ (pH 7.3). Patches were held at +50 to +80 mV (Δ 10 mV), and only those patches that were silent initially after excision were used (i.e., those without native channel activities). Purified Casp3 was applied in the proximity of the patch to a final bath concentration of ~ 1 -2 μ g/ml. Stable steady-state channel activity was recorded ~ 5 -10 min after Casp3 addition before switching to an inside-out bath solution containing CBX (50 μ M). Channel amplitudes were obtained from all-points amplitude histograms at multiple patch potentials using Clampfit 10 (Molecular Devices).

ImageStream Flow Cytometry

Proteoliposomes (50 μ L) were incubated in liposome buffer with Casp3 (75 μ g/mL final) overnight at 4°C. SR-B dye was added to the reaction and incubated for 3 hours. The reaction was diluted to obtain a final SR-B concentration of 100 μ M prior to flow cytometry analysis. The entire mixture was loaded on to an Amnis ImageStream®^X MkII imaging flow cytometer (Luminex Corporation, Austin, TX). The 488 nm laser was used to capture eGFP signal and the 560 nm laser was used to capture Sulforhodamine-B. Amnis IDEAS® was utilized for data processing. A decrease in GFP fluorescence was used to verify caspase-mediated fPanx1-GFP cleavage for experiments included in the statistical analysis.

Dye Loading into Proteoliposomes

Proteoliposomes were filled with dye as previously described (Karasawa, Michalski, Mikhelzon, & Kawate, 2017). Briefly, fPanx1-containing proteoliposomes or empty liposomes (i.e., without fPanx1) were incubated with each dye: Sulforhodamine B, Rhodamine B, (all 1 mM; Sigma Aldrich, St. Louis, MO); Alexa 594 Carboxylic Acid, Alexa 555 Carboxylic Acid, Dextran Tetramethylrhodamine 3000 MW (all 1 mM; Thermo Fisher Scientific, Waltham, MA); ATTO 550 Phalloidin (25 μ M ATTO-TEC, Siegen, Germany), and loaded by 3 sequential freeze-

thaw cycles in liquid N₂ and room temperature water bath. After the final thaw, the mixture was extruded through a 100 nm extruder (T&T Scientific, Knoxville, TN). The proteoliposomes containing dye were eluted through a GE Healthcare PD MiniTrap column containing G-25 resin equilibrated with liposome buffer (GE Healthcare, Chicago, IL). The eluant was spun at 100,000 x g for one hour at 4°C. The proteoliposome/liposome pellet filled with dye was resuspended with cold liposome buffer.

TIRF Microscopy, Data Analysis of TIRF

A Zeiss AxioObserver Z1 fluorescence microscope (Carl Zeiss, Oberkochen, Germany) with a 63x water immersion objective (N.A.= 0.95) and a prism-based illumination was utilized. The light sources for excitation were an OBIS 488 LX and an OBIS 561 LS laser (Coherent Inc., Santa Clara, CA). An OptoSplit (Andor, Belfast, Northern Ireland) was used to separate two spectral fluorescence bands with band pass filters BP525/50 and BP607/70 (Idex-Semrock, Rochester, NY). Images were acquired every 10s with an EMCCD iXon DV887ESC-BV (Andor). Laser intensity, shutter, and camera were controlled by homemade software written in LabVIEW (National Instruments, Austin, TX). Custom chambers were filled with liposomes (1:1000

liposome:buffer dilution) and injected with Casp3 diluted in liposome buffer (to ~0.01 mg/mL).

Image series were analyzed by extracting the central pixel values from both spectral channels from regions of interests around each observed liposome by custom software written in LabVIEW (National Instruments; software has been made available:

https://github.com/VolkerKirchheim/VK_TIRFsinglevesicleStep1)

(Volker Kiessling, 2020; V. Kiessling, Crane, & Tamm, 2006). Efflux amounts were quantified by measuring the decrease of fluorescence intensity relative to the intensity before the onset of the decay and the background. Flux rates were determined by fitting mono exponential decay curves to the data starting at the onset of the decay over a range of 1200 s.

Bulk Dye Uptake Assay

Proteoliposomes (50 μ L) were incubated overnight with Casp3 (75 μ g/mL) at 4°C in liposome buffer (20 mM Tris pH 7.4, 140 mM NaCl). Dye (1mM SR-B) was added to the mixture (final volume 100 μ L) and gently agitated at 4°C for 3 h. CBX in liposome buffer was added to the liposome reaction (50 μ M, in 200 μ L final volume). The reaction was gently layered onto GE Healthcare PD MiniTrap columns containing G-

25 resin pre-equilibrated with liposome buffer containing 100 μM CBX (GE Healthcare, Chicago, IL). The column was spun at 1000 \times g for one minute at 4°C. The eluted liposomes were read on a FlexStation 3 Multi-Mode Microplate Reader (excitation 565 nm, emission 586 nm) (Molecular Devices, San Jose, CA).

Metabolite Uptake Assay

As previously described (Johnson & Lee, 2015), frozen liposomes were thawed on ice and subjected to three freeze/thaw cycles using liquid N_2 and a room temperature water bath. Following the third freeze/thaw cycle, liposomes were extruded through 1.0 μm polycarbonate membranes in a Mini-Extruder (Avanti Polar Lipids Inc., Alabaster, AL). Proteoliposomes (100 μL) were incubated overnight with Casp3 (~ 75 $\mu\text{g}/\text{mL}$) at 4°C in liposome buffer (20 mM Tris pH 7.4, 140 mM NaCl). We examined uptake of each of the potential permeants independently. For this, metabolites were added to caspase-treated proteoliposome mixtures to final concentrations of 1 mM ATP, 0.8 mM glutamate, 8 μM spermidine, together with 0.02 $\mu\text{Ci}/\mu\text{L}$ of ^{32}P -ATP, ^3H -Glutamate or ^3H -Spermidine (200 μL final volume; all from PerkinElmer, Waltham, MA). Note that we used a 100-fold lower final concentration of spermidine to avoid potential disruption of the proteoliposomes (Creutz, Hira, Gee, & Eaton, 2012)

and thus the hot:cold molar ratio for spermidine was ~100-fold greater than for glutamate. Following gentle agitation at room temperature for 3 h, the radioactive mixture was diluted with ice cold liposome buffer containing unlabeled metabolite at the relevant final concentrations (to 1 mL) and filtered through a Whatman GF/B filter pre-equilibrated with liposome buffer containing unlabeled metabolite. The filter was washed 3 times with ice cold liposome buffer containing unlabeled metabolite, immersed in 5 mL of Ecoscint A (National Diagnostics, Atlanta, GA) and read with a LS6500 Multipurpose Scintillation Counter (Beckman Coulter, Brea, CA).

Chemical Structures

All chemical structures were rendered in ChemDraw (Cambridgesoft, Cambridge, MA) with the base structures (carboxylic acids of Alexa 594 and Alexa 555, and the dextran conjugate of tetramethylrhodamine (Thermo Fisher Scientific; see Gebhardt, Lehmann, Reif, Zacharias, & Cordes, 2020); the precise site of the conjugate for these proprietary dyes was not provided so the figures depict approximate structures. The chemical structure of ATTO 550 Phalloidin was provided by ATTO-TEC.

Acknowledgements

This work was supported by P01 HL120840 (KSR, DAB, MY); R01 HL138241 (PQB); R01 GM099490 (JEC); R01 GM138532 (MY) and R01 HL48908 (MY); and P01 GM072694 (LKT) and R01 GM051329 (LKT). AKN was supported by F30 CA236370, T32 GM007267, and the University of Virginia Whitfield-Randolph Scholarship, and AKN and CBM were supported by T32 GM007055. YHC was supported by MOST 108-2320-B-007-007-MY2. The authors are grateful for sample preparation by Sandra Poulos, liposome preparation advice from Raghavendar Reddy Sanganna Gari and Patrick Seelheim, helpful early advice on liposome bulk dye uptake assays from Joseph A. Mindell (NINDS), and the University of Virginia flow cytometry core facility. The authors are grateful to Elizabeth Gonye, Keyong Li, and Yingtang Shi (Bayliss Laboratory) for helpful discussions and suggestions.

References

- Abascal, F., & Zardoya, R. (2012). LRRC8 proteins share a common ancestor with pannexins, and may form hexameric channels involved in cell-cell communication. *Bioessays*, *34*(7), 551-560. doi:10.1002/bies.201100173
- Adair, B. D., & Yeager, M. (2007). Electron Microscopy of Integrins. In *Integrins* (pp. 337-373).
- Bao, L., Locovei, S., & Dahl, G. (2004). Pannexin membrane channels are mechanosensitive conduits for ATP. *FEBS Lett*, *572*(1-3), 65-68. doi:10.1016/j.febslet.2004.07.009
- Baranova, A., Ivanov, D., Petrash, N., Pestova, A., Skoblov, M., Kelmanson, I., . . . Panchin, Y. (2004). The mammalian pannexin family is homologous to the invertebrate innexin gap junction proteins. *Genomics*, *83*(4), 706-716. doi:10.1016/j.ygeno.2003.09.025
- Bargiotas, P., Krenz, A., Hormuzdi, S. G., Ridder, D. A., Herb, A., Barakat, W., . . . Schwaninger, M. (2011). Pannexins in ischemia-induced neurodegeneration. *Proc Natl Acad Sci U S A*, *108*(51), 20772-20777. doi:10.1073/pnas.1018262108
- Beckel, J. M., Daugherty, S. L., Tyagi, P., Wolf-Johnston, A. S., Birder, L. A., Mitchell, C. H., & de Groat, W. C. (2015). Pannexin 1 channels mediate the release of ATP into the lumen of the rat urinary bladder. *J Physiol*, *593*(8), 1857-1871. doi:10.1113/jphysiol.2014.283119
- Billaud, M., Lohman, A. W., Straub, A. C., Looft-Wilson, R., Johnstone, S. R., Araj, C. A., . . . Isakson, B. E. (2011). Pannexin1 regulates alpha1-adrenergic receptor- mediated vasoconstriction. *Circ Res*, *109*(1), 80-85. doi:10.1161/CIRCRESAHA.110.237594
- Bravo, D., Ibarra, P., Retamal, J., Pelissier, T., Laurido, C., Hernandez, A., & Constandil, L. (2014). Pannexin 1: a novel participant in neuropathic pain signaling in the rat spinal cord. *Pain*, *155*(10), 2108-2115. doi:10.1016/j.pain.2014.07.024
- Chekeni, F. B., Elliott, M. R., Sandilos, J. K., Walk, S. F., Kinchen, J. M., Lazarowski, E. R., . . . Ravichandran, K. S. (2010). Pannexin 1 channels mediate 'find-me' signal release and membrane permeability during apoptosis. *Nature*, *467*(7317), 863-867. doi:10.1038/nature09413
- Chiu, Y. H., Jin, X., Medina, C. B., Leonhardt, S. A., Kiessling, V., Bennett, B. C., . . . Bayliss, D. A. (2017). A quantized mechanism for activation of pannexin channels. *Nat Commun*, *8*, 14324. doi:10.1038/ncomms14324

- Chiu, Y. H., Schappe, M. S., Desai, B. N., & Bayliss, D. A. (2018). Revisiting multimodal activation and channel properties of Pannexin 1. *J Gen Physiol*, *150*(1), 19-39. doi:10.1085/jgp.201711888
- Creutz, C. E., Hira, J. K., Gee, V. E., & Eaton, J. M. (2012). Protection of the membrane permeability barrier by annexins. *Biochemistry*, *51*(50), 9966-9983. doi:10.1021/bi3013559
- Dahl, G. (2015). ATP release through pannexon channels. *Philos Trans R Soc Lond B Biol Sci*, *370*(1672). doi:10.1098/rstb.2014.0191
- Deneka, D., Sawicka, M., Lam, A. K. M., Paulino, C., & Dutzler, R. (2018). Structure of a volume-regulated anion channel of the LRRC8 family. *Nature*, *558*(7709), 254-259. doi:10.1038/s41586-018-0134-y
- Deng, Z., He, Z., Maksaev, G., Bitter, R. M., Rau, M., Fitzpatrick, J. A. J., & Yuan, P. (2020). Cryo-EM structures of the ATP release channel pannexin 1. *Nat Struct Mol Biol*, *27*(4), 373-381. doi:10.1038/s41594-020-0401-0
- Farsi, Z., Preobraschenski, J., van den Bogaart, G., Riedel, D., Jahn, R., & Woehler, A. (2016). Single-vesicle imaging reveals different transport mechanisms between glutamatergic and GABAergic vesicles. *Science*, *351*(6276), 981-984. doi:10.1126/science.aad8142
- Gaete, P. S., Lillo, M. A., Lopez, W., Liu, Y., Jiang, W., Luo, Y., . . . Contreras, J. E. (2020). A novel voltage-clamp/dye uptake assay reveals saturable transport of molecules through CALHM1 and connexin channels. *J Gen Physiol*, *152*(11). doi:10.1085/jgp.202012607
- Gebhardt, C., Lehmann, M., Reif, M. M., Zacharias, M., & Cordes, T. (2020). Molecular and spectroscopic characterization of green and red cyanine fluorophores from the Alexa Fluor and AF series. *bioRxiv*. doi:10.1101/2020.11.13.381152
- Good, M. E., Chiu, Y. H., Poon, I. K. H., Medina, C. B., Butcher, J. T., Mendu, S. K., . . . Ravichandran, K. S. (2018). Pannexin 1 Channels as an Unexpected New Target of the Anti-Hypertensive Drug Spironolactone. *Circ Res*, *122*(4), 606-615. doi:10.1161/CIRCRESAHA.117.312380
- Good, M. E., Eucker, S. A., Li, J., Bacon, H. M., Lang, S. M., Butcher, J. T., . . . Isakson, B. E. (2018). Endothelial cell Pannexin1 modulates severity of ischemic stroke by regulating cerebral inflammation and myogenic tone. *JCI Insight*, *3*(6). doi:10.1172/jci.insight.96272
- Hernandez, J. M., Stein, A., Behrmann, E., Riedel, D., Cypionka, A., Farsi, Z., . . . Jahn, R. (2012). Membrane fusion intermediates

- via directional and full assembly of the SNARE complex. *Science*, 336(6088), 1581-1584. doi:10.1126/science.1221976
- Iglesias, R., Locovei, S., Roque, A., Alberto, A. P., Dahl, G., Spray, D. C., & Scemes, E. (2008). P2X7 receptor-Pannexin1 complex: pharmacology and signaling. *Am J Physiol Cell Physiol*, 295(3), C752-760. doi:10.1152/ajpcell.00228.2008
- Jin, Q., Zhang, B., Zheng, X., Li, N., Xu, L., Xie, Y., . . . Ye, S. (2020). Cryo-EM structures of human pannexin 1 channel. *Cell Res*, 30(5), 449-451. doi:10.1038/s41422-020-0310-0
- Johnson, Z. L., & Lee, S. Y. (2015). Liposome reconstitution and transport assay for recombinant transporters. *Methods Enzymol*, 556, 373-383. doi:10.1016/bs.mie.2014.11.048
- Kang, H. J., Lee, Y. M., Jeong, Y. J., Park, K., Jang, M., Park, S. G., . . . Chung, S. J. (2008). Large-scale preparation of active caspase-3 in *E. coli* by designing its thrombin-activatable precursors. *BMC Biotechnol*, 8, 92. doi:10.1186/1472-6750-8-92
- Karasawa, A., Michalski, K., Mikhelzon, P., & Kawate, T. (2017). The P2X7 receptor forms a dye-permeable pore independent of its intracellular domain but dependent on membrane lipid composition. *Elife*, 6. doi:10.7554/eLife.31186
- Kiessling, V. (2020). TIRF Single Vesicle. GitHub. Retrieved from https://github.com/VolkerKirchheim/VK_TIRFsinglevesicleStep1
- Kiessling, V., Crane, J. M., & Tamm, L. K. (2006). Transbilayer effects of raft-like lipid domains in asymmetric planar bilayers measured by single molecule tracking. *Biophys J*, 91(9), 3313-3326. doi:10.1529/biophysj.106.091421
- Lutter, D., Ullrich, F., Lueck, J. C., Kempa, S., & Jentsch, T. J. (2017). Selective transport of neurotransmitters and modulators by distinct volume-regulated LRRC8 anion channels. *J Cell Sci*, 130(6), 1122-1133. doi:10.1242/jcs.196253
- Ma, W., Compan, V., Zheng, W., Martin, E., North, R. A., Verkhratsky, A., & Surprenant, A. (2012). Pannexin 1 forms an anion-selective channel. *Pflugers Arch*, 463(4), 585-592. doi:10.1007/s00424-012-1077-z
- Medina, C. B., Mehrotra, P., Arandjelovic, S., Perry, J. S. A., Guo, Y., Morioka, S., . . . Ravichandran, K. S. (2020). Metabolites released from apoptotic cells act as tissue messengers. *Nature*, 580(7801), 130-135. doi:10.1038/s41586-020-2121-3
- Michalski, K., Syrjanen, J. L., Henze, E., Kumpf, J., Furukawa, H., & Kawate, T. (2020). The Cryo-EM structure of pannexin 1 reveals unique motifs for ion selection and inhibition. *Elife*, 9. doi:10.7554/eLife.54670

- Mou, L., Ke, M., Song, M., Shan, Y., Xiao, Q., Liu, Q., . . . Deng, D. (2020). Structural basis for gating mechanism of Pannexin 1 channel. *Cell Res*, 30(5), 452-454. doi:10.1038/s41422-020-0313-x
- Nielsen, B. S., Toft-Bertelsen, T. L., Lolansen, S. D., Anderson, C. L., Nielsen, M. S., Thompson, R. J., & MacAulay, N. (2020). Pannexin 1 activation and inhibition is permeant-selective. *J Physiol*, 598(2), 361-379. doi:10.1113/JP278759
- Panchin, Y., Kelmanson, I., Matz, M., Lukyanov, K., Usman, N., & Lukyanov, S. (2000). A ubiquitous family of putative gap junction molecules. *Curr Biol*, 10(13), R473-474. doi:10.1016/s0960-9822(00)00576-5
- Penuela, S., Gehi, R., & Laird, D. W. (2013). The biochemistry and function of pannexin channels. *Biochim Biophys Acta*, 1828(1), 15-22. doi:10.1016/j.bbamem.2012.01.017
- Poon, I. K., Chiu, Y. H., Armstrong, A. J., Kinchen, J. M., Juncadella, I. J., Bayliss, D. A., & Ravichandran, K. S. (2014). Unexpected link between an antibiotic, pannexin channels and apoptosis. *Nature*, 507(7492), 329-334. doi:10.1038/nature13147
- Qu, R., Dong, L., Zhang, J., Yu, X., Wang, L., & Zhu, S. (2020). Cryo-EM structure of human heptameric Pannexin 1 channel. *Cell Res*, 30(5), 446-448. doi:10.1038/s41422-020-0298-5
- Qu, Y., Misaghi, S., Newton, K., Gilmour, L. L., Louie, S., Cupp, J. E., . . . Dixit, V. M. (2011). Pannexin-1 is required for ATP release during apoptosis but not for inflammasome activation. *J Immunol*, 186(11), 6553-6561. doi:10.4049/jimmunol.1100478
- Romanov, R. A., Bystrova, M. F., Rogachevskaya, O. A., Sadovnikov, V. B., Shestopalov, V. I., & Kolesnikov, S. S. (2012). The ATP permeability of pannexin 1 channels in a heterologous system and in mammalian taste cells is dispensable. *J Cell Sci*, 125(Pt 22), 5514-5523. doi:10.1242/jcs.111062
- Ruan, Z., Orozco, I. J., Du, J., & Lu, W. (2020). Structures of human pannexin 1 reveal ion pathways and mechanism of gating. *Nature*, 584(7822), 646-651. doi:10.1038/s41586-020-2357-y
- Sandilos, J. K., Chiu, Y. H., Cheleni, F. B., Armstrong, A. J., Walk, S. F., Ravichandran, K. S., & Bayliss, D. A. (2012). Pannexin 1, an ATP release channel, is activated by caspase cleavage of its pore-associated C-terminal autoinhibitory region. *J Biol Chem*, 287(14), 11303-11311. doi:10.1074/jbc.M111.323378
- Siebert, A. P., Ma, Z., Grevet, J. D., Demuro, A., Parker, I., & Foskett, J. K. (2013). Structural and functional similarities of calcium homeostasis modulator 1 (CALHM1) ion channel with connexins,

- pannexins, and innexins. *J Biol Chem*, 288(9), 6140-6153.
doi:10.1074/jbc.M112.409789
- Silverman, W. R., de Rivero Vaccari, J. P., Locovei, S., Qiu, F., Carlsson, S. K., Scemes, E., . . . Dahl, G. (2009). The pannexin 1 channel activates the inflammasome in neurons and astrocytes. *J Biol Chem*, 284(27), 18143-18151.
doi:10.1074/jbc.M109.004804
- Syrjanen, J. L., Michalski, K., Chou, T. H., Grant, T., Rao, S., Simorowski, N., . . . Furukawa, H. (2020). Structure and assembly of calcium homeostasis modulator proteins. *Nat Struct Mol Biol*, 27(2), 150-159. doi:10.1038/s41594-019-0369-9
- Taruno, A. (2018). ATP Release Channels. *Int J Mol Sci*, 19(3).
doi:10.3390/ijms19030808
- Thompson, R. J. (2015). Pannexin channels and ischaemia. *J Physiol*, 593(16), 3463-3470. doi:10.1113/jphysiol.2014.282426
- Wang, J., Ambrosi, C., Qiu, F., Jackson, D. G., Sosinsky, G., & Dahl, G. (2014). The membrane protein Pannexin1 forms two open-channel conformations depending on the mode of activation. *Sci Signal*, 7(335), ra69. doi:10.1126/scisignal.2005431
- Wang, J., & Dahl, G. (2018). Pannexin1: a multifunction and multiconductance and/or permeability membrane channel. *Am J Physiol Cell Physiol*, 315(3), C290-C299.
doi:10.1152/ajpcell.00302.2017
- Wang, J., Ma, M., Locovei, S., Keane, R. W., & Dahl, G. (2007). Modulation of membrane channel currents by gap junction protein mimetic peptides: size matters. *Am J Physiol Cell Physiol*, 293(3), C1112-1119. doi:10.1152/ajpcell.00097.2007
- Weaver, J. L., Arandjelovic, S., Brown, G., S, K. M., M, S. S., Buckley, M. W., . . . Bayliss, D. A. (2017). Hematopoietic pannexin 1 function is critical for neuropathic pain. *Sci Rep*, 7, 42550.
doi:10.1038/srep42550
- Weilinger, N. L., Lohman, A. W., Rakai, B. D., Ma, E. M., Bialecki, J., Maslieieva, V., . . . Thompson, R. J. (2016). Metabotropic NMDA receptor signaling couples Src family kinases to pannexin-1 during excitotoxicity. *Nat Neurosci*, 19(3), 432-442.
doi:10.1038/nn.4236
- Yang, D., He, Y., Munoz-Planillo, R., Liu, Q., & Nunez, G. (2015). Caspase-11 Requires the Pannexin-1 Channel and the Purinergic P2X7 Pore to Mediate Pyroptosis and Endotoxic Shock. *Immunity*, 43(5), 923-932. doi:10.1016/j.immuni.2015.10.009
- Zhang, Y., Laumet, G., Chen, S. R., Hittelman, W. N., & Pan, H. L. (2015). Pannexin-1 Up-regulation in the Dorsal Root Ganglion

Contributes to Neuropathic Pain Development. *J Biol Chem*,
290(23), 14647-14655. doi:10.1074/jbc.M115.650218

CHAPTER 3

Stoichiometry and function of Pannexin 1 channels

The chapter is still in progress and will be submitted for publication:

Please note: Yu-Hsin Chiu (Bayliss Lab, now independent PI) made the concatemeric constructs, HEK293T Panx-KO cell line, and provided the methods for these respective parts of the chapter. I performed the electrophysiology using these reagents. Christopher Medina made the Jurkat T-cell Panx-KO cell line with assistance from Mahmut Parlak. Christopher Medina and Brady Baron (Ravichandran Lab) performed and analyzed the flow-cytometry data.

Abstract

Determining the oligomeric state of ion channels is crucial to understanding how they function and ultimately the larger signaling role they play. Pannexin 1 was thought to function as a hexamer until recently. In this chapter I use concatenated Pannexin 1 constructs in electrophysiology and flow cytometry experiments to decipher the functional oligomeric state of Pannexin 1.

Introduction

Pannexin 1 (Panx1) channels were initially predicted to be hexamers based on their topological homology to connexin channels (Ambrosi et al., 2010; Chiu et al., 2017; Panchin et al., 2000). Recent structural studies have now shown that Panx1 is likely a heptamer (Deng et al., 2020; Jin et al., 2020; Michalski et al., 2020; Mou et al., 2020; Qu et al., 2020; Ruan, Orozco, Du, & Lu, 2020). Determining the oligomeric

state of ion channels is difficult due to the homomeric nature of the monomers. Previous attempts to answer the oligomeric state of Panx1 have included negative-stain electron microscopy, single-molecule photobleaching using GFP-tagged protein, and structural studies of the channel using cryo-electron microscopy (Chiu et al., 2017). The first two of these methods suggested that the channel was a hexamer whereas new cryo-EM structures indicate that the channel is heptameric. Interestingly, functional studies from our group suggested that the channel could be functional as a hexamer as currents from hexameric concatemers were identical to monomers expressed in HEK293T cells (Boassa et al., 2007; Chiu et al., 2017; Penuela, Gehi, & Laird, 2013; Sosinsky et al., 2011). With these discrepancies we set out to determine whether Panx1 can function as a hexamer, heptamer, or both.

Chiu et al. utilized an elegant approach in which Panx1 subunits were concatenated to form higher order oligomers with the prediction that only a hexamer would form active channels (**Figure 3.1**) (Chiu et al., 2017). As predicted, dimeric, trimeric, and hexameric concatemers formed active channels; however, tetrameric concatemers did not form active channels (Chiu et al., 2017). Interestingly, hexameric concatemers that had all of their C-termini intact were inactive and

sequential removal of C-terminal tails resulted in a channel with progressively larger unitary conductance. In this chapter I present the concatemers with the following notation: #of subunits (# of C-terminal tails left intact). For example, a heptameric concatemer with all tails truncated is denoted as 7(0).

Recent structural studies have all concluded that the Panx1 channel is a heptamer (Deng et al., 2020; Jin et al., 2020; Michalski et al., 2020; Mou et al., 2020; Qu et al., 2020; Ruan et al., 2020). Numerous groups using two orthologues (*Xenopus tropicalis* and *Homo sapiens*) observed heptamers in both the full-length and C-terminal Caspase-3 cleavage site truncated constructs.

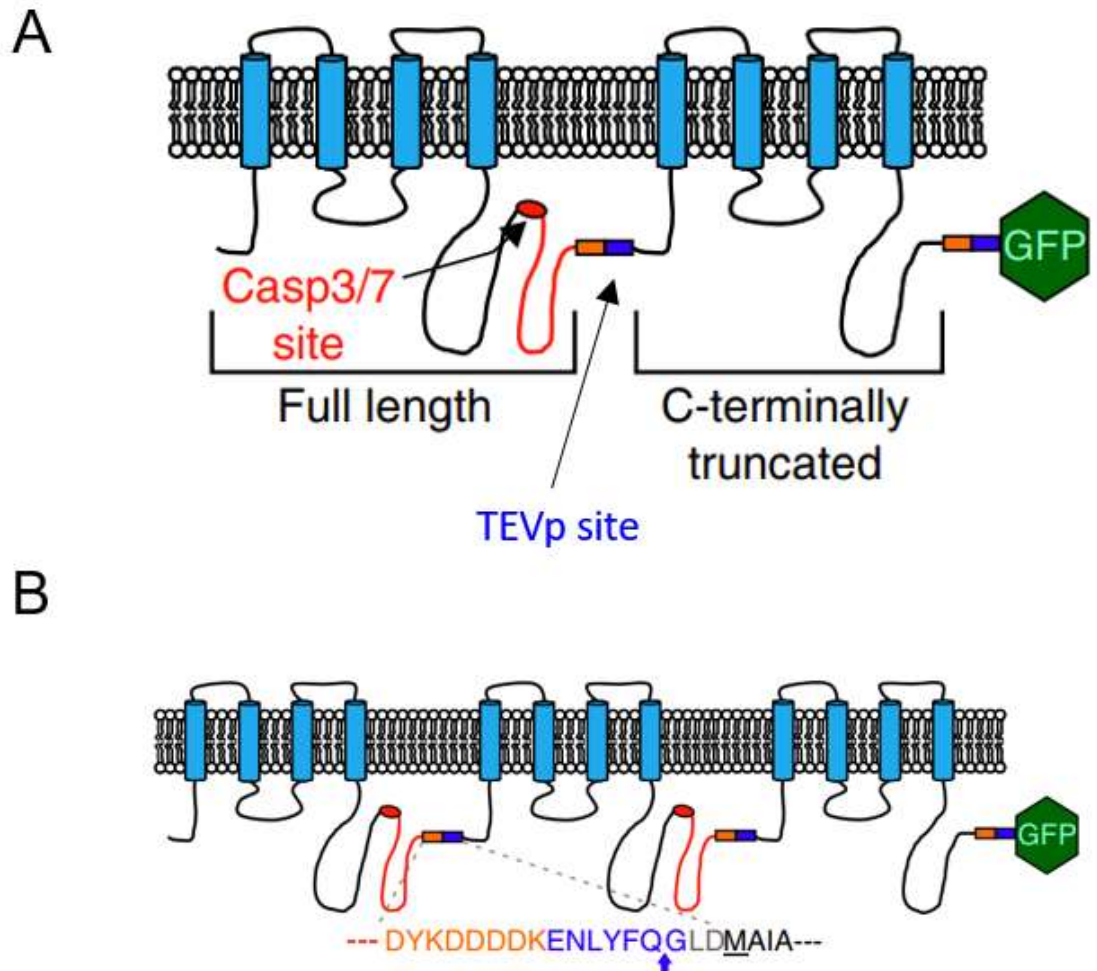


Figure 3.1 Concatemeric Constructs

Concatemeric construct for Panx1 was generated by Yu-Hsin Chiu. **A)** Each subunit in the concatemer is either full length or is truncated at the C-terminal caspase-cleavage site. Each construct has a GFP tag. **B)** Monomers are joined by a linker sequence which contains a TEV-protease cleavage sequence; cleavage at this site is required for activity, presumably to relieve a steric hindrance.

Further, both C-1 and C-7 symmetry imposed during model refinement results in a heptamer. C-1 symmetry models did not yield any hexameric 2D class averages.

With these unambiguous results from numerous structural groups our hexameric functional data are in clear contrast to the structural heptameric data. If the channel assembles as a heptamer, how is possible that our hexameric constructs are able to generate currents that resemble those of channels formed by expressing a monomer? We examine a few potential mechanisms by which this may occur: 1) In wild-type HEK293T an endogenous Panx1 subunit may incorporate into the transfected hexamer to actually form a heptamer; 2) Six subunits from one concatemer could combine to form a heptameric channel by borrowing one subunit from a second concatemer, leaving 5 subunits excluded; 3) both hexamers and heptamers are functional channels with very little electrophysiological differences.

To test these various possibilities, Yu-Hsin Chiu generated new concatemeric constructs (heptamers) and Panx1-KO HEK293T cells for electrophysiology studies (**Figure 3.2**). In addition, we also utilized Panx1-KO Jurkat T-cells and the different concatemeric constructs to explore dye uptake. Thus, these experiments examine both ionic currents and large molecule permeation which are each important

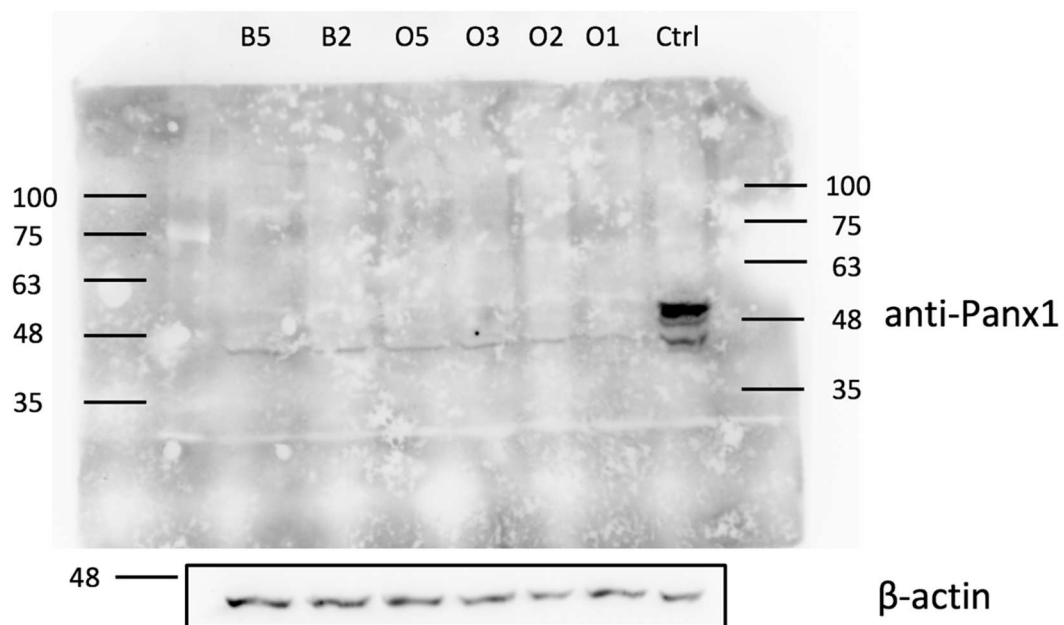


Figure 3.2 Western Blot of Panx1KO HEK293T Cells

Panx1KO HEK293T clones and a Cas9-expressing parental control cell line were tested for Panx1 expression. β -actin was used as a loading control. Clone B2 was used in our studies.

properties of Panx1 that may be differentially affected by channel subunit stoichiometry.

Results

For these studies, we used the Panx1 ortholog from *Homo sapiens* (i.e. human Panx1, hPANX1) that has been examined in recent structural studies (Deng et al., 2020; Jin et al., 2020; Mou et al., 2020; Qu et al., 2020; Ruan et al., 2020).

Pannexin 1 heptameric concatemers form functional ion channels

Currently, all functional data regarding the oligomeric state of hPANX1 has been from monomers that assemble into oligomeric channels of undefined stoichiometry. To determine if heptameric hPANX1 is functional, we expressed heptameric concatemers in HEK293T cells and activated the constructs with TEV-protease via the patch-pipette. The TEV-protease cleaves the TEV recognition sequence (ENLYFQG) within the linker that connects each monomer. As the monomers are released, a presumed steric constraint is relieved and the channel is functional. When TEV-protease is introduced to the cell via the patch pipette and not by transfection, ideally the protease will only activate channels that are in the cell membrane. The stoichiometry of the channel may change after the channel is embedded in the membrane, although this is less likely.

We transfected 4 concatemer constructs: 1) a hexamer with all tails intact [6(6)], 2) a hexamer with all tails deleted [6(0)], 3) a heptamer with all tails intact [7(7)], and 4) a heptamer with all tails deleted [7(0)]. As TEV-protease was perfused into the cell via diffusion from the patch-pipette, an outwardly-rectifying current slowly developed in 7(0)-expressing cells as constructs were activated by cleavage of the linkers (**Figure 3.3**). The 7(0) construct lacks C-termini on any of the subunits, so the constructs are expected to mimic a heptameric channel with all of its C-terminal tails cleaved. By contrast, while a current occasionally developed after TEV perfusion (>5 minutes) in cells expressing 7(7) channels (with all intact C-tails), this current was smaller than observed with in cells expressing 7(0) channels (**Figure 3.3**). For both 7(0) channels and 7(7) channels, the TEV-activated currents were CBX-sensitive and outwardly-rectifying, as also observed after caspase-cleavage of oligomeric Panx1 channels formed from wild-type monomeric Panx1 subunits. (**Figure 3.3**)

Hexameric and heptameric Pannexin 1 concatemers form functional ion channels in Panx1 KO HEK293T Cells

We postulated that perhaps 6(0) constructs were functional in wild-type HEK293T cells due to possible incorporation of an endogenous

HEK293 CELLS WITH ENDOGENOUS PANX1

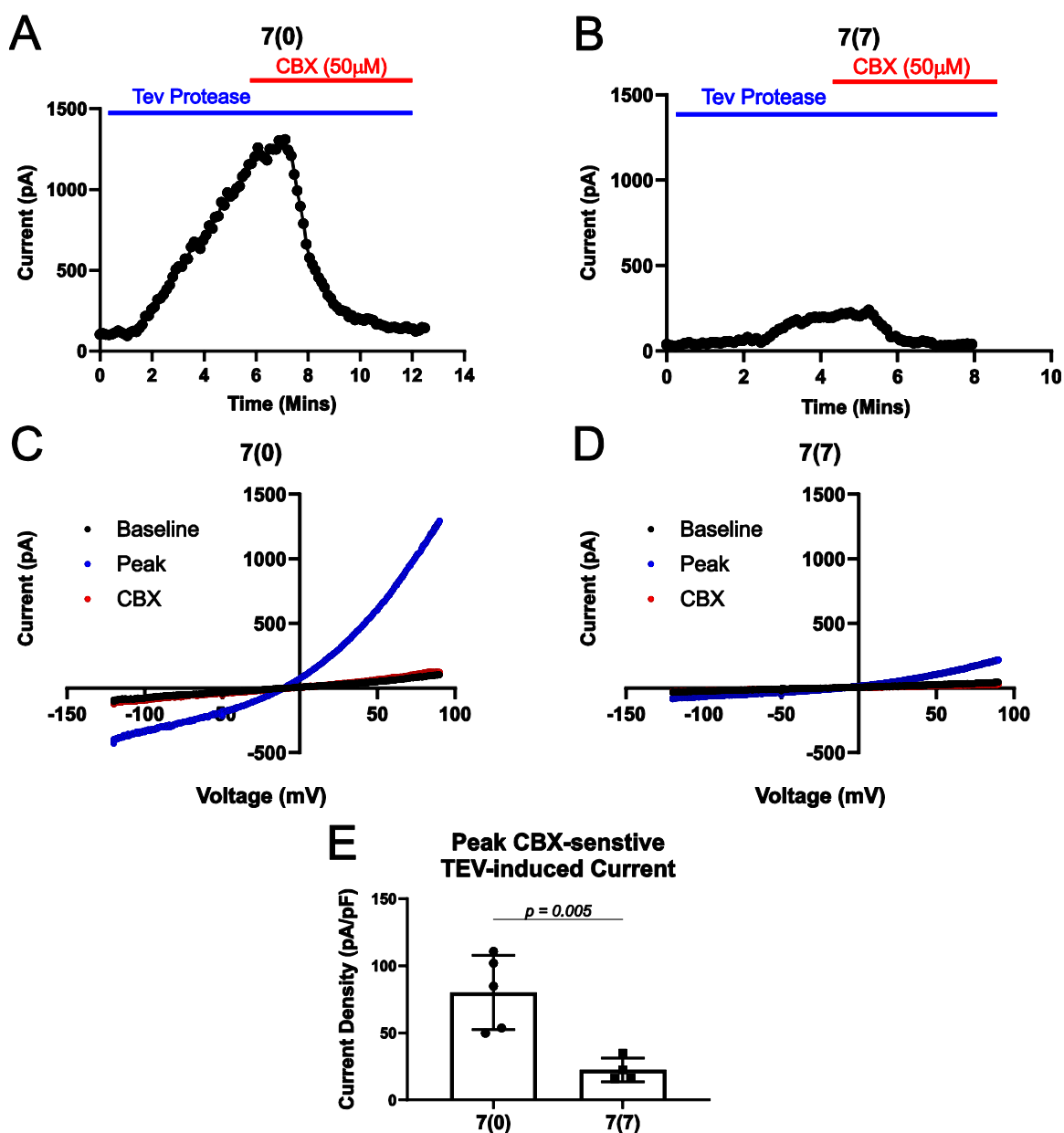


Figure 3.3 Heptameric Pannexin 1 Forms Functional Channels in wild-type HEK293T Cells

A) Time course of currents evoked from Panx1 7(0)-expressing cells after TEV-protease infusion via pipette solution. Current measurements were taken at +80mV. **B)** Time course of 7(7) after TEV-protease infusion via pipette solution. Current measurements were taken at +80mV. **C)** Current-

voltage trace of 7(0) displaying current at the beginning of the recording (baseline), peak current after TEV-protease infusion (Peak), and current after CBX inhibition (CBX). **D**) Current-voltage trace of 7(7) displaying current at the beginning of the recording (baseline), peak current after TEV-protease infusion (Peak), and current after CBX inhibition (CBX). **E**) Cumulative data of CBX-sensitive peak current (+80mV) for both 7(0) and 7(7). An unpaired t-test was performed ($p = 0.0054$). One outlier was removed from 7(7) using the Grubbs outlier test (Alpha = 0.05).

subunit. Therefore, we utilized a Panx1KO HEK293T cell line (**Figure 3.2**) which eliminates the possibility of endogenous subunit contribution. We performed a similar experiment as in (**Figure 3.3**) and transfected either 6(0), 6(6), 7(0), or 7(7) into our knockout cell line (**Figure 3.4, Figure 3.5**). We used WT HEK293T cells as our control and Cas9-containing HEK293T cells with guide RNAs to knock out hPANX1 (Panx1KO). Unsurprisingly, both 6(6) and 7(7) were silent and did not produce any current (**Figure 3.6**). To our surprise, both 6(0) and 7(0) constructs yielded nearly identical outwardly rectifying currents similar to currents observed when monomers are transfected and activated (Chiu et al., 2017).

HEK293 CELLS WITH NO ENDOGENOUS PANX1

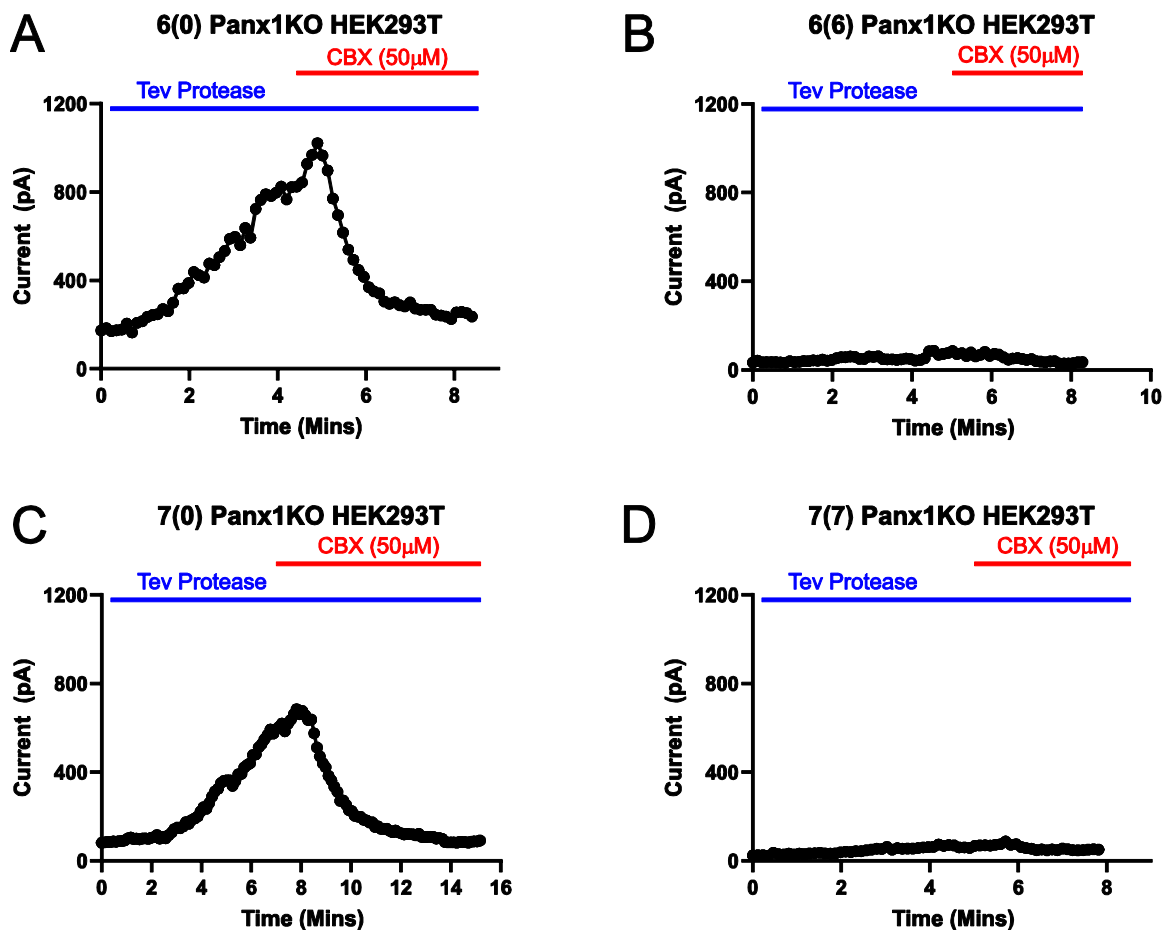


Figure 3.4 Hexameric Pannexin 1 Forms Functional Channels in Panx1KO HEK293T Cells

A) Time course of 6(0) after TEV-protease infusion via pipette solution. Current measurements were taken at +80mV. **B)** Time course of 6(6) after TEV-protease infusion via pipette solution. Current measurements were taken at +80mV. **C)** Current-voltage trace of 6(0) displaying current at the beginning of the recording (baseline), peak current after TEV-protease infusion (Peak), and current after CBX inhibition (CBX). **D)** Current-voltage trace of 6(6) displaying current at the beginning of the recording (baseline), peak current after TEV-protease infusion (Peak), and current after CBX inhibition (CBX).

HEK293 CELLS WITH NO ENDOGENOUS PANX1

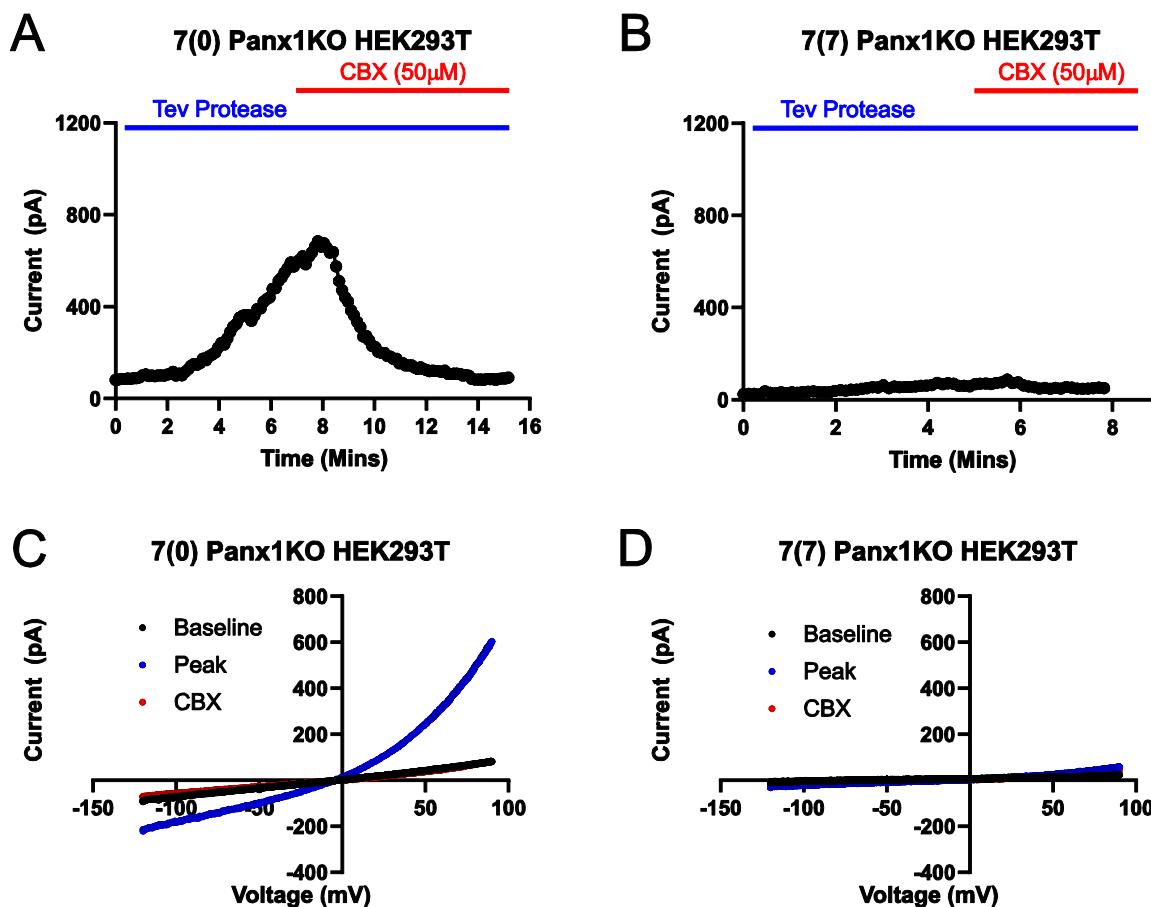


Figure 3.5 Heptameric Pannexin 1 Forms Functional Channels in Panx1KO HEK293T Cells

A) Time course of 7(0) after TEV-protease infusion via pipette solution. Current measurements were taken at +80mV. **B)** Time course of 7(7) after TEV-protease infusion via pipette solution. Current measurements were taken at +80mV. **C)** Current-voltage trace of 7(0) displaying current at the beginning of the recording (baseline), peak current after TEV-protease infusion (Peak), and current after CBX inhibition (CBX). **D)** Current-voltage trace of 7(7) displaying current at the beginning of the recording (baseline), peak current after TEV-protease infusion (Peak), and current after CBX inhibition (CBX).

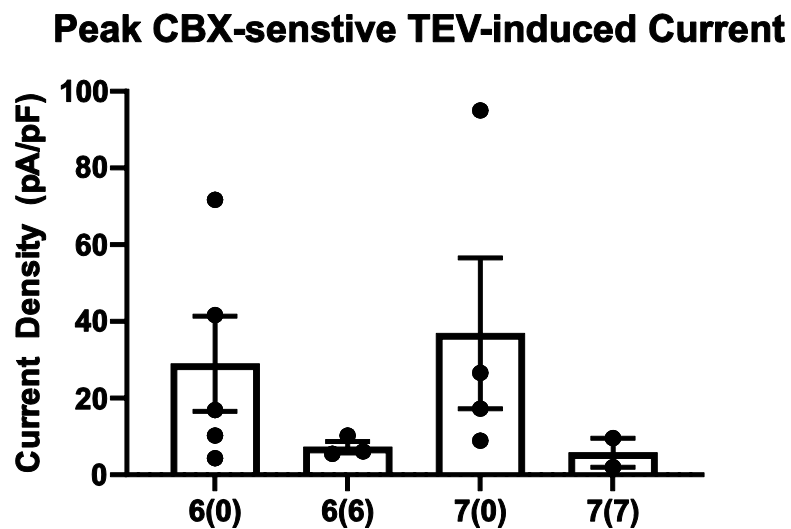


Figure 3.6 Both hexameric and heptameric Pannexin 1 concatemers form functional channels

Aggregate data of current density from whole-cell electrophysiology recordings in Panx1 deficient HEK293T cells. Peak current was recorded at +80mV and is shown as current density (Current/membrane capacitance). TEV-protease was perfused via the patch pipette.

Pannexin 1 heptameric concatemers permit dye flux

Large molecule flux is a unique property of Panx1 channels. In order to test whether our Panx1 concatemers permit dye flux, we employed Cas9-containing Jurkat T-cells without guide RNAs to ablate hPANX1 (Cas9) and the same cells containing guide RNAs to knock out hPANX1 (Panx1KO). We transfected 4 concatemeric constructs: 6(0), 6(6), 7(0), 7(7). Both Cas9 and Panx1KO Jurkat T-cells were transfected with either 6(0), 6(6), 7(0), 7(7). These cells were also transfected with or without a construct to express TEV-protease, and incubated with ToPro3. Cells were gated to exclude Annexin-V⁺ and 7-AAD⁺ cells (apoptotic) and gated to include GFP⁺ cells (cells containing GFP-tagged concatemer). Cells were gated to exclude these Annexin-V⁺ and 7-AAD⁺ populations because late apoptotic cells, necrotic cells, and pyroptotic cells lead to membrane permeabilization. Membrane permeabilization leads to nonspecific ToPro3 uptake through the membrane and not via Panx1 channels (Jiang et al., 2016). ToPro3 MFI (mean fluorescence intensity) was measured in cells (**Figure 3.7**). Each experiment was normalized to the GFP MFI to control for concatemer expression. Each concatemer has one GFP tag and a higher number of channels expressed will result in a higher GFP MFI. As expected, experiments where TEV was not transfected resulted in

no dye uptake. Under these conditions, the linkers were intact and therefore the channels were not activated (even those with all C-tails truncated). As previously demonstrated by Chiu et al. ToPro3 uptake was observed in control Cas9 cells for 6(0) (Chiu et al., 2017). Higher dye uptake was observed with the 7(0) construct. Predictably, no dye uptake was observed with the respective "uncleaved" 6(6) and 7(7) constructs. In Panx1KO cells, only 7(0) demonstrated dye uptake and these levels were at the levels of dye uptake in Cas9 cells. 6(0) dye uptake was negligible compared to controls. These results indicate that a hexamer likely does not form a functional channel that permits the uptake of a dye with ~670 dalton size whereas a heptameric channel does form a functional channel in this regard.

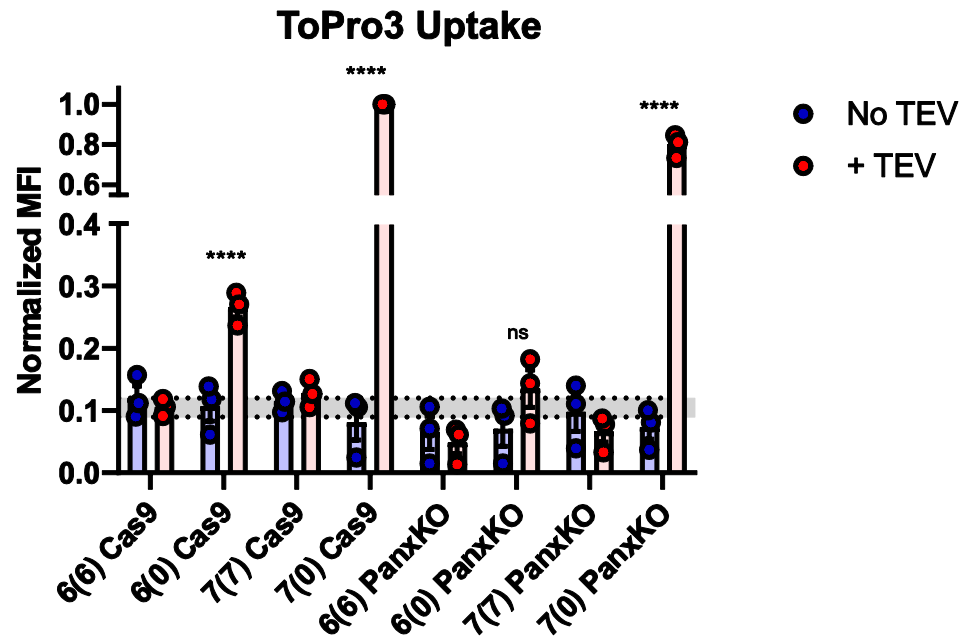


Figure 3.7 ToPro3 Uptake into Jurkat T-cells expressing Panx1 concatemeric constructs

Concatemeric constructs 6(0), 6(6), 7(0), or 7(7) were expressed in both Cas9 containing Jurkat T-cells or in Panx1KO Jurkat T-cells and ToPro3 MFI (mean fluorescence intensity) was measured via flow cytometry. ToPro3 MFI is presented as a fraction of the highest ToPro3 signal (7(0) + TEV in Cas9 cells). All experiments are normalized by GFP MFI to account for concatemer expression levels. Both 6(0) and 7(0) display ToPro3 uptake in Cas9 cells but only 7(0) has dye uptake in Panx1KO cells. A two-way ANOVA with Sidak's post-hoc test was performed (**** $p < 0.0001$, ns = not significant)

Discussion

The oligomeric state of Panx1 has been a puzzling issue after numerous groups reported structures of a heptameric channel. Our group had previously reported functional data on concatenated hexameric channels, including whole-cell recordings, single channel recordings, total internal reflection fluorescence (TIRF) microscopy photobleaching experiments, and low-resolution negative-stain electron microscopy (Chiu et al., 2017). After the structural studies were reported, we generated heptameric constructs for testing in our assays.

Heptameric concatemers yielded functional channels that resembled monomers expressed in WT HEK293T cells: large outwardly-rectifying currents that are carbenoxolone sensitive. However, we aimed to decipher if hexameric constructs are also active in a similar manner. In order to prevent potential contribution from endogenous subunits, we utilized a PanxKO HEK293T cell line. Even within these cells, both hexameric and heptameric constructs revealed nearly identical currents, suggesting that both hexameric and heptameric Panx1 channels form functional channels.

Surprisingly, hexameric concatemers did not permit dye flux in a PANX1-dependent manner in Panx1KO Jurkat T-cells, whereas heptameric concatemers did permit dye flux into cells. We are considering that there may be a delineation between atomic ion flux (patch-clamp) and large molecule flux (flow cytometry) between the two oligomeric states of the channel. This may be due to steric hindrance if, for example, the hexamer presents with a smaller pore that permits atomic ion flux but is not favorable for ToPro3 flux.

A second possible explanation for the observed differences in our two assays is that we perfused TEV-protease into the cell via the patch pipette in the electrophysiology recordings. In these dye uptake experiments, TEV-protease was expressed at the same time as the Panx1 concatemers. It is possible that the linkers in the Panx1 concatemer are cleaved before the channels reach the membrane and could account for the delineation between our electrophysiology and dye uptake flow cytometry data. The heptameric channel permits dye flux and cleavage of the linkers in the hexamer could result in reassembly into a heptamer (in similar fashion monomers expressed in cells assemble into heptamers based on structural data). Our data do not suggest that this occurs as the hexameric concatemer does not allow for ToPro3 uptake. The stability of the heptameric concatemer

even after linker cleavage during protein biogenesis may allow for normal trafficking to the membrane and channel function. It is possible that the hexameric concatemer is stable enough to traffic to the membrane and form a functional channel if the linkers are cleaved at the membrane, but the channel is unable to form a functional channel that can flux dye if the linkers are cleaved prior to the channel reaching the cell membrane. Further experiments will be necessary in order to determine the true functional oligomeric state(s) of the channel.

There are a few limitations and assumptions being made in this set of studies. One major assumption being made is that our concatenated constructs are remaining "intact" and trafficking to the membrane in the intended stoichiometry. We are aided by the fact that previous work by Chiu et al. show that hexameric concatemers with progressive C-terminal tail deletion had functional increases in unitary conductance (Chiu et al., 2017). We are limited in our flow cytometry assays by having to co-express the concatemeric construct and TEV-protease construct at the same time. We lose our ability to control when TEV-protease can cleave the inter-subunit linkers. Finally, we did not control for the different expression levels of concatemers in our electrophysiology studies beyond transfecting the same amount of

construct in each experiment. While we observe similar current densities in 7(0) and 6(0) constructs, these results may be confounded by varying expression levels.

Materials and Methods

Whole Cell Recordings

Whole cell voltage clamp recordings hPANX1 were performed in transiently transfected HEK293T cells (ATCC, Manassas, VA. Cells were authenticated originally by ATCC STR profiling and negative for mycoplasma at time of purchase), as described previously (Chiu et al., 2017). In short, expression plasmids for hPANX1 concatemers +/- mCherry, were transfected into HEK293T cells using Lipofectamine 2000 (Thermo Fisher Scientific, Waltham, MA) and incubated with 20 μ M Q-VD-OPh (Sigma Aldrich). After 16-18 hours, whole cell recordings were performed at room temperature using borosilicate glass micropipettes (Harvard Apparatus, Holliston, MA) that were pulled on a P-97 puller (Sutter Instrument Company, Novato, CA) to a resistance of 3-5 M Ω and coated with Sylgard 184 (Dow Corning Corporation, Midland, MI). Recordings were obtained with an Axopatch 200B amplifier, a Digidata 1322 A board, and Clampex software (all Molecular Devices, San Jose, CA) with a HEPES-bath solution composed of (mM): 140 NaCl, 3 KCl, 2 MgCl₂, 2 CaCl₂, 10 HEPES and 10 glucose (pH 7.3) and an internal solution composed of (mM): 100 CsMeSO₄, 30 TEACl, 4 NaCl, 1 MgCl₂, 10 HEPES, 10 EGTA, 3 ATP-Mg, and 0.3 GTP-Tris (pH 7.3). Purified TEV protease³ was added in the

internal solution (2 $\mu\text{g}/\text{mL}$) to activate concatemers before bath application of CBX (50 μM). CBX-sensitive currents were obtained from ramp voltage commands, and normalized to the peak current to compare current-voltage relationships.

Flow Cytometry

Five μg of concatemer and ten μg of human TEV protease cDNA was transfected into 10×10^6 jurkat cells using an electroporater for one pulse at 250mV for 25 msec in a 0.4cm cuvette (BioRad). After 10 minutes of incubation the cells were transferred to a well and incubated at 37°C overnight for 16-18 hours. The following day, cells were pelleted and resuspended in 250 μL of staining buffer (2.5 mM CaCl_2 , 140 mM NaCl, 10mM HEPES, 1 ng/mL (ThermoFisher), 1 μM ToPro3 (ThermoFisher), and 1:100 Annexin-V Pacific Blue (BioLegend). Cells were incubated for 15 minutes at room temperature and diluted with 250 μL of Annexin-V buffer (2.5 mM CaCl_2 , 140mM NaCl, and 10mM HEPES).

Cloning of hPANX1 2 \times sgRNA construct

A pLX-sgRNA-BfuAI-2k plasmid was a gift from Dr. Ren-Jang Lin (Addgene #112915) (Kurata & Lin, 2018). The plasmid was built to encode for two different small guide RNAs (sgRNAs) against the human

PANX1 gene. First, the blasticidin resistance gene of pLX-sgRNA-BfuAI-2k was replaced by a zeocin resistance gene, and an additional U6 promoter was subcloned into this plasmid (pLX-2×sgRNA). Oligonucleotides encoding complementary sequences of two small guide RNAs, targeting exon 1 of human PANX1 gene, were sequentially inserted into pLX-2×sgRNA at BsbI and BsmMI sites using T4 DNA ligase (New England BioLabs). The oligonucleotide sequences were AATCGAGATCTCCTGCGCGA and GATGGTCACGTGCATTGCGG. All constructs were verified by Sanger's sequencing.

Generation of PANX1-deleted HEK293T cell line

HEK293T cells stably expressing Cas9 nucleases and GFP proteins were purchased from GeneCopoeia (#SL502; Rockville, MD), and were cultured using DMEM containing 10% FBS, penicillin, streptomycin, sodium pyruvate, and puromycin (1 µg/mL; #A1113803; Thermo Fisher Scientific) at 37 °C with humidified air containing 5% CO₂. The cells were transfected with the abovementioned hPANX1 2×sgRNA plasmids using Transporter5 (#26008; Polysciences, Warrington, PA), following manufacturer's instruction. After 24 hr, transfected cells were selected in culture media supplemented with 400 µg/mL zeocin (Thermo Fisher Scientific) for more than 4 weeks. Individual clones of zeocin-resistant

HEK293T cells were generated by a serial dilution approach and PANX1 deletion of individual clones was verified by using immunoblotting.

Immunoblotting

HEK293T cells were lysed by using PBS containing 1% Triton X-100, 10 mM NaF, 10 mM NaVO₃, and a cocktail of protease inhibitors (#HY-K0010; MedChemExpress, NJ). Protein samples were separated by SDS-PAGE, transferred onto 0.2 μm PVDF membrane, blocked by 5% non-fat dry milk in a Tris-based buffer (10 mM Tris, 150 mM NaCl, and 0.1% Tween 20, pH 7.4) for 1 hr at room temperature, followed by probing with a rabbit anti-Panx1 antibody (1:1000, Cell Signaling #91137S) in the Tris-based buffer containing 5% BSA at 4 °C overnight with gentle shaking. HRP-conjugated goat anti-rabbit antibody (1:5000; Jackson ImmunoResearch #111-035-003) and T-Pro LumiLong Plus (T-Pro Biotechnology, Taiwan) were used to visualize chemoluminescent signals. Anti-β actin (1:5000; Sigma-Aldrich # A5441) and goat anti-mouse IgG-HRP (1:5000; Jackson ImmunoResearch #115-035-003) were used as a loading control. Images were taken by using ImageQuant LAS4000 Mini (GE Healthcare).

References

- Ambrosi, C., Gassmann, O., Pranskevich, J. N., Boassa, D., Smock, A., Wang, J., . . . Sosinsky, G. E. (2010). Pannexin1 and Pannexin2 channels show quaternary similarities to connexons and different oligomerization numbers from each other. *J Biol Chem*, *285*(32), 24420-24431. doi:10.1074/jbc.M110.115444
- Boassa, D., Ambrosi, C., Qiu, F., Dahl, G., Gaietta, G., & Sosinsky, G. (2007). Pannexin1 channels contain a glycosylation site that targets the hexamer to the plasma membrane. *J Biol Chem*, *282*(43), 31733-31743. doi:10.1074/jbc.M702422200
- Chiu, Y. H., Jin, X., Medina, C. B., Leonhardt, S. A., Kiessling, V., Bennett, B. C., . . . Bayliss, D. A. (2017). A quantized mechanism for activation of pannexin channels. *Nat Commun*, *8*, 14324. doi:10.1038/ncomms14324
- Deng, Z., He, Z., Maksaev, G., Bitter, R. M., Rau, M., Fitzpatrick, J. A. J., & Yuan, P. (2020). Cryo-EM structures of the ATP release channel pannexin 1. *Nat Struct Mol Biol*, *27*(4), 373-381. doi:10.1038/s41594-020-0401-0
- Jiang, L., Tixeira, R., Caruso, S., Atkin-Smith, G. K., Baxter, A. A., Paone, S., . . . Poon, I. K. (2016). Monitoring the progression of cell death and the disassembly of dying cells by flow cytometry. *Nat Protoc*, *11*(4), 655-663. doi:10.1038/nprot.2016.028
- Jin, Q., Zhang, B., Zheng, X., Li, N., Xu, L., Xie, Y., . . . Ye, S. (2020). Cryo-EM structures of human pannexin 1 channel. *Cell Res*, *30*(5), 449-451. doi:10.1038/s41422-020-0310-0
- Kurata, J. S., & Lin, R. J. (2018). MicroRNA-focused CRISPR-Cas9 library screen reveals fitness-associated miRNAs. *RNA*, *24*(7), 966-981. doi:10.1261/rna.066282.118
- Michalski, K., Syrjanen, J. L., Henze, E., Kumpf, J., Furukawa, H., & Kawate, T. (2020). The Cryo-EM structure of pannexin 1 reveals unique motifs for ion selection and inhibition. *Elife*, *9*. doi:10.7554/eLife.54670
- Mou, L., Ke, M., Song, M., Shan, Y., Xiao, Q., Liu, Q., . . . Deng, D. (2020). Structural basis for gating mechanism of Pannexin 1 channel. *Cell Res*, *30*(5), 452-454. doi:10.1038/s41422-020-0313-x
- Panchin, Y., Kelmanson, I., Matz, M., Lukyanov, K., Usman, N., & Lukyanov, S. (2000). A ubiquitous family of putative gap junction molecules. *Curr Biol*, *10*(13), R473-474. doi:10.1016/s0960-9822(00)00576-5

- Penuela, S., Gehi, R., & Laird, D. W. (2013). The biochemistry and function of pannexin channels. *Biochim Biophys Acta*, 1828(1), 15-22. doi:10.1016/j.bbamem.2012.01.017
- Qu, R., Dong, L., Zhang, J., Yu, X., Wang, L., & Zhu, S. (2020). Cryo-EM structure of human heptameric Pannexin 1 channel. *Cell Res*, 30(5), 446-448. doi:10.1038/s41422-020-0298-5
- Ruan, Z., Orozco, I. J., Du, J., & Lu, W. (2020). Structures of human pannexin 1 reveal ion pathways and mechanism of gating. *Nature*, 584(7822), 646-651. doi:10.1038/s41586-020-2357-y
- Sosinsky, G. E., Boassa, D., Dermietzel, R., Duffy, H. S., Laird, D. W., MacVicar, B., . . . Dahl, G. (2011). Pannexin channels are not gap junction hemichannels. *Channels (Austin)*, 5(3), 193-197. doi:10.4161/chan.5.3.15765

CHAPTER 4

Conclusions and Future Studies

In this dissertation, I have presented two new sets of data which have advanced our understanding of Pannexin 1 channels. Each chapter was presented with a discussion and conclusions. In this chapter, I will evaluate these conclusions, expand on them, and suggest future experimental studies to continue these projects.

Permeation properties and selectivity of Pannexin 1

Prior to starting our studies on the permeation properties and metabolite permeation of Panx1 channels, the field of Pannexin biology vastly disagreed on whether caspase-activated Panx1 channels were responsible for the flux of large signaling metabolites (Bao, Locovei, & Dahl, 2004; Chekeni et al., 2010; Lutter, Ullrich, Lueck, Kempa, & Jentsch, 2017; Medina et al., 2020; Siebert et al., 2013; Taruno, 2018). In fact, some members of the field were unsure if Panx1 was an ion channel that displayed any form of selectivity (Chiu, Ravichandran, & Bayliss, 2014; Deng et al., 2020; Ma et al., 2012; Michalski et al., 2020; Nielsen et al., 2020; Nomura et al., 2017; Ruan, Orozco, Du, & Lu, 2020; Wang & Dahl, 2018). Understanding if

the channel can form a conduit for the flux of large signaling metabolites with any resemblance of charge preference is paramount to understanding the role it plays in a larger biological picture. We have answered outstanding questions in the field using simple, reduced approaches.

Purified Pannexin 1 Protein is an electrophysiologically active channel

With assistance from the Yeager lab, we were able to purify recombinant Panx1 which was required for implementing our proteoliposome system. In order to evaluate the electrical properties of the channel, we performed planar lipid bilayer recordings. Panx1 was incorporated into DPhPC (1,2-diphytanonyl-sn-glycero-3-phosphocholine) bilayers and activated with purified Caspase-3. Panx1 was silent prior to activation. Interestingly, recent reports have suggested that a side tunnel may be responsible for a basal current observed by two groups (Mou et al., 2020; Ruan et al., 2020). We observed no basal current with our channels and only observed current after activating the channel with caspase. Our experiments are very similar to data from fPanx1 and hPANX1 from cell expression systems. Surprisingly, we observed that purified *Xenopus* Panx1 has two conductance states. One state (100pS) is similar to the conductance

observed in heterologous expressed Panx1, whereas a second state (~189pS) was higher than our group's previous observations (Chiu et al., 2017). A few possible reasons for this are that 1) certain lipids (PIP₂ or cholesterol) may be required for physiologic regulation of the channel (Hilgemann, Feng, & Nasuhoglu, 2001; Karasawa, Michalski, Mikhelzon, & Kawate, 2017; Levitan, Singh, & Rosenhouse-Dantsker, 2014; Poveda et al., 2014; H. Zhang, He, Yan, Mirshahi, & Logothetis, 1999), 2) accessory proteins play a role in channel modulation and those are not present in the liposome system (Buraei & Yang, 2010; Li, Um, & McDonald, 2006; J. Zhang, Bal, Bierbower, Zaika, & Shapiro, 2011), and 3) these conductance states may be a consequence of the symmetrical recording solutions used in these experiments. It is possible that asymmetrical solutions in cell-based recordings may lead to the single conductance state that was found in those experiments (Bao et al., 2004; Chiu et al., 2017; Good et al., 2018; Locovei, Wang, & Dahl, 2006; Romanov et al., 2012).

Panx1 forms a dye-permeable pore

Our proteoliposome approach presented in this paper, established a biochemically reduced system that permits control of ions, lipids, proteins, and other molecules. Our proteoliposomes were composed of brain PC, cholesterol, PI(4,5)P₂, and brain polar lipid extract. In this

lipid environment, Panx1 formed a dye-permeable pore in a Caspase-3 activation-dependent manner. Performing these experiments in an isolated system allows us to conclude that Panx1 does indeed form a pore for dye to flux through and that some secondary mechanism is not required for the dye uptake that was observed in cells. In short, Panx1 is sufficient and necessary for dye uptake in Panx1-dependent dye flux experiments. Panx1 does not require any accessory proteins, at least in our system, for this activity.

Panx1 prefers anionic large molecule permeants

The majority of our experiments were performed with Sulforhodamine B (SR-B), an anionic dye that has a molecular mass of 559 daltons. We performed experiments with dye fluxing into the liposomes by adding dye outside the liposomes. To test if dye flux can occur in the opposite direction, we pre-filled liposomes with dye and activated the channel with caspase. The dye fluxed through the channel in this direction as well. Utilizing a TIRF-based assay we tested dyes of various sizes and charges for flux rates through Panx1. One advantage of using this TIRF system is that we can measure dye flux from individual liposomes. By fitting the exponential decay of dye signal from each liposome (when the liposome was activated to when dye flux stopped), we were able to calculate the rate at which dye fluxed through Panx1. We were not

able to control for the number of channels within each liposome, but the distribution of decrease in GFP fluorescence (indicating C-tail cleavage and channel activation) was similar across all conditions. We found that small, anionic dyes, such as SR-B, flux through the channel faster than not only larger anionic dyes (880, 980 daltons) but also faster than a small cationic dye (\sim 480 daltons). Finally, we found that a dye of \sim 1300 daltons was unable to flux through the activated channel.

Pannexin 1 is a metabolite channel

Panx1 has canonically been dubbed an ATP channel (Bao et al., 2004; Beckel et al., 2015; Chekeni et al., 2010; Lutter et al., 2017; Medina et al., 2020; Siebert et al., 2013; Taruno, 2018). Utilizing our proteoliposome system, we were able to clearly demonstrate that ATP does indeed flux directly through activated Panx1 channels. Previously, ATP release through Panx1 was correlated with Panx1 activation. This did not preclude the possibility that ATP was being released via a secondary mechanism. However, we show that Panx1 is not only an ATP channel but also a conduit for other important signaling metabolites such as glutamate and spermidine. Implications of Panx1 being critical during inflammation and apoptosis suggest that its role in “good-bye” signals and “find-me” signals is tightly regulated. Further,

when we evaluated ATP and spermidine flux in tandem, both metabolites fluxed through the channel albeit at lower levels compared to when they were tested individually. In the complex environment of a cell where Panx1 is activated, numerous atomic ions and metabolites are likely permeants. Understanding the preferential selectivity of Panx1 and release of these metabolites needs to be explored in future experiments. In conclusion, we have shown that a caspase-activated Panx1 channel is able to permit ATP and other large metabolite flux.

Suggested Future Experiments

1) Test activation dependent selectivity of Pannexin 1

There are numerous methods of activating Panx1 (see introduction). Two highly characterized methods of activation are GPCR-mediated activation of the channel (reversible posttranslational modification) and caspase-mediated activation (irreversible modification) of the channel. These two modes of activation render Panx1 with two sets of properties: 1) GPCR-activated Panx1 has a smaller mean open time (1.3 ms) and the channel opens and closes far more frequently, 2) caspase-activated Panx1 has longer mean open times (7.9 ms) and the channel does not open and close as frequently. However, the unitary conductance of the two differentially activated channels is

nearly identical. It is possible that the same channel with two sets of channel properties depending on the mode of activation, can permit the flux of different permeants. Shorter open times may only permit smaller permeants and longer open times may allow for flux of bulkier permeants that take more time to flux through the conduit. One possible way to test GPCR-mediated activation of the channel is to modify the channel to mimic posttranslational modifications such as phosphorylation or deacetylation (unpublished data). These experiments can be performed by purifying a GPCR-activation mimetic channel (serine to aspartic acid mutations) that is incorporated into proteoliposomes and tested across an array of permeants alongside wild-type Panx1 proteoliposomes that are activated by caspase as presented in this dissertation. Some limitations with this method are that the mutation may render the channel to have longer open times than a naturally activated channel. One potential way to address this limitation is to follow the concatemer approach described previously, except in this case the posttranslational modification is made rather than a C-terminal tail deletion.

2) Test atomic ion selectivity of Pannexin 1

In the present studies, we have only tested large molecule permeants of Panx1. Via patch-clamp studies, we know that Panx1 is active via

whole-cell recordings and single-channel recordings when one C-terminal tail (in a hexameric concatemer) is cleaved; however, dye uptake and ATP release were not observed (Chiu et al., 2017). Due to difficulties in conventional impermeant ion replacement and observing E_{rev} changes, using our proteoliposome system offers advantages for testing atomic ion permeation. Specific ion sensitive dyes can be filled into proteoliposomes (for calcium, chloride, sodium, and potassium) and these ions can be added into the extraliposomal bath solution. Caspase-3 can be added to the reaction and fluorescence of the reaction can be recorded to observe atomic ion flux. One advantage of this method is that we can carefully select the presence or absence of specific ions and their concentration in the reaction. These experiments will allow us to evaluate the atomic ion selectivity of Panx1. We currently understand large molecule flux, but understanding the atomic ion flux will be important to understanding other Panx1 signaling mechanisms.

3) Refinement of Pannexin 1 Permeants

In our initial studies, we only tested a few predicted metabolite permeants in our assays (ATP, glutamate, and spermidine). Medina et al. have reported certain metabolites that they did not find released from apoptotic cells in a Panx1-activation dependent manner (Alanine,

pyruvate, and creatinine) (Medina et al., 2020). In these experiments, differential release of metabolites in live cells or during apoptosis was tested in WT Jurkat T-cells, dominant negative Panx1 Jurkat T-cells (Caspase-3 site was mutated such that it could not be cleaved), or WT Jurkat T-cells treated with a Panx1 inhibitor. We have now tested alanine in our proteoliposome flux assay. Our initial observations suggest that alanine (neutral, 89 daltons) does not flux through activated Panx1 channels (**Figure 4.1**). This result is quite peculiar as it suggests that the channel has further mechanisms of permeant selectivity than just size or charge. A few neutral metabolites are predicted to flux through the channel, so the mechanism by which the channel differentiates between these various metabolites remains elusive (Medina 2020). Testing metabolites of various sizes and charges will allow us to refine our understanding of the molecular weight, shape, and charge of molecules capable of fluxing through Panx1. Further, we have not performed any kinetic analysis with radiolabeled metabolite uptake experiments. Fluorescent dyes are surrogates used for experimental convenience, but exploring differential permeation rates between cationic and anionic metabolites will provide more physiologically relevant data about the flux of

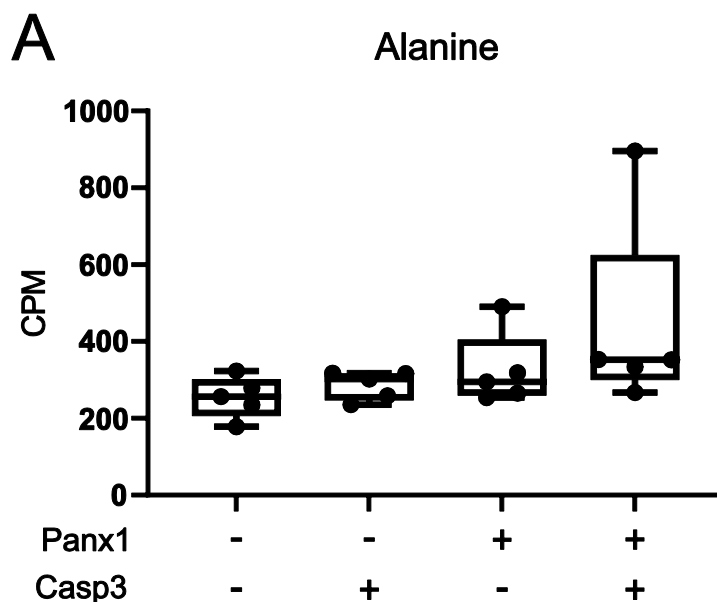


Figure 4.1 Alanine may not flux through Pannexin 1

A) Liposomes were incubated recombinant Casp3 overnight at 4°C before incubation with with 4 μ Ci of [3 H]-Alanine (0.8mM; \sim 1:2000) for 3 h and filtered using a Whatman GF/B filter (n = 5). Statistical analysis was performed by repeated-measures one-way ANOVA $F_{3,16} = 2.095$, $p = 0.2187$; and no significance is present between groups using Tukey's multiple comparisons tests.

metabolites out of cells during apoptosis and other contexts during which Panx1 is activated by C-terminal tail cleavage. These kinetic experiments can be performed by combining different isotopes of radiolabeled metabolites (similar to **Figure 2.17**) while also utilizing a time course to determine metabolite flux rates. Finally, Panx1 is activated in a quantized manner as each successive C-terminal tail is cleaved (Chiu et al., 2017). If these concatemeric constructs can be purified and incorporated into proteoliposomes, we may be able to artificially capture “snapshots” of Panx1 at various stages of activation to determine its ability to flux atomic ions and larger molecules with each successive C-terminal tail cleavage. For example, early on during apoptosis, fewer C-tails may be cleaved and a set of “early” signaling metabolites may be released compared to later on in apoptosis when almost all C-tails are cleaved and a set of “late” signaling may be released.

Stoichiometry and function of Pannexin 1 channels

Pannexin 1 was predicted to be a hexamer until quite recently (Ambrosi et al., 2010; Chiu et al., 2017; Panchin et al., 2000). With the recent publication of numerous structural studies indicating that Panx1 is a heptamer (Deng et al., 2020; Jin et al., 2020; Michalski et al., 2020; Mou et al., 2020; Qu et al., 2020; Ruan et al., 2020), determining whether the channel can function as both a hexamer in certain contexts or is only functional as a heptamer is important to understanding channel assembly and function. Other channels are known to function with different stoichiometric states compared to members of their channel family or as heteromers (Demura et al., 2020; Naulin et al., 2020; Syrjanen et al., 2020).

Pannexin 1 is functional as both a hexamer and heptamer

First, we utilized heptameric concatemers and found that they were functional in wild-type HEK293T cells. The channel exhibits outwardly rectifying currents similar to both hexameric concatemers and to monomers expressed in HEK293T cells. Previous studies found that hexameric concatemers are also active in wild-type cells (Chiu et al., 2017). In order to prevent any potential contribution from endogenous Panx1 subunits, we utilized Panx1KO HEK293T cells. Surprisingly both

hexameric and heptameric channels were active in these cells also. In light of the heptameric structure reported by numerous groups, we predicted that hexameric channels may not be active in Panx1KO cells. However, both constructs were active and can form functional channels. Next, we utilized both hexameric and heptameric constructs to test dye uptake in Jurkat T-cells using flow cytometry. Surprisingly, we found that both 6(0) and 7(0) permitted dye uptake in Cas9 control cells, but only 7(0) allowed for dye uptake in Panx1KO Jurkat T-cells. This difference observed in patch-clamp experiments and flow cytometry experiments suggests that both 6(0) and 7(0) form channels that permit atomic ion flux, but possibly not large dye flux. Dye flux was found in experiments in wild-type Jurkat-T cells; however, the presence of an endogenous subunit does not preclude the possibility of forming a 7(1) channel (Chiu et al., 2017). Further experiments are needed in order to determine if the channel is physiologically a hexamer or heptamer and what conditions drive the oligomeric state.

Suggested Future Experiments

1) Single channel recordings of hexameric and heptameric concatemers

Determining the single channel properties of these two constructs compared to monomeric channels expressed in Panx1KO cells will allow us to determine if the monomeric channel is more similar to a hexameric channel or heptameric channel. Single channel properties such as open probability, mean open time, and channel conductance may allow us to conclude what the oligomeric state of the channel is physiologically. However, hexameric concatemers were identical to monomers which assembled into an oligomer of unknown stoichiometry (Chiu et al., 2017). We may find that heptamers and hexamers are indistinguishable from channels assembled from monomeric expression. In this case, it is possible that the channel can function as both a 6-mer and a 7-mer. Further experiments will be necessary to visualize if monomeric channels assemble into hexamers or heptamers.

2) Perform Atomic Force Microscopy with Purified Panx1 Channels

Currently, all of the structural data that has been published has relied on cryo electron microscopy (cryo-EM) or negative-stain electron microscopy. These are powerful techniques with a few technical limitations. High resolution structure determination relies on the averaging of many particles. It is possible that hexamers are formed and functional, but in a very low number and therefore are not

classified into a class average. Atomic force microscopy (AFM) allows for the imaging of single particles, albeit at low resolution. The resolution of AFM is high enough to count subunits and therefore the oligomeric state of Panx1 across many individual channels can be explored. The technique was recently used to determine the arrangement of heteromeric Connexin26/30 channels by tagging one of the constructs with an HA tag (Naulin et al., 2020). A second advantage to AFM is that the channels are incorporated in a lipid bilayer that does not have to be frozen in order to image them. A full-length channel can be imaged before and after Caspase-3 activation. The time resolution provided on an individual channel scale may allow for interpretations of gating via domain shifts which may be difficult to capture in non-mobile conditions required for cryo-EM.

Summary & Conclusions

In summary, I have shown in this dissertation that Caspase-3 cleaved Pannexin 1 channels form conduits capable of permeating both cationic and anionic large molecules such as dyes, ATP, and other large signaling metabolites. Using our cell-free proteoliposomes system, these experiments provide direct evidence for the channel being a pathway for these signaling metabolites to be released from cells. Further, I have started to characterize the functional oligomeric state of Pannexin 1 channels. These preliminary experiments suggest that the Panx1 channel may be functional as both a hexamer and a heptamer. I have suggested further studies to complete this body of work.

References

- Ambrosi, C., Gassmann, O., Pranskevich, J. N., Boassa, D., Smock, A., Wang, J., . . . Sosinsky, G. E. (2010). Pannexin1 and Pannexin2 channels show quaternary similarities to connexons and different oligomerization numbers from each other. *J Biol Chem*, *285*(32), 24420-24431. doi:10.1074/jbc.M110.115444
- Bao, L., Locovei, S., & Dahl, G. (2004). Pannexin membrane channels are mechanosensitive conduits for ATP. *FEBS Lett*, *572*(1-3), 65-68. doi:10.1016/j.febslet.2004.07.009
- Beckel, J. M., Daugherty, S. L., Tyagi, P., Wolf-Johnston, A. S., Birder, L. A., Mitchell, C. H., & de Groat, W. C. (2015). Pannexin 1 channels mediate the release of ATP into the lumen of the rat urinary bladder. *J Physiol*, *593*(8), 1857-1871. doi:10.1113/jphysiol.2014.283119
- Buraei, Z., & Yang, J. (2010). The ss subunit of voltage-gated Ca²⁺ channels. *Physiol Rev*, *90*(4), 1461-1506. doi:10.1152/physrev.00057.2009
- Chekeni, F. B., Elliott, M. R., Sandilos, J. K., Walk, S. F., Kinchen, J. M., Lazarowski, E. R., . . . Ravichandran, K. S. (2010). Pannexin 1 channels mediate 'find-me' signal release and membrane permeability during apoptosis. *Nature*, *467*(7317), 863-867. doi:10.1038/nature09413
- Chiu, Y. H., Jin, X., Medina, C. B., Leonhardt, S. A., Kiessling, V., Bennett, B. C., . . . Bayliss, D. A. (2017). A quantized mechanism for activation of pannexin channels. *Nat Commun*, *8*, 14324. doi:10.1038/ncomms14324
- Chiu, Y. H., Ravichandran, K. S., & Bayliss, D. A. (2014). Intrinsic properties and regulation of Pannexin 1 channel. *Channels (Austin)*, *8*(2), 103-109. doi:10.4161/chan.27545
- Demura, K., Kusakizako, T., Shihoya, W., Hiraizumi, M., Nomura, K., Shimada, H., . . . Nureki, O. (2020). Cryo-EM structures of calcium homeostasis modulator channels in diverse oligomeric assemblies. *Sci Adv*, *6*(29), eaba8105. doi:10.1126/sciadv.aba8105
- Deng, Z., He, Z., Maksaev, G., Bitter, R. M., Rau, M., Fitzpatrick, J. A. J., & Yuan, P. (2020). Cryo-EM structures of the ATP release channel pannexin 1. *Nat Struct Mol Biol*, *27*(4), 373-381. doi:10.1038/s41594-020-0401-0
- Good, M. E., Chiu, Y. H., Poon, I. K. H., Medina, C. B., Butcher, J. T., Mendu, S. K., . . . Ravichandran, K. S. (2018). Pannexin 1 Channels as an Unexpected New Target of the Anti-Hypertensive

- Drug Spironolactone. *Circ Res*, 122(4), 606-615.
doi:10.1161/CIRCRESAHA.117.312380
- Hilgemann, D. W., Feng, S., & Nasuhoglu, C. (2001). The complex and intriguing lives of PIP2 with ion channels and transporters. *Sci STKE*, 2001(111), re19. doi:10.1126/stke.2001.111.re19
- Jin, Q., Zhang, B., Zheng, X., Li, N., Xu, L., Xie, Y., . . . Ye, S. (2020). Cryo-EM structures of human pannexin 1 channel. *Cell Res*, 30(5), 449-451. doi:10.1038/s41422-020-0310-0
- Karasawa, A., Michalski, K., Mikhelzon, P., & Kawate, T. (2017). The P2X7 receptor forms a dye-permeable pore independent of its intracellular domain but dependent on membrane lipid composition. *Elife*, 6. doi:10.7554/eLife.31186
- Levitan, I., Singh, D. K., & Rosenhouse-Dantsker, A. (2014). Cholesterol binding to ion channels. *Front Physiol*, 5, 65. doi:10.3389/fphys.2014.00065
- Li, Y., Um, S. Y., & McDonald, T. V. (2006). Voltage-gated potassium channels: regulation by accessory subunits. *Neuroscientist*, 12(3), 199-210. doi:10.1177/1073858406287717
- Locovei, S., Wang, J., & Dahl, G. (2006). Activation of pannexin 1 channels by ATP through P2Y receptors and by cytoplasmic calcium. *FEBS Lett*, 580(1), 239-244. doi:10.1016/j.febslet.2005.12.004
- Lutter, D., Ullrich, F., Lueck, J. C., Kempa, S., & Jentsch, T. J. (2017). Selective transport of neurotransmitters and modulators by distinct volume-regulated LRRC8 anion channels. *J Cell Sci*, 130(6), 1122-1133. doi:10.1242/jcs.196253
- Ma, W., Compan, V., Zheng, W., Martin, E., North, R. A., Verkhratsky, A., & Surprenant, A. (2012). Pannexin 1 forms an anion-selective channel. *Pflugers Arch*, 463(4), 585-592. doi:10.1007/s00424-012-1077-z
- Medina, C. B., Mehrotra, P., Arandjelovic, S., Perry, J. S. A., Guo, Y., Morioka, S., . . . Ravichandran, K. S. (2020). Metabolites released from apoptotic cells act as tissue messengers. *Nature*, 580(7801), 130-135. doi:10.1038/s41586-020-2121-3
- Michalski, K., Syrjanen, J. L., Henze, E., Kumpf, J., Furukawa, H., & Kawate, T. (2020). The Cryo-EM structure of pannexin 1 reveals unique motifs for ion selection and inhibition. *Elife*, 9. doi:10.7554/eLife.54670
- Mou, L., Ke, M., Song, M., Shan, Y., Xiao, Q., Liu, Q., . . . Deng, D. (2020). Structural basis for gating mechanism of Pannexin 1 channel. *Cell Res*, 30(5), 452-454. doi:10.1038/s41422-020-0313-x

- Naulin, P. A., Lozano, B., Fuentes, C., Liu, Y., Schmidt, C., Contreras, J. E., & Barrera, N. P. (2020). Polydisperse molecular architecture of connexin 26/30 heteromeric hemichannels revealed by atomic force microscopy imaging. *J Biol Chem*, *295*(49), 16499-16509. doi:10.1074/jbc.RA119.012128
- Nielsen, B. S., Toft-Bertelsen, T. L., Lolansen, S. D., Anderson, C. L., Nielsen, M. S., Thompson, R. J., & MacAulay, N. (2020). Pannexin 1 activation and inhibition is permeant-selective. *J Physiol*, *598*(2), 361-379. doi:10.1113/JP278759
- Nomura, T., Taruno, A., Shiraishi, M., Nakahari, T., Inui, T., Sokabe, M., . . . Marunaka, Y. (2017). Current-direction/amplitude-dependent single channel gating kinetics of mouse pannexin 1 channel: a new concept for gating kinetics. *Sci Rep*, *7*(1), 10512. doi:10.1038/s41598-017-10921-x
- Panchin, Y., Kelmanson, I., Matz, M., Lukyanov, K., Usman, N., & Lukyanov, S. (2000). A ubiquitous family of putative gap junction molecules. *Curr Biol*, *10*(13), R473-474. doi:10.1016/s0960-9822(00)00576-5
- Poveda, J. A., Giudici, A. M., Renart, M. L., Molina, M. L., Montoya, E., Fernandez-Carvajal, A., . . . Gonzalez-Ros, J. M. (2014). Lipid modulation of ion channels through specific binding sites. *Biochim Biophys Acta*, *1838*(6), 1560-1567. doi:10.1016/j.bbamem.2013.10.023
- Qu, R., Dong, L., Zhang, J., Yu, X., Wang, L., & Zhu, S. (2020). Cryo-EM structure of human heptameric Pannexin 1 channel. *Cell Res*, *30*(5), 446-448. doi:10.1038/s41422-020-0298-5
- Romanov, R. A., Bystrova, M. F., Rogachevskaya, O. A., Sadovnikov, V. B., Shestopalov, V. I., & Kolesnikov, S. S. (2012). The ATP permeability of pannexin 1 channels in a heterologous system and in mammalian taste cells is dispensable. *J Cell Sci*, *125*(Pt 22), 5514-5523. doi:10.1242/jcs.111062
- Ruan, Z., Orozco, I. J., Du, J., & Lu, W. (2020). Structures of human pannexin 1 reveal ion pathways and mechanism of gating. *Nature*, *584*(7822), 646-651. doi:10.1038/s41586-020-2357-y
- Siebert, A. P., Ma, Z., Grevet, J. D., Demuro, A., Parker, I., & Foskett, J. K. (2013). Structural and functional similarities of calcium homeostasis modulator 1 (CALHM1) ion channel with connexins, pannexins, and innexins. *J Biol Chem*, *288*(9), 6140-6153. doi:10.1074/jbc.M112.409789
- Syrjanen, J. L., Michalski, K., Chou, T. H., Grant, T., Rao, S., Simorowski, N., . . . Furukawa, H. (2020). Structure and assembly of calcium homeostasis modulator proteins. *Nat Struct Mol Biol*, *27*(2), 150-159. doi:10.1038/s41594-019-0369-9

- Taruno, A. (2018). ATP Release Channels. *Int J Mol Sci*, 19(3).
doi:10.3390/ijms19030808
- Wang, J., & Dahl, G. (2018). Pannexin1: a multifunction and multiconductance and/or permeability membrane channel. *Am J Physiol Cell Physiol*, 315(3), C290-C299.
doi:10.1152/ajpcell.00302.2017
- Zhang, H., He, C., Yan, X., Mirshahi, T., & Logothetis, D. E. (1999). Activation of inwardly rectifying K⁺ channels by distinct PtdIns(4,5)P₂ interactions. *Nat Cell Biol*, 1(3), 183-188.
doi:10.1038/11103
- Zhang, J., Bal, M., Bierbower, S., Zaika, O., & Shapiro, M. S. (2011). AKAP79/150 signal complexes in G-protein modulation of neuronal ion channels. *J Neurosci*, 31(19), 7199-7211.
doi:10.1523/JNEUROSCI.4446-10.2011